AUTOMATIC SYNTHESIS OF SEQUENTIAL CIRCUITS FOR LOW POWER DISSIPATION

A DISSERTATION

SUBMITTED TO THE DEPARTMENT OF ELECTRICAL ENGINEERING

AND THE COMMITTEE ON GRADUATE STUDIES

OF STANFORD UNIVERSITY

IN PARTIAL FULFILLMENT OF THE REQUIREMENTS

FOR THE DEGREE OF

DOCTOR OF PHILOSOPHY

Luca Benini

February, 1997

I certify that I have read this thesis and that in my opinion it is fully adequate, in scope and in quality, as a dissertation for the degree of Doctor of Philosophy.

Giovanni De Micheli(Principal Adviser)

I certify that I have read this thesis and that in my opinion it is fully adequate, in scope and in quality, as a dissertation for the degree of Doctor of Philosophy.

Teresa Meng(Associate Adviser)

I certify that I have read this thesis and that in my opinion it is fully adequate, in scope and in quality, as a dissertation for the degree of Doctor of Philosophy.

Stephen Boyd

Approved for the University Committee on Graduate Studies:

Abstract

In high-performance digital CMOS systems, excessive power dissipation reduces reliability and increases the cost imposed by cooling systems and packaging. Power is obviously is the primary concern for portable applications, since battery technology cannot keep the fast pace imposed by Moore's Law, and there is large demand for devices with light batteries and long time between recharges.

Computer-Aided Engineering is probably the only viable paradigm for designing state-of-the art VLSI and ULSI systems, because it allows the designer to focus on the high-level trade-offs and to concentrate the human effort on the most critical parts of the design. We present a framework for the computer-aided design of low-power digital circuits. We propose several techniques for automatic power reduction based on paradigms which are widely used by designers. Our main purpose is to provide the foundation for a new generation of CAD tools for power optimization under performance constraints. In the last decade, the automatic synthesis and optimization of digital circuits for minimum area and maximum performance has been extensively investigated. We leverage the knowledge base created by such research, but we acknowledge the distinctive characteristics of power as optimization

Dedication

To Natasha, with gratitude and love.

Acknowledgments

I have many people to thank for this dissertation. First of all, my advisor, Professor Giovanni De Micheli, who guided my efforts and never denied his help. I am very grateful to the members of my reading committee, Professor Teresa Meng and Professor Stephen Boyd, for the time and patience spent in reading these pages. This research was sponsored by a scholarship from NSF, under grant MIP-9421129. I wish to thank NSF for the economic support that made possible this work.

I also wish to thank all current and past members of the CAD group: Claudionor Coelho, David Filo, David Ku, Vincent Mooney, Polly Siegel (who also read part of this thesis), Matja Siljak, Frederick Vermeulen, Patrick Vuillod and Jerry Yang. Their help has been invaluable in many occasions.

Special thanks to my first mentor, Professor Bruno Riccó and to my friends and colleagues at DEIS, Universitá di Bologna. I am also deeply in debt with the friends of Politecnico di Torino for long, sleepless nights of work. I would especially like to mention two good friends and great co-workers, Alessandro Bogliolo and Enrico Macii, for sharing with me the pains of bringing ideas to practice.

Lastly, I am deeply in debt with my family who gave me support during the hard moments, and with my wife Natasha, for her love and the wonderful gift of her presence.

Contents

List of Tables

List of Figures

Chapter 1

Introduction

When Gordon Moore of Intel Corporation observed in 1965 that the number of transistors per chip had been doubling every year for a period of 15 years, he was formulating one of the fundamental laws of the semiconductor industry [moor96]. The so-called "Moore's Law" has held for the last 35 years, although recently the rate has slowed to about 1.5 times per year, or to quadrupling every three years [mein95]. In the dominant CMOS technology the increase in integration comes with numerous beneficial effects. Transistors become faster (the delay of a ring oscillator stage in in $0.1\mu m$ technology with $1.0V$ supply voltage is less than $5ps$) and performance increases. In 1996, commercially available microprocessors run with clock speed exceeding 500MHz and contain more than 9 million transistors [alpha96, expo96]. Processors in the GHz clock frequency range are expected to be announced in the next two to three years.

While top-of-the line microprocessors provide impressive computational power and lead the way addressing the formidable challenges of *Ultra-Large Scale of Integration* (ULSI) design, less aggressive products target the rapidly expanding market of portable electronic devices for personal communication, automotive systems, biomedical instruments and many other applications. In both kinds of applications,

the reduction of power consumption is a primary concern. In high-performance systems, excessive power dissipation reduces reliability and increases the cost imposed by cooling systems and packaging. Power is obviously is the primary concern for portable applications, since battery technology cannot keep the fast pace imposed by Moore's law, and there is large demand for devices with light batteries and long time between recharges.

The design of electronic circuits with low power dissipation is an old art. Several micropower techniques were introduced in the 1970's and commercially exploited in the first low-power applications: electronic wristwatches and implantable units for biomedical applications [bult96]. Although the basic issues are unchanged, the designers of today's low-power systems are faced with a much more complex task: power must be minimized while maintaining high performance. To further complicate the problem, the pressure for fast time-to-market has become extremely high, and it is often unacceptable to completely re-design a system just to reduce its power dissipation.

Computer-Aided Engineering (CAE) and *Computer-Aided Design* (CAD) are probably the only viable paradigms for designing state-of-the art *Very Large Scale of Integration* (VLSI) and ULSI systems, because they allow the designer to focus on the high-level trade-offs and to concentrate the human effort on the most critical parts of the design. Low-power VLSI systems are no exception: although human contribution is essential for taking architectural decisions and providing creative solutions of the most critical problems, computer-aided design support reduces the turn-around time and improves the efficiency of the design process.

In this thesis we present a framework for the computer-aided design of low-power digital circuits. We propose several techniques for automatic power reduction based on paradigms which are widely used by designers. Our main purpose is to provide the foundation for a new generation of CAD tools for power optimization under

tight performance constraints. In the last decade, the automatic synthesis and optimization of digital circuits for minimum area and maximum performance has been extensively investigated. We leverage the knowledge base created by such research, but we acknowledge the distinctive characteristics of power as optimization target. It will become clearer in the following sections that power is a complex cost measure whose optimization poses original and exciting new challenges.

The remaining of this chapter is organized as follows. Section 1.1 describes the main sources of power consumption in the dominant CMOS technology. Section 1.2 describes the basic design techniques to reduce power dissipation. Section 1.3 is a review of related work in synthesis techniques for low power. Section 1.4 is a summary of the contributions of this thesis.

1.1 Sources of power consumption

As power dissipation becomes a high-priority cost metric, researchers and designers have increased their efforts in understanding its sources and minimizing its impact. In this section we review the main causes of power dissipation in CMOS digital circuits, then we discuss the most effective strategies for power minimization. Power dissipation is not constant during the operation of a digital device. The *peak power* is an important concern. Excessive peak power may cause a circuit to fail because of electromigration and voltage drops on power and ground lines. Fortunately, correct and reliable circuit operation can be ensured by designing for worst-case conditions. For this reason peak power *estimation* is the main focus and we do not address it here (see [najm95] for an excellent overview). On the other hand, the *time-averaged* power consumption is inversely proportional to the battery life time. Hence, minimization of average power consumption is a key issue for the success of numerous electronic products, and it is the primary focus of the following treatment.

The average power dissipation in a CMOS circuit can be described by a simple equation that summarizes the four most important contributions to its final value

$$P_{avg} = P_{dynamic} + P_{short} + P_{leakage} + P_{static} \tag{1.1}$$

The four components are respectively $P_{dynamic}$, *dynamic*, P_{short} *short-circuit*, P_{lk} *leakage* and P_{static} *static* power consumption. The partition of P_{avg} among its component strongly depends on the application and the technology. We analyze each contribution in detail, using a simple combinational static CMOS gate as a motivating example. Dynamic circuits and sequential gates show similar behavior.

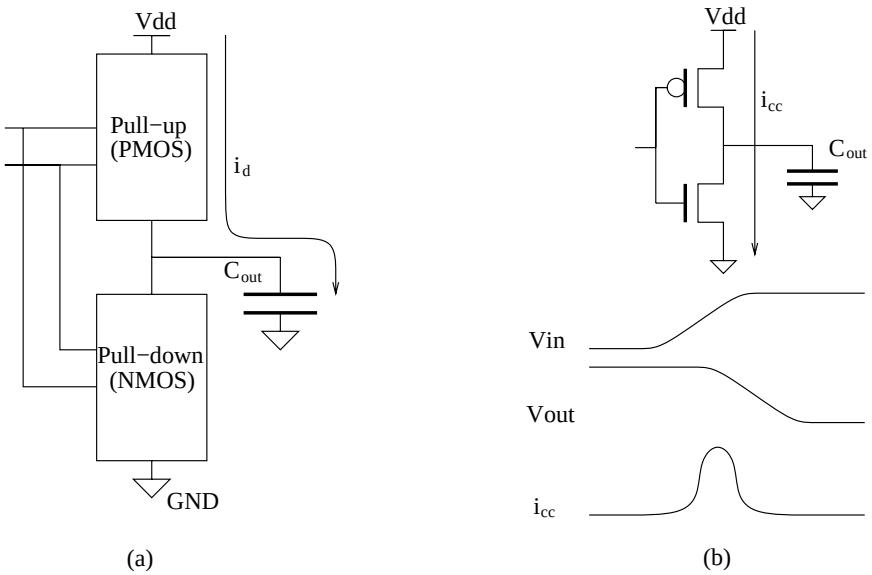

Figure 1: CMOS gate structure and power dissipation

Dynamic power consumption, $P_{dynamic}$ is the power consumed during the output switching of a CMOS gate. Figure 1 (a) shows the structure of a generic static CMOS gate. The *pull-up* network is generally built with PMOS transistors and connects the output node *Out* to the power supply *Vdd*. The *pull-down* network is generally composed of NMOS transistors and connects the output node to the ground node

GND. In a CMOS gate, the structure of the pull-up and pull-down networks is such that when the circuit is stable (i.e. the output rise or fall transients are exhausted) the output is never connected to both Vdd and GND at the same time.

When a transition on the inputs causes a change in the conductive state of the pull-up and the pull-down network, electric charge is transferred from the power supply to the output capacitance C_{out} or from the output capacitance to ground. The transition causes power dissipation on the resistive pull-up and pull-down networks. Let us consider a rising output transition. Power is by definition $P_{dynamic}(t) = dE(t)/dt = i_d(t)v(t)$, where $i_d(t)$ is the current drawn from the supply and $v(t)$ is the supply voltage ($v(t) = Vdd$). The total energy provided by the supply is:

$$E_r = \int_0^{T^r} i_d(t)v(t)dt = V_{dd}\int_0^{V_{dd}} C_{out}dV_{out} = C_{out}V_{dd}^2 \tag{1.2}$$

where T^r is a time interval long enough to allow transient exhaustion. Notice that we implicitly assumed that all current provided by V_{dd} is used to charge the output capacitance. We also assumed that the output capacitance is a constant.

At the end of the transition, the output capacitance is charged to V_{dd}, and the energy stored in it is $E_s = 1/2C_{out}V_{dd}^2$. Hence, the total energy dissipated during the output transition is $E_d = C_{out}V_{dd}^2 - 1/2C_{out}V_{dd}^2 = 1/2C_{out}V_{dd}^2$. If we now consider a falling transition, the final value of the output node is 0, and the output capacitance stores no energy. For conservation of energy, the total energy dissipated during a falling transition of the output is again $1/2C_{out}V_{dd}^2$.

This simple derivation leads us to the fundamental formula of dynamic power consumption:

$$P_{dynamic} = K\frac{C_{out}V_{dd}^2}{T} = KC_{out}V_{dd}^2 f \tag{1.3}$$

where T is the clock period of the circuit and $f = 1/T$ is the clock frequency. The factor K is the average number of transitions of the output node in a clock cycle

divided by two. Setting $K = 1/2$ is equivalent to assuming that the gate performs a single transition every cycle. Clearly, in any digital circuit the clock cycle is much longer than the time for a gate transition. Hence, a single gate may have multiple transitions in any given clock cycle. On the other hand, the output of a gate may not switch at all during a clock cycle. Equation 1.3 is important mainly because it includes the most important parameters influencing power dissipation, namely supply voltage, capacitance switched, clock frequency and the average number of output transitions per clock cycle.

Figure 1 (b) illustrates the origin of the short circuit power dissipation P_{short}. While in deriving $P_{dynamic}$ we assumed that all charge drawn from the power supply is collected by the output capacitance, this is not the case in realistic digital circuits. Since the inputs have finite slope, or, equivalently, the input transit time $t_{r/f}$ is larger than 0, the pull-down and the pull-up are both on for a short period of time. During this time, there is a connection between power and ground and some current is drawn from the supply and flows directly to ground. We call this current *short-circuit current*. The total current drawn from V_{dd} is therefore $i(t) = i_d(t) + i_{short}(t)$. The following formula was proposed to describe the short circuit power dissipation of an inverter with no external load (the analytical derivation of the formula under several simplifying assumption is carried out in [veen84]):

$$P_{short} = \frac{\beta}{12}(V_{dd} - 2V_T)^3 \tau f \tag{1.4}$$

where β is the gain factor of a MOS transistor, V_T is its threshold voltage and τ is the rise (or fall) of the input of the inverter. The analysis in [veen84] shows that P_{short} depends on the ratio between the transit time of the output and the transit time of the input, the worst case being slow input edges and fast output edges. Although the P_{short} of a single gate is minimized for very fast input edges and slow output edges, the best design point for cascade of gates is when the transit times of all gate outputs

is kept roughly constant [veen84].

Several authors observed that short-circuit power dissipation is usually a small fraction (around 10%) of the total power dissipation, in "well-designed" CMOS circuits. The rationale for the observation is that P_{short} becomes sizable when a gate is driven by an excessively loaded driver which generates slow transitions at its input. This situation is generally avoided in circuits designed for high performance. As a consequence, it is reasonable to expect that traditional design techniques for high performance lead to circuits where short-circuit power dissipation is not a major concern.

The third component of the total power dissipation in Equation 1.1 is $P_{leakage}$, the power dissipated by leakage currents. Leakage power is mainly caused by two phenomena: *diode leakage* current due to the reverse saturation currents in the diffusion regions of the PMOS and NMOS transistors and *sub-threshold leakage* current of transistors which are nominally off. Both currents have an exponential dependence on the voltage: diode leakage depends on the voltage across the source-bulk and drain-bulk junctions of the transistors, while sub-threshold current depends on both the voltage across source and drain and across gate and source.

Diode leakage is an important concern for circuits that are in standby mode for a very large fraction of operation time and it is usually reduced by adopting specialized device technologies with very small reverse saturation current. Sub-threshold leakage is becoming increasingly important because of reductions in power supply. As power supply voltages decrease, the transistor threshold is lowered to keep turned-on transistors well within the conductive region of operation. Consequently, transistors operating in a non-conductive region are only weakly turned off, and conduct some current even in their "OFF" state.

In today's VLSI circuits $P_{leakage}$ is still a small fraction (less than 10%) of the total power dissipation. Reductions in $P_{leakage}$ is achieved mainly through device

technology improvements (diffusion region engineering and threshold control), and by enforcing stricter design rules. It may be possible, however, that specialized design techniques for minimizing $P_{leakage}$ may be required, as power supply voltages continue to decrease.

The last component in Equation 1.1 is the static power dissipation, P_{static}, caused by DC current flow from V_{dd} to GND when the pull-up and pull-down are both conducting and the gate output is not transitioning. Correctly designed CMOS circuits do not have static power dissipation, and it is fair to say that the absence (in nominal conditions) of static power dissipation is probably the most important distinctive characteristic of the CMOS technology. Unfortunately P_{static} may become non null in faulty circuits. Circuits where $P_{static} \neq 0$ must be detected and discarded because i) if present, P_{static} becomes the major contributor to the total power dissipation ii) static current is often associated with incorrect or unpredictable functional behavior. As an example of a faulty circuit with $P_{static} \neq 0$ consider the inverter of Figure 1 (b) and assume that the gate of the PMOS transistor is connected GND. When the input is high, both PMOS and NMOS transistors are conducting and current flows from V_{dd} to GND even if the input is stable.

Summarizing the discussion on the contributions to power dissipation in CMOS circuits, we conclude that the dominant fraction (around 80%) of P_{avg} is attributed to $P_{dynamic}$, the dynamic power dissipation caused by switching of the gate outputs. The reader should refer to the detailed survey by Chandrakasan [chan95] for more information. The vast majority of power reduction techniques concentrate on minimizing the dynamic power dissipation by reducing one or more factors on the right hand side of Equation 1.3. In the next section we will consider each controlling variable in greater detail, and give a brief overview of the techniques currently employed by designers to reduce power dissipation.

1.2 Design techniques for low power

1.2.1 Power minimization by frequency reduction

Probably the most obvious way to reduce power consumption is to decrease the clock frequency f. Decreasing the clock frequency causes a proportional decrease in power dissipation. However, in digital systems we are interested in performing a given task (e.g. adding two numbers). Slowing the clock merely results in a slower computation, but no effective savings for that task. The power consumption over a given period of time is reduced, but the total amount of useful work is reduced as well. In other words, the energy dissipated to complete the task has not changed.

Assume that we want to perform the task with a portable battery-operated system. Assume the system is clocked with a clock period T_1, and the task takes NT_1 clock cycles to complete. During each cycle, the system dissipates an average power P_1.

If we now decrease the frequency in half, we will dissipate $P_2 = 1/2P_1$, over the original time period, because average power is directly proportional to the clock frequency. However, it now takes a total time of $2NT_1$ to complete the task. As a consequence, the average energy consumed by the system is $E = P_1NT_1$ in both cases. It is true that we consumed less power per cycle with the slower frequency, but we *had to operate the system for a longer time* to execute the same task.

Under the assumption that the total amount of energy provided to complete the task is a constant, decreasing the clock frequency has negative consequences, because it just increases the time needed to complete the given task. This observation has been often reported in the literature [chan95, burd95].

For portable systems, we are interested in power reduction as a way to maximize battery life. Recent studies [mart96] have shown that the total amount of energy provided by actual batteries is *not* a constant, but depends on the rate of discharge of the battery, so the frequency of operation comes back into play here. According to

an empiric equation known as *Peukert's formula* we have [mart96]:

$$C = \frac{\chi}{I^{\alpha}} \tag{1.5}$$

where C is the total energy that can be drawn from a battery (also know as the *energy capacitance*), χ is a technology-dependent constant (a characteristic of the particular type of battery used), I is the average discharge current and α is a technology-dependent fitting factor. For typical $NiCd$ batteries, for instance, α ranges between 0.1 and 0.3. The most important consequence of Equation 1.5 is that if we decrease the discharge current, we can actually increase the total amount of energy that is provided by the battery. In other words, there may be some advantage in reducing the clock frequency, because batteries are more proficiently utilized when the discharge current is small.

Although this interesting and somewhat counterintuitive observation may open a new avenue of research for portable systems where clock frequency is reduced (thereby reducing the average current per clock cycle) to maximize the energy capacitance, there are still other important factors that limit the impact of power optimization techniques based on clock frequency reduction. One factor is the constraint on *peak performance*. For many digital systems such as microprocessors, the peak performance is very important, beacuse it allows to favorably compare to the competitor's products when running benchmark programs and it is related to the user waiting time which is subject to hard limits.

Even if peak performance is not the primary objective, a very large fraction of digital systems are throughput-constrained. In order for the system to meet the design specifications, a given number of computations per second must be performed. This kind of specification is typical of signal processing systems where the sampling rate is often decided by high-priority system-level constraints. For both peak-performance-constrained and throughput-constrained systems, clock frequency reduction is not a

viable alternative for power optimization. Since such systems are the vast majority of VLSI applications implemented today, clock frequency control is used only in conjunction with other techniques to achieve power savings [chan95].

1.2.2 Power minimization by voltage scaling

Voltage scaling is the most effective way to reduce power consumption. This is apparent from Equation 1.3, since $P_{dynamic}$ has quadratic dependence on the power supply voltage. A large body of research has been devoted to voltage scaling for power reduction. The most complete work in the area is the pioneering research of Chandrakasan and Brodersen, summarized in [chan95].

In CMOS, reducing supply voltage causes the circuit to run slower. The delay of a CMOS inverter can be described by the following formula [chan95]:

$$T_d = \frac{C_{out}V_{dd}}{I} = \frac{C_{out}V_{dd}}{\eta(W/L)(V_{dd} - V_t)^2} \tag{1.6}$$

where η is a technology-dependent constant, W and L are respectively the transistor width and length, and V_t is the threshold voltage. Many simplifying assumption are made in the derivation of Equation 1.6. The most important assumptions are: i) the current through the MOS transistor is well fitted by the quadratic model, ii) during the transient, the device controlling the charge (discharge) of the output capacitance is in saturation.

Unfortunately, deep sub-micron devices such as those used in modern VLSI systems are *velocity saturated* and are not modeled correctly by the simple quadratic model. A MOS transistor is said to be velocity saturated if no improvement in transit time of the electrons through the conductive channel can be obtained by increasing the drain-source voltage. Equation 1.6 should not be regarded as an accurate analytical model of gate delay (not even for a simple inverter) because it assumes that T_d

can be arbitrarily reduced by increasing V_{dd}.

Nevertheless, the equation is important because it contains the variables on which gate delay actually depend, and the nature of their effect is correctly represented. In other words, T_d increases with C_{out} and $1/(W/L)$, and it strongly depends on the voltage supply and the threshold voltage.

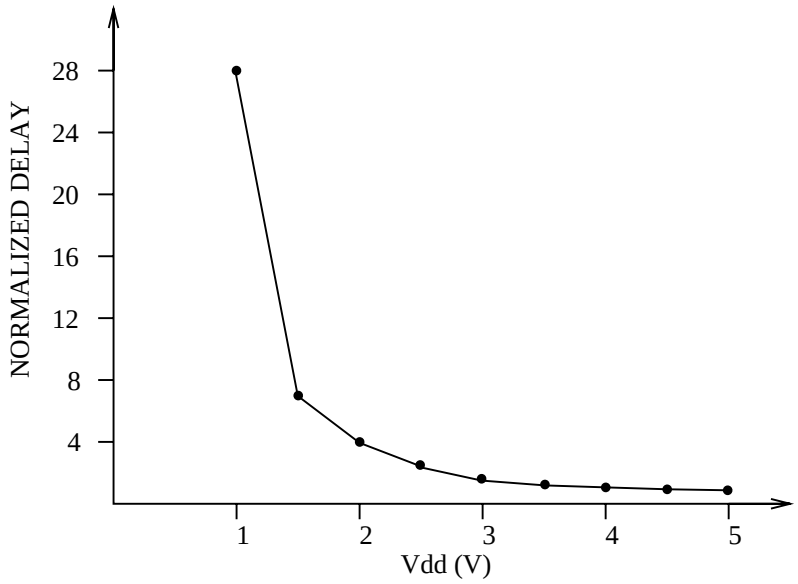

Figure 2: Normalized gate delay versus supply voltage

We can study T_d as a function of the voltage supply with all other parameters fixed. A plot depicting the functional dependency of delay from V_{dd} is shown in Figure 2. Two main features emerge from the analysis of the plot: i) further increasing the supply voltage above 3V has little impact on performance; ii) the speed decreases abruptly as V_{dd} gets closer to the threshold voltage V_t. The physical phenomena responsible for this behavior are respectively the velocity saturation of the MOS transistors at high V_{ds} [chan95] and the low conductivity of the channel when V_{gs} approximates V_t.

If speed decreases when we decrease the power supply, power decreases as well, and quadratically. Clearly there is no point in increasing the supply voltage beyond

velocity saturation, because little, if any, performance advantage can be obtained. This straightforward observation explains the supply voltage reduction observed in CMOS circuits in the last few years. However, if power dissipation is the primary target, we may push power supply reduction in the region where some speed penalty is paid.

In the following discussion we target power reduction of a digital system with throughput constraints and a fixed cycle time T. We assume that the system was originally designed just to meet the throughput constraints (i.e. the critical path of the circuitry is matched to the cycle time T). If we lower the power supply, the circuit becomes slower and the computation does not complete within a single clock cycle.

However, the designer can still use voltage scaling to reduce power consumption if design modifications are made to satisfy the throughput constraints. This approach is known as *architecture-driven voltage scaling* [chan95]. The transformations employed in architecture-driven voltage scaling are based on increasing the level of concurrency in the system: more hardware is used and several tasks are performed in parallel. Typical transformations are *pipelining* and *parallelization*. But, pipelining and parallelization result in an area penalty, because they require additional hardware. Increased area in turn implies increased capacitance, which increases power dissipation. However, power decreases quadratically with V_{dd}, but increases only linearly with switched capacitance. Thus, there will be a net reduction in power with these techniques.

Example 1.2.1. This example is taken from [chan95]. Consider the add-compare circuit shown in figure 3 (a). The power consumed by the circuit is

$$P_{ref} = C_{ref} V_{ref}^2 \frac{1}{T}$$

The cycle time is matched to the critical path $T = T_{add} + T_{cmp}$ and the throughput constraint is $1/T$ add-compares per second. Hence, we cannot simply reduce the supply voltage. However, we can pipeline the circuit. The pipelined implementation is shown in Figure 3 (b). The critical path becomes

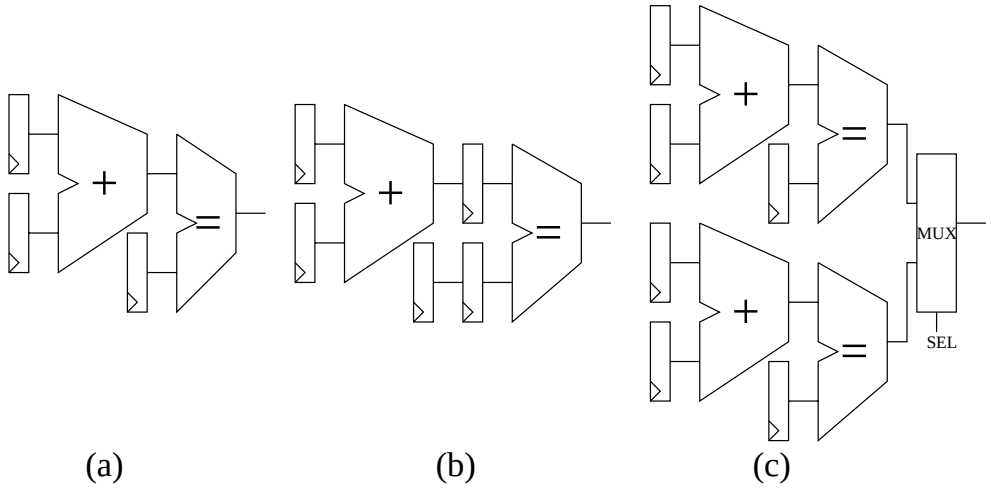

Figure 3: Transformation for architecture-driven voltage scaling

$Max\{T_{add}, T_{cmp}\} < T$. Now we can lower the power supply until the new critical path matches T. Notice that the switched capacitance is increased, because of the additional pipeline registers. The power consumed by the pipelined implementation is, for this example [chan95]:

$$P_{pipe} = C_{pipe}V_{pipe}^2 1/T_{pipe} = (1.15C_{ref}) \cdot (.58V_{ref})^2 \cdot \frac{1}{T} = .39P_{ref}.$$

Alternatively, we can utilize a parallel architecture, as shown in Figure 3 (c). Notice that the two parallel data-paths are clocked respectively on the odd and even clock cycles, and the multiplexer selects alternatively the result of one or the other data-path. In the parallel implementation, every add-compare circuit has $2T - T_{mux}$ to complete the computation, and we can lower the voltage supply until the critical path matches the available time. The power dissipation of the parallel implementation is

$$P_{par} = C_{par}V_{par}^2 1/T_{par} = (2.15C_{ref}) \cdot (.58V_{ref})^2 \cdot \frac{1}{2T} = .36P_{ref}$$

The two transformations can be combined to obtain a parallel and pipelined implementation, with even better power savings (and higher hardware overhead). The power dissipation of the combined parallel and pipelined implementation is $P_{parpipe} = .2P_{ref}$. □

Obviously there is a point of diminishing returns for architecture-driven voltage

scaling. As V_{dd} approaches V_t, the incremental speed reduction paid for an incremental voltage reduction becomes larger. Moreover, the area cost of highly parallel implementation increases more than linearly because of the communications overhead.

Several other voltage scaling techniques for low power have been proposed (the book by Chandrakasan contains an excellent survey [chan95]), however the main limitation of all voltage scaling approaches is that they assume the designer has the freedom of choosing the voltage supply for his/her design. Unfortunately this is almost always impossible. For many real-life systems, the power supply is part of the specification and not a variable to be optimized. Accurate voltage converters are expensive, and multiple supply voltages complicate board and system-level design and increase overall system cost. Thus, it may not be economically acceptable to arbitrarily control the supply voltage.

Even if low-cost reliable voltage converters became widely available [stra94], there is a more fundamental limitation. Device technologies are designed to perform optimally at a given supply voltage. Since sub-micron devices are velocity saturated, and there is almost no advantage to choose a high voltage supply, the semiconductor industry is moving to low-voltage technologies (the current standard is $3.3V$ and advanced microprocessors are already operating at $2V$). In current (and future) technologies, voltage scaling will become almost impossible because of reduced noise margins and deterioration of device characteristics. Since the best supply voltage for a technology is set by higher priority items than power dissipation, it appears that voltage scaling techniques will have only a marginal practical impact.

1.2.3 Power optimization by capacitance reduction

Equation 1.3 shows that there is a linear dependence of $P_{dynamic}$ on the capacitance. The capacitive load C_{out} of a CMOS gate G consists mainly of i) gate capacitance of transistors in gates driven by G, ii) capacitance of the wires that connect the gates,

iii) parasitic (junction and gate-source or gate-drain) capacitance of the transistors in gate G. In symbols:

$$C_{out} = C_{fo} + C_w + C_p \tag{1.7}$$

where C_{fo} is the capacitance of fan-out gates, C_w is the wiring capacitance and C_p is the parasitic capacitance. We analyze the three components in more detail.

The fan-out capacitance depends on the number of logic gates driven by G and the size of their transistors. The capacitance of a MOS transistor depends on the technology (more precisely, the gate oxide thickness) and the dimensions of the transistor, $C_g = WL\epsilon_{ox}/t_{ox}$, where ϵ_{ox} is the electric permittivity of the silicon oxide and t_{ox} is the oxide thickness. Since t_{ox} is set by the technology, and it is not under the designer's control, the gate capacitance can be reduced only by shrinking the dimension of the transistors. Another way to reduce the contribution of C_{fo} is to reduce the number of fan-out gates. In technologies with channel length above $1\mu m$, C_{fo} is by far the most important component in C_{out}. Unfortunately, this is not the case for today's *deep sub-micron* devices, with channel length in the order of $.3\mu m$.

For deep sub-micron technologies, the wiring capacitance C_w is becoming the dominant component of C_{out}. It is extremely hard to accurately estimate C_w. If the circuit is manually laid out, the topology of the wires and their sizing can be decided by the designer (or at least estimated with some accuracy). Unfortunately, state-of-the art technologies have multiple levels of metal and extremely small minimum feature size and therefore wires are very close to each other. Hence, the coupling between wires is becoming the most important factor for determining the wiring capacitance. Accurate modeling of such *cross-talk* capacitance can be achieved only through computationally expensive computations of two and three-dimensional electric field. Even a rough approximation of these effects requires a good deal of engineering ingenuity.

For automatically laid-out circuits, the situation is even worse, because the designer does not know what the wire's topology and sizing will be. The wiring capacitance can be estimated *after* placement and routing, but it is not clear how the knowledge of the wiring capacitance after placement and routing can be exploited to reduce the impact of C_w. Currently the estimation, and worse, the control of wiring capacitance is a problem for which no satisfactory solution is available.

The parasitic capacitance C_p is probably the component causing the least concern, because it is well characterized and constant (to a first approximation) since it depends only on the transistors of the gate itself, and it is relatively small compared to the other two contributions.

In summary, in state-of-the art technologies, approximatively 50% of C_{out} is due to C_{fo}, 40% is due to C_w and 10% is due to C_p. The wiring capacitance already dominates C_{out} for data busses and global control wires, and will become largely dominant in the next two to three years.

Reducing C_{out} not only improves power, but also reduces area and increases speed. For this reason, techniques for capacitance minimization have been practiced for a long time, in practice since the birth of VLSI technology. Capacitance minimization is *not* the distinctive feature of low-power design, since in CMOS technology power is consumed only when the capacitance is switched. Focusing on reducing power by decreasing C_{out} is a tempting alternative since it allows to exploit the mature technology for area minimization (capacitance is proportional to active silicon area).

What differentiates power optimization from capacitance minimization is the fact that we do not need to minimize capacitance if it is seldom switched. Although a minimum capacitance (i.e. minimum area) circuit has generally low power dissipation, a minimum power circuit does not necessary have minimum capacitance. Pure capacitance reduction is not generally the most effective to reduce power dissipation, because it is useless to reduce capacitance when there is little activity. Moreover, as

we will see later, a slight capacitance increase (i.e. the addition of some redundant circuitry) may lead to remarkable power reduction.

1.2.4 Power optimization by switching activity reduction

We can summarize the previous subsections as follows: the supply voltage V_{dd} is usually not under designer control; the clock frequency, or more generally, the system throughput is a constraint more than a design variable; capacitance is important only if switched. What really distinguishes power is its dependence on the switching activity (i.e. factor K in Equation 1.3). More precisely, power minimization techniques should target the reduction of the *effective capacitance*, defined as $C_{eff} = K \cdot C_{out}$. The fundamental equation of dynamic power dissipation can be rewritten as:

$$P_{dynamic} = C_{eff} V_{dd}^2 f \tag{1.8}$$

Equation 1.8 helps clarifying our fundamental claim: power minimization is achieved through the reduction of C_{eff}. It is important to reiterate the assumptions behind this claim. First, $P_{dynamic}$ is the dominant factor in power dissipation. Second, V_{dd} is a technology-related parameter that cannot be directly controlled. Third, the performance (in terms of amount of work carried out in given amount of time) of the system is constrained.

The implications of Equation 1.8 have been clear to digital designers for a long time. In surveying the description of commercial chips with low power consumption, it is obvious that once a technology and a supply voltage have been set, power savings come from the careful minimization of the switching activity.

We can define types of switching activity: *functional* and *useless*. Functional switching activity is required to compute the desired results. For example, the switching activity in an arithmetic unit that computes a fast Fourier transform is functional.

Useless switching activity is produced by units that are not taking active part in a computation or whose computation is redundant. For example, the result of an arithmetic operation is useless when an exception is raised that invalidates it.

Thus, the key to designing low-power VLSI systems is to minimize the amount of switching activity needed to carry out a given task within its performance constraints. There are many examples of effective applications of this idea.

- *Nap* and *doze* modes of operation in portable computers [elli91, harr95, debn95, slat95]. With these techniques, power is reduced by stopping the clock of parts of the microprocessor, or of the entire system, when the system is not performing any useful task. This is an example of minimizing useless switching activity.

- Dynamic power management through the use of *gated clocks* [harr95]. The same principle of the processor-level low-power modes of operation is applied at a finer granularity: the clock distribution to a unit in a chip can be disabled at run time if the unit is not needed for a given computation. The clock is enabled as soon as the unit is required.

- Algorithmic transformations for signal processing tasks [meng95, chan95b, mehr96]. Reducing the number of operations needed to carry out a give computation may not be always useful in terms of performance (if the operations are parallelizable), but it is often useful for reducing power. In this case the functional switching activity is reduced.

- Communication protocol design [mang95]. Communication protocols can be modified to improve the activity patterns. For example, an asynchronous communication protocol for pagers may be less power efficient than a synchronous protocol, because in the first case the receiving unit must be continuously turned on, while in the second case it must be on only during the time slots where some incoming data is expected.

Notice that in many cases the reduction in C_{eff} comes with a concomitant increase of C_{out}. For example, the addition of the circuitry for controlling the *Nap* mode in a microprocessor marginally increases the area, and consequently the total capacitance. However, the C_{out} increase is more than paid off by the reduction of the switching activity. Whenever investigating some power reduction technique that implies some area overhead, we should always consider the trade off between increasing C_{out} and decreasing K, to guarantee an overall decrease in C_{eff}.

Design techniques that reduce the useful switching activity are inherently harder to apply than those targeting useless switching. Reducing useful switching is usually accomplished through algorithm redesign and optimization, a task that largely relies on human skills. In this thesis we will investigate examples of both techniques, and propose practical ways to partially automate the process of reducing C_{eff}.

1.2.5 Revolutionary approaches

Before concluding the section we briefly mention techniques for power reduction that adopt a more radical approach by removing one of more of the assumption leading to the conclusions of Subsection 1.2.4. We call these approaches *revolutionary* to contrast with the *evolutionary* nature of the power optimization strategies previously discussed. We consider two revolutionary approaches that have been proposed in the literature in the last few years, namely: asynchronous circuits and adiabatic circuits.

Asynchronous circuits [birt95] are an interesting alternative to standard synchronous circuits for low-power design. Synchronous circuits define one or more clock signals that are used used to synchronize the sequential elements. Although a common clock simplifies the interface of sub-modules in complex systems, clocking circuitry is hard to design and power consuming. The C_{eff} of the clock is almost invariably the largest of the chip, since it has large switching activity and capacitance. Asynchronous design techniques eliminate the need for clock signals. Units

interface through handshake signals which are activated only when necessary and do not require global synchronization. Several asynchronous chips have been designed targeting low power [niel94, mars94, gars96].

It is often claimed that asynchronous circuits are inherently more power efficient than synchronous circuits, because they eliminate global synchronization signals that do not actually perform any "useful computation". Furthermore, as the size and clock speed of VLSI circuits increases, new clocking paradigms are emerging that have much in common with asynchronous circuits: sub-units of a large digital systems are clocked at different speeds and require handshaking to communicate among them.

Unfortunately, asynchronous circuits have not yet become a mainstream technology, mainly because of the lack of computer-aided design tools to help engineers design large chips and the overhead of local handshaking signals that erode the claimed power savings. The few large asynchronous designs described in the literature have not incontrovertibly proven that there are substantial advantages with respect to synchronous designs, mainly because they compared to functionally equivalent synchronous designs that were not optimized for power. Although the author is a believer in asynchronous design methodologies, their final success as a revolutionary design style for low power is yet to be realized.

Design techniques typical of asynchronous design have been employed within the realm of synchronous circuits: a typical example is *clock gating*. With clock gating, power is reduced by stopping the clock of idle units. Clock gating can be seen as a specialized use of asynchronous techniques, because the clock becomes an activation signal that is provided to a sub-system only when its computation is required. It is likely that asynchronous design techniques will be integrated in the mainstream synchronous paradigm in an evolutionary fashion.

Adiabatic computation has been proposed as a low-power design technique [benn88, atha94, denk94]. The principles of adiabatic computation are rooted in a simple

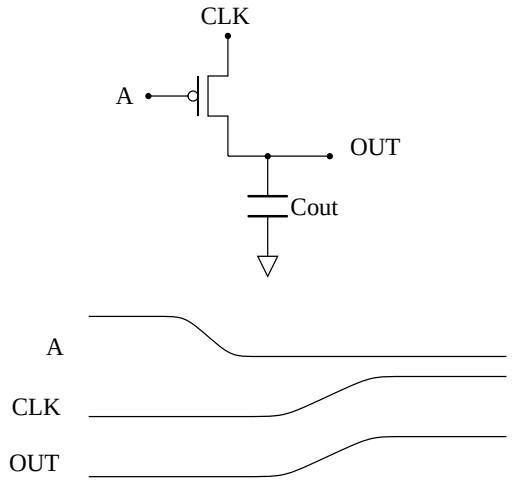

Figure 4: Simple adiabatic inverter

physical principle: since power is $p(t) = i(t)v(t)$, little power is dissipated if the charge transfer needed to perform computation is performed at $v(t) \approx 0$. Obviously, if $v(t) = 0$ no charge is transferred. If we keep $v(t)$ small and change it slowly, we can transfer charge (i.e. perform useful computation) with minimal power dissipation. Key to the practical applicability of adiabatic computation is the quantitative meaning of the word "slowly". For charge transfer to be adiabatic, the transfer time must be $T_t >> \tau$, where τ is the RC time constant of the circuit performing the computation.

The simplest adiabatic circuit is the *adiabatic inverter* [denk94] shown in Figure 4. When the input A switches, the CLK line is low. The transistor is turned on, but no power is dissipated through it, because the voltage across its drain and source is zero. When the transient on A is exhausted, the CLK line is raised with a slow transition. In this case, "slow" means that the rise time of CLK T_r has to be $T_r >> C_{out}R$, where R is the equivalent resistance of the transistor and C_{out} is the load capacitance. Since T_r is slow, the output voltage V_{out} tracks the clock waveform and the voltage across the source and drain of the transistor is always very close to zero ($V_{ds} \approx 0$). Since power is dissipated on the transistor resistance, $P = VI = V_{ds}^2/R \approx 0$.

Theoretically, $lim_{T_r \to \infty} P = 0$. In practice $T_r \approx 10 C_{out} R$ is sufficient for the circuit to operate adiabatically, with negligible power dissipation. Notice that, at the end of the transition on CLK, OUT is equal to A', thus the circuit behaves as an inverter.

Several *adiabatic logic families* have been proposed [raba96] and actually implemented in silicon, showing extremely low power dissipation. Unfortunately there are numerous practical and theoretical objections to the concept of adiabatic circuits. Probably the most convincing one has been proposed by Indermaur and Horowitz [inde94]. In their paper, the authors claim that adiabatic circuits should be compared to voltage-scaled CMOS circuits with similar performance, and show that the operation frequencies at which adiabatic circuits become more power-efficient than voltage-scaled CMOS are extremely low.

Nevertheless, many papers have been presented where adiabatic circuits are implemented successfully within standard CMOS systems [raba96]. It appears that adiabatic techniques may help in designing critical sub-units and save some power, but it is unlikely that fully adiabatic designs will ever become a practical alternative to mainstream CMOS.

1.3 CAD techniques for low power

Designers faced with the challenges of tight power constraints optimize power dissipation following the basic principles outlined in the previous section. Designing for low power is at least as difficult as designing for maximum speed or minimum area. Power is a pattern-dependent cost function, unlike area, which is constant with respect to input patterns. Delay is pattern dependent as well, but as far as delay is concerned, we are interested in reducing its worst case value (i.e. the *critical path delay*) and relatively simple and fast estimates of the worst case can be obtained. The main source of difficulty in low-power design is the dependence of power on the switching activity

of the internal and output nodes, which in turn depends on the input statistics.

As design turnaround time decreases, designers must rely on automatic optimization techniques, to speed up the design process. Low-power designs are no exception. Since power becomes increasingly important as a design evaluation metric, a new generation of computer-aided design tools targeting power minimization is urgently needed by the design community. In the last few years, significant research and development effort has been undertaken by numerous academic and commercial institutions targeting the creation of a new generation of CAD tools for low power. As a result, hundreds of papers and several books have been published on the subject.

We will focus on approaches that target the reduction of the effective capacitance C_{eff}. More precisely, we will outline optimization techniques for sequential circuits. The reasons for this decision are the following.

- When automatic power optimization techniques are applied, high-level decisions such as the choice of the supply voltage or the device technology have already been taken. Hence, we do not consider power minimization techniques based on voltage scaling, although voltage scaling is an important weapon in the early phases of the design process.

- The original contribution of this thesis is the formulation of techniques for power minimization of sequential circuits. An overview of the literature on the same topic will help the understanding of the novelty and specificity of our work. Moreover, good overviews of power minimization algorithms targeting combinational logic do exist [deva95, raba96].

In the next subsections we will review several low-power synthesis techniques that have been recently proposed. All optimization techniques discussed in this section share a common model of synchronous sequential circuit with single clock and sequential elements which sample their input value only on the raising edges of the clock

signal (*edge-triggered* flip-flops). Some of the techniques described in the following subsections can be applied to different clocking schemes, but we will assume a single clock scheme for the sake of simplicity.

1.3.1 High-level optimizations

We first consider techniques that operate at high level of abstraction, more precisely at the *behavioral level.* At the behavioral level, the gate-level structure is abstracted away, and the circuit is represented by a graph (called *control-data-flow or sequencing graph* [dmc94]) where vertices are operations and edges represent functional or control dependencies between operations. The mapping of this abstract structure to hardware is done in two steps: *scheduling* and *resource allocation.*

During scheduling, operations are assigned to the clock cycles in which they will be executed. During resource allocation the operations are mapped to actual hardware resources (such as adders, multipliers, etc.). If the result of an operation is to be used in a clock cycle following its computation, it must be stored in a sequential element (a register). *Register binding* is the part of the resource allocation step where the outputs of operations are assigned to registers. The last part of resource allocation is *steering logic generation*, where the hardware connections among units or between units and registers are created. Steering logic consists of multiplexers, decoders, encoders and data busses. A good overview of behavioral synthesis can be found in [dmc94].

There are two basic approaches to high-level power minimization. One approach attempts to minimize the *switching activity* of the circuit, because accurate estimation of the capacitance is not available at this level of abstraction. In other words, this approach attempts to minimize the average activity factor K of Equation 1.3. The second approach tries to minimize of $C_{eff} = KC_{out}$, by taking the active area into account as well. This approach relies on behavioral power estimation tools that

provide accurate information on C_{out}.

We first outline the synthesis flow followed by techniques in the first approach. To collect information about the switching activity of the initial design, the behavioral description of the design is simulated, prior to scheduling and resource allocation. Each edge of the sequencing graph is associated with a unique identifier called a *variable*. Information on the switching activity of all variables is collected. More precisely, an *activity matrix* is constructed. An element of the matrix is the average number of bit differences between a variable and all other variables.

The sequencing graph is then scheduled, usually with constraints on resource usage, latency and throughput. After scheduling, resource allocation is performed targeting the minimization of switching activity. The key idea is to assign hardware resources trying to minimize the average functional switching activity at their inputs and outputs, since it is experimentally observed that low input and output activity is accompanied by low internal power dissipation in register and data-path units. Moreover, low switching on the input and outputs implies that the capacitance associated to the steering logic is switched less frequently.

Raghunatan and Jha [ragh94] focus on allocation of data-path units to minimize their input-output switching activity, while Chang and Pedram [chan95] focus on register allocation. Mussol and Cortadella [muss95] modify the scheduling algorithm as well in order to approximatively take into account switching activity.

The reduction of the switching activity in the steering logic is targeted in the papers by Dasgupta and Karri [dasg95] and by Raghunatan et al. [ragh96a, ragh96b]. In the first paper, the authors target functional switching activity in bus-based systems: exploiting the same intuition as in the resource allocation case, they assign data transfers to the bus in a sequence that minimize the average number of transitions between values output on the bus in successive cycles. By contrast, Ragunathan et al. target the useless switching activity on the steering logic when it is not used to

communicate data required for the computation. Such switching activity is doubly harmful because it dissipates power in both the steering logic and the units connected to it.

The techniques targeting minimization of C_{eff} leverage the behavioral power estimation capability of a class of power analysis tools that has been recently developed [land96, sanm96]. The key improvement of these analysis tools with respect to behavioral simulation is that they exploit power information on data-path units, steering logic and registers that have been pre-characterized once for all in a preliminary step.

Behavioral power analysis tools are fast, therefore they can be used in the inner loop of an optimization algorithm. The basic flow of power optimization is the following. First, a scheduling and resource allocation is generated, then the analysis tool is used to estimate its power. Alternative solutions are then generated and their power consumption is estimated as well. Finally, the solution with minimum estimated power is chosen.

What differentiates the approaches in this area is the strategy used to generate alternative solutions and the behavioral power estimation tool used. Chandrakasan et al. [chan95b] propose a *transformation-based* approach. The synthesis tool operates a set of power-optimizing transformations on the original specification. Transformations that deeply modify the structure of the circuit are first applied one at a time using heuristic rules. The best resulting circuits are then memorized and become the starting points for a probabilistic algorithm that attempts to further improve power dissipation by local, low-impact transformations. The power analysis tool used to estimate the quality of the generated solutions is *pattern independent*. The power of an implementation is estimated using only information on the switching activities of the variables in the control data-flow graph (collected once for all at the beginning of the synthesis process) and the back-annotated library of hardware component used

for synthesis [land96].

In contrast, Kumar et al. [kuma95], propose an approach based on *pattern-dependent* power estimation. A fast simulation with a user-specified input pattern set is performed on a candidate solution, and the power is estimated using the switching activities and the back-annotated library of components. Notice that, differently from the approach of Chandrakasan et al., a new simulation is performed for each candidate solution. The candidate solutions are generated from a set of valid solutions that satisfy timing and area constraint using simple enumerative techniques.

Concluding this brief overview, we notice that all algorithms surveyed so far rely on transformations and optimization tools developed for traditional cost functions (power and timing), with the important difference that the quality of a solution generated by the transformations is estimated using a power-related cost measure (i.e. either K or C_{eff}).

1.3.2 Logic-level sequential optimizations

Logic-level synthesis techniques operate on a specification at a level of abstraction lower than behavioral-level synthesis. We could view logic-level synthesis as a post-optimization step on the results produced by behavioral-level synthesis. Alternatively, since many digital system are directly specified at the logic level, logic-level synthesis may be applied in a stand-alone fashion on the original specification.

Logic-level specifications describe sequential circuits as *finite-state machines* (FSMs). A finite state machine can be represented in an *abstract* or a *structural* fashion. The abstract representation of a FSM is the *state transition graph* (STG), where nodes represent states and edges state transition. The main limitation of STG representation is that its size is proportional to the number of states.

Practical sequential circuits may have billions or more states. For such circuits the STG representation is simply too large. A structural representation is then used,

called *synchronous network*. A synchronous network is a graph consisting of two kinds of nodes: combinational and sequential. Combinational nodes represent logic functions, while sequential nodes represent state elements (i.e. flip-flops). The main advantage of this representation is that the number of sequential nodes is only logarithmic in the number of states. The synchronous network representation has several disadvantages as well, since it hides many important properties of the sequential circuit that are apparent in the STG representation.

Logic-level sequential synthesis may target circuits specified by STGs or by synchronous networks. The algorithms and data structures employed are remarkably different, therefore we use the specification format as a distinguishing factor in our overview.

Algorithms for low-power state assignment target sequential circuits specified by a STG, where each state (node of the STG) is uniquely identified by a symbolic name. State assignment algorithms choose the binary codes to assign to the symbolic states so as to minimize a given cost function.

When minimum power is the target, the state codes are chosen trying to minimize the switching activity on the state variable inputs and outputs. This is because a limited switching activity of the state lines, if combined with an appropriate implementation of the combinational logic, may lead to a dramatic decrease in power of the circuit implementation.

Since state codes are binary strings that uniquely identify each state, the switching activity of the state lines reaches a minimum when all admissible state transitions require only one bit change. Notice that the theoretical minimum is often not reachable, but it can be used at (loose) lower bound to estimate the quality of a state encoding.

Numerous state encoding algorithms for low power have been proposed in the literature [roy93, olso94, hahe94, tsui94]. They differentiate among themselves mainly

by the heuristic algorithms used for choosing the state codes, but they have similar cost functions. Although the problem of minimizing the average switching activity of the state lines lends itself to a clean mathematical formulation, an important issue is the impact of state assignment on the power dissipation of the combinational logic that implements the computation of the next state and output given the present state and output. Hence, another distinctive factor for state assignment algorithm is the heuristic used to take combinational logic into account, so as to minimize the *global power* and not only the switching activity on the state lines.

We do not describe here in detail the analogies and differences among state assignment algorithms. A more complete comparative analysis will be given in Chapter 6, when the necessary formalism and background will be available.

A sequential optimization that is applied to synchronous networks is *retiming* [dmc94]. Similarly to all other techniques described so far, retiming was originally formulated to improve the performance of sequential circuits, by moving sequential elements within a synchronous network. The retiming transformation does not change the input-output behavior of the network, but it completely changes the state space. Retiming for low power has been proposed by Monteiro et al. [mont93]. The basic idea is that sequential elements can be moved to positions where their presence reduces the global C_{eff}. If the wire where the flip-flop is moved by retiming has high capacitance and large switching activity due to spurious transitions, the flip-flop will only latch the last value appearing on the wire before the clock edge, and will therefore propagate a maximum of one transition to the high capacitive load.

Obviously, retiming for power has to be constrained. The cycle time of the circuit must not increase because of retiming, and bounds on the maximum increase in the number of registers may be specified as well. The strongest objection to retiming for low power is that it is very difficult to accurately estimate the spurious switching activity in a logic circuit without layout data back-annotation and accurate (and

slow) simulation. When a flip-flop is moved, glitches disappear on its output, but other glitches may be generated because the timing of the combinational logic is changed. Consequently, it is hard to estimate not only the opportunity of a retiming move, but also its impact on the power dissipation of the final implementation.

1.3.3 Power management schemes

All power minimization strategies discussed so far leverage ideas and algorithms originally developed for traditional cost functions (timing and area). A criticisms that may be moved to these approaches is that they try to use "old weapons for a new enemy". The technique analyzed in this section is specific to the power minimization problem and rely on an important basic observation that is valid for power, but incorrect for area and timing.

While area depends on the totality of the hardware instantiated in a system and performance is controlled by the worst-case path, power depends only on the hardware that is actively switching. Thus it is neither an extensive nor an intensive quantity. For instance, the cycle time of a circuit may be set by a critical path that is exercised one time on a million. Similarly, circuits that are almost never used contribute to the total area. On the contrary, parts of the chip that have low effective switched capacitance contribute very little to the total power dissipation. Thus, it may be beneficial to insert some redundant circuitry (which increases area) if it allows to shut down large parts of the chip for a substantial fraction of the operation time.

This intuition is at the basis of a power minimization technology introduced by Alidina et al. [alid94] known as *precomputation*. Consider the sequential circuit shown in Figure 5 (a). The blocks marked with A and B represent combinational networks, while blocks $R1$ and $R2$ represents registers (i.e. banks of flip-flops). The key idea in precomputation is that some additional logic can be added to A to *pre-compute* the value of B one cycle in advance. If B can be pre-computed, we can disable register

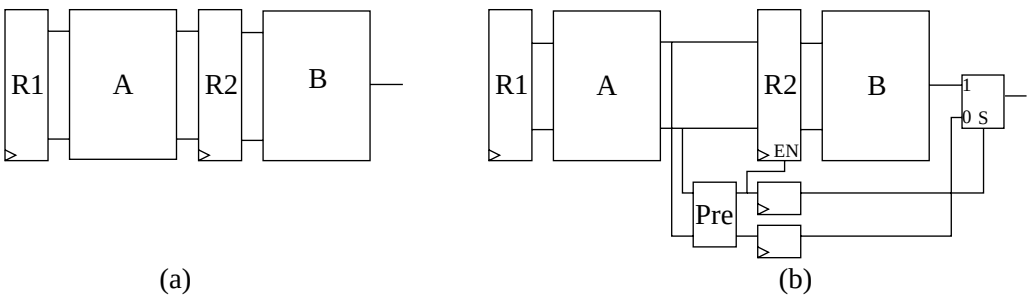

Figure 5: A precomputation architecture

$R1$ for one clock cycle and save power in B, since the inputs of B are held constant and no transition activity takes place.

Two are the main requirements for precomputation to be successful. First, we need to generate circuitry not only to recompute B, but also to recognize the conditions for which B can actually be precomputed. Second, the precomputation logic added in A should be small, otherwise the power it dissipates may swamp the power saved by stopping B. The modified circuit including precomputation logic (i.e. the block Pre) is shown in figure 5 (b). Notice that i) the precomputation logic has one additional output that is used to disable register $R1$ when B can be precomputed, ii) the precomputed output is delayed by one clock cycle and multiplexed on the output of block B. The multiplexer is controlled by the same signal used to disable $R1$ delayed by one clock cycle.

We presented here just one flavor of precomputation. The work by Alidina et al. describes several similar architectures, and discusses the details of efficiently generating precomputation logic. One important issue to be taken into account is that precomputation logic increases area and may degrade performance (if the critical path of the circuit goes through it). Hence, the technique is applicable only if it does not lead to violations of timing or area constraints.

A technique similar to precomputation, called *guarded evaluation* is applicable to combinational circuits as well. Guarded evaluation has been proposed by Tiwari et.

al [tiwa95] as a general-purpose power reduction technique. Unfortunately, guarded evaluation requires the insertion of transparent latches within combinational logic and imposes increased effort in timing verification. Moreover, the experimental results obtained by the authors seem to indicate that the power savings enabled by guarded evaluation may not fully compensate the increase in circuit complexity and analysis efforts to ensure correctness.

1.4 Thesis contribution

We focus on control-dominated application-specific integrated circuits (ASICs) synthesized starting from a high-level description in a *hardware description language* (HDL). Within the synthesis-based design flow, we propose a set of techniques for *automatically* detecting opportunities for power optimization and generating low-power implementations.

More in detail, the work presented in this thesis is an attempt to address the problem of reducing power consumption of sequential circuits using techniques targeting the distinctive characteristics of power dissipation as a cost metric. Similarly to the precomputation-based approach (which was concurrently and independently proposed), we exploit the ideas at the basis of all dynamic power management schemes illustrated in Section 1.2.4.

Our techniques are applicable in a bottom-up as well as a top-down fashion. In the top-down paradigm, we synthesize low-power implementations from a behavioral specification of the target system. In the bottom-up paradigm, we start from a logic-level structural description of the target system, and we re-optimize the original description.

Power management techniques are applied in two flavors: reduction of wasted

power and reduction of functional power. In the first case, the dynamic power dissipation of unused units is nullified by stopping their clocks. Power is saved not only by avoiding useless switching activity in the disabled logic, but also in the clock distribution network, which is probably the main single contributor to the total power dissipation. In the second case, power is saved even for units that are never idle. This result is achieved by transforming the initial specification in a functionally equivalent description whose implementation has reduced power consumption.

Power optimization is not possible without tight integration with analysis tools to steer the search for optimal solutions. A comprehensive analysis framework is developed to this purpose. Given the knowledge of input statistics, we derive the information needed to estimate i) power optimization opportunities during optimization and ii) the quality of the final results. The tight relationship between power estimation and optimization is one of the recurring themes in our treatment.

Throughout all our research work, a substantial effort has been dedicated to bridging the gap between theory and practical application. Experimental results are always provided and carefully discussed, in order to show the practical applicability of our power optimization techniques. Moreover, the importance of timing and/or area constraints is always acknowledged and taken into account, since all realistic VLSI synthesis problems involve the minimization of a cost measure subject to some kind of constraints on other metrics.

The application of the techniques presented in this thesis on several benchmark designs shows that sizable reduction of power dissipation can be achieved. For some designs, the average power consumption is reduced by more than a factor of two. It is however important to stress the fact that the quality of the results is strongly influenced by the initial specification and the input statistics.

1.5 Outline of the following chapters

In the first part of this thesis, we target wasted power dissipation by stopping the clock when the system is idle (a clock that can be conditionally disabled is called *gated clock*). In the second part, we propose two techniques, namely *decomposition* and *state encoding*, to reduce the power of a system even when it is performing useful computation.

In Chapters 3 and 4, we propose a set of techniques for *automatically* detecting clock-gating opportunities and generating clock-gating circuitry. The pattern-dependent nature of power dissipation is taken into account in our methodology and our algorithms automatically detect the most likely input conditions for clock gating. We develop an analysis framework to direct the synthesis tool towards the generation of optimal clock control logic that dissipates minimum power, has minimum area and performance overhead and stops the clock with maximum efficiency. Heuristic and exact algorithms are developed to accomplish the synthesis task. In Chapter 3 we follow a top-down paradigm and we target sequential circuits of small and medium size, while in Chapter 4 we describe a bottom-up methodology that is suitable for much larger sequential circuits.

A decomposition approach is proposed in Chapter 5, where a behavioral specification of a sequential circuit is decomposed in several smaller, interacting components. The circuit is then synthesized using an implementation style in which only one component at a time is performing useful computation, while all other components are shut down. The decomposition approach reduces the power dissipation even for systems that are *never* idle, since only a small part of the system is active at any given time. Algorithms are developed to direct the search for optimal decompositions which have minimum interface cost and maximum locality of computation.

In Chapter 6 we formulate state encoding algorithms that reduce the power dissipation of flip-flops in the implementation of controllers specified as finite state machines. We propose exact and heuristic solutions for the minimization of the average transition activity on the state lines. Additionally, we heuristically take into account the impact of state encoding on the complexity of the combinational logic of the state machine. Thus, we produce encodings that reduce the power dissipation due to the activity on the state lines and, at the same time, keep the area an power dissipation of the combinational logic under control.

Finally, Chapter 7 contains a summary of the theoretical and experimental results obtained in this thesis and a discussion of future direction of research and development.

Chapter 2

Background

The main purpose of this chapter is to provide the necessary background for the ideas and algorithms presented in the following chapters. In the first section we define the basic concepts of Boolean algebra and of finite state machines with binary inputs and outputs. This material is prerequisite for all following sections.

In the second section, we delve into the algorithms and data structures that allow the manipulation of large Boolean functions and finite state machines. We will then extend our treatment to similar structures and algorithms for dealing with a generalization of Boolean functions known as discrete functions.

Finally, in the third section we will describe the analysis techniques that allow the accurate estimation of the power-related cost functions used in our algorithms. The theory of finite Markov chains will be briefly introduced and algorithms for dealing with small and large-size Markov chains will be described.

2.1 Boolean algebra and finite state machines

The following treatment is by no means complete. The reader is referred to the many books on Boolean algebra and sequential machines published in the last few decades

(see, for example [koha70, davi78, brow90]). We adopt the formalism and terminology used by De Micheli [dmc94]. We will use boldface fonts for vectors and matrices.

2.1.1 Boolean algebra

A *binary Boolean algebra* is defined by the set $B = \{0, 1\}$ and the operations *disjunction* and *conjunction* which are represented by the symbols $+$, $\cdot$, respectively. Disjunction is often called *sum* or OR, while conjunction is called *product* or AND. We will use these terms interchangeably.

The multi-dimensional space spanned by n binary-valued variables is denoted by B^n. A point in B^n is a binary-valued vector of dimension n. Every variable is associated with a dimension of the Boolean space and is called *Boolean variable*. In addition, any Boolean variable a with values in B has a *complement*, denoted by a', such that $a + a' = 1$, $a \cdot a' = 0$. A *literal* is an instance of a variable or its complement. For convenience, we define the *exclusive or* (XOR) operation, denoted by the symbol $\oplus$, as $a \oplus b = ab' + a'b$.

A *completely specified* Boolean function is a mapping between Boolean spaces: $f : B^n \rightarrow B^m$. An *incompletely specified* Boolean function is defined over a subset of B^n. The points where the function is not defined are called *don't care* conditions. For the sake of compactness, incompletely specified functions can be represented as $f : B^n \rightarrow \{0, 1, -\}^m$, where the symbol "$-$" denotes a *don't care* condition. For each output, the subset of the domain for which the function assumes values 1, 0 and $-$ are respectively called *on set*, *off set* and *don't care set*.

In order to simplify the following treatment, we restrict ourselves to *single-output Boolean functions*, i.e. $f : B^n \rightarrow B$. Generic (*multiple output*) Boolean functions can be represented as arrays of single-output Boolean functions $\mathbf{f} = (f_1, f_2, ..., f_m)$. We also define two special Boolean functions: i) $\mathbf{1} : B^n \rightarrow \{1\}$ (also known as *tautology*) and ii) $\mathbf{0} : B^n \rightarrow \{0\}$ (the *null function*). Tautology maps all points in B^n to the

point 1 in B. The null function maps all points in B^n to the point 0.

Let $f(x_1, x_2, ..., x_n)$ be a Boolean function of n variables. We call the set $\{x_1, x_2, ..., x_n\}$ the *support* of the function. We now give some definitions that will be extensively used.

Definition 2.1 *The positive cofactor of* $f(x_1, x_2, ..., x_n)$ *with respect to variable* x_i *is*

$$f_{x_i} = f(x_1, x_2, ..., x_{i-1}, 1, x_{i+1}, ..., x_n).$$

The negative cofactor is

$$f_{x_i'} = f(x_1, x_2, ..., x_{i-1}, 0, x_{i+1}, ..., x_n).$$

In words, a cofactor of a Boolean function w.r.t x_i is the restriction of the function to the semi-space where variable x_i has a fixed value. Hence, the support of the cofactor does not contain x_i, because f_{x_i}, $f_{x_j'}$ do not depend on x_i. The definition of cofactor allow us to define three important operators of Boolean algebra, namely Boolean difference (Boolean derivative), consensus (universal quantifier) and smoothing (existential quantifier).

Definition 2.2 *The Boolean difference of* $f(x_1, x_2, ..., x_n)$ *with respect to variable* x_i *is* $\partial f/\partial x_i = f_{x_i} \oplus f_{x_i'}$.

The Boolean difference represents the sensitivity of the value of f to the value of x_i, in other words, $\partial f/\partial x_i = 1$ for all values of input variables (different from x_i) for which a value change on x_i causes a value change of f.

Definition 2.3 *The consensus of* $f(x_1, x_2, ..., x_n)$ *with respect to variable* x_i *is* $\forall_{x_i} f = f_{x_i} \cdot f_{x_i'}$

The consensus is a fundamental operator in Boolean algebra and will be often used in this thesis. It represents the component of f whose value is independent of x_i. In other words, $\forall_{x_i} f = 1$ for all values of input variables (different from x_i) for which $f = 1$ no matter what is the value of x_i. We will often call consensus the *universal quantifier* with respect to x_i, because it represents conditions that make $f = 1$ for all values of x_i

Definition 2.4 *The smoothing of* $f(x_1, x_2, ..., x_n)$ *with respect to variable* x_i *is* $\exists_{x_i} f = f_{x_i} + f_{x_i'}$.

The smoothing is the dual of the consensus: $\exists_{x_i} f = 0$ for all values of input variable (different from x_i) for which $f = 0$ no matter what the value of x_i is. The smoothing is often called *existential quantifier.*

The *greater or equal* relation between two Boolean functions $f \geq g$ holds if and only if $f \cdot g' = \mathbf{1}$. An equivalent notation is $g \Rightarrow f$. The definition given so far will be clarified through an example.

Example 2.1.1. Consider the Boolean function $f(a, b, c) = ab + b'c + a'b'c'$. The positive cofactor w.r.t c is $f_c = f(a, b, 1) = ab + b'1 + a'b'0 = ab + b'$. The negative cofactor is $f_{c'} = f(a, b, 0) = ab + b'0 + a'b'1 = ab + a'b'$. The partial derivative is $\partial f/\partial c = f_c \oplus f_c' = (ab + b') \oplus (ab + a'b') = ab'$ The universal quantifier is $\forall_c f = f_c f_c' = (ab + b') \cdot (ab + a'b') = ab + a'b'$. Finally, the existential quantifier is $\exists_c f = f_c + f_c' = (ab + b') + (ab + a'b') = ab + b'$. Notice that all operations involving cofactors reduce the support of the function by eliminating the variable with respect to which the cofactors are taken. As an example of $\geq$ relation, observe that $\exists_c f \geq \forall_c f$ (this is actually true for any Boolean function f). □

Boolean functions can be represented as sets (there is an isomorphism between set algebra and binary Boolean algebra). We will sometimes adopt the set representation, because it helps clarifying some concepts. A *minterm* is a point in the n-dimensional Boolean domain of a Boolean function where the function has value 1. Thus, a

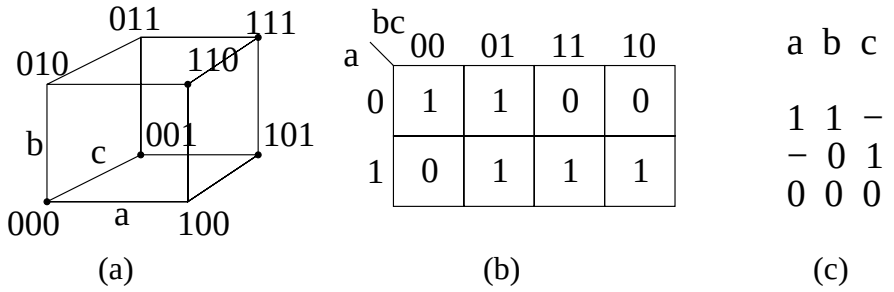

Figure 6: Pictorial representations of a Boolean Function

completely specified Boolean function can be represented by the set of its minterms (i.e. *on set*). An incompletely specified Boolean function is defined by two sets (either *on set* and *off set*, or *on set* and *don't care set*, or *off set* and *don't care set*).

Any Boolean function can be represented as a *sum of products* (SOP) of literals, or as a *product of sums* of literals. A product of literals is often called a *cube*. One particular *sum of product* representation is the *minterm canonical form*, where each product has n literals. Each product in the minterm canonical form is a minterm of the function. This representation is unique for any given function.

Example 2.1.2. Refer to function f of Example 1. $f = ab + b'c + a'b'c'$ is a sum of product representation, but so is $f = abc + abc' + b'c + a'b'c'$. Hence, there are many SOP representations for a single Boolean function. The minterm canonical form of f is: $f = abc + abc' + ab'c + a'b'c + a'b'c'$. The function has five minterms. Figure 6 shows three equivalent graphical representations of f. In Figure 6 (a), the three-dimensional cube represents B^3 and the darkened vertices are the *on set* of f. In Figure 6 (b), the Karnaugh map of the function is shown [mccl86]. Finally, Figure 6 (c) shows the representation of the function as a list of cubes: the ones, represent positive literals, the zeros negative literals and the "$-$" literals that do not appear in the product. For instance, $ab' \rightarrow 10-$ and $ab'c' \rightarrow 100$. □

Several important definitions and concepts are related to the SOP representation of Boolean functions.

Definition 2.5 *An implicant of a Boolean function f is a product of literals such that $f \geq p$.*

Any product in a SOP representation is obviously an implicant of f. Particular relevance has the concept of *prime implicant.*

Definition 2.6 *A prime implicant of f is an implicant of f is not contained in any other implicant.*

To better understand the definition, notice that a product in a SOP represents a set of minterms. If we drop a literal from a product we *expand* the product (i.e. we increase the number of minterms it contains by a factor of 2). A prime implicant is a product that cannot be expanded. If we expand a prime implicant, some of its minterm will not be contained in the *on set* of f. Thus, the product is not an implicant any more.

Definition 2.7 *A cover of a Boolean function is a set (list) of implicants that covers all its minterms*

Any SOP representation of a Boolean function is a cover. A *minimum* cover is a cover of minimum cardinality. The concept of minimum cover is important because there is correlation between the number of implicants in a cover of a function (and the number of literals in a cover) and the area of the hardware implementation of the function [dmc94, mccl86]. Numerous algorithms for the minimization of covers have been developed in the recent past (the book by De Micheli [dmc94] contains a good overview). All these algorithms are based on a the following theorem:

Theorem 2.1 [*Quine theorem*]. *There is a minimum cover that is prime.*

The most important implication of this theorem is that it defines the search space where a minimum cover can be found. If we restrict our search to covers formed by prime implicants only, we are guaranteed to find a minimum cover. Although the number of prime implicants can be exponential in the number of inputs of a Boolean

function, several efficient algorithms for SOP minimization based on Quine theorem have been developed and successfully applied in industrial-strength CAD tools.

Boolean algebra provides a convenient framework for reasoning about properties of digital circuits. In particular, the steady-state input-output behavior of a feedback-free digital circuits (a.k.a. combinational circuits) can be modeled by a multi-output Boolean function. Large combinational circuits are often better described in a *structural* fashion by *logic networks* (also called *combinational networks*). A logic network is an interconnection of *modules*, representing input/output ports, logic gates or single-output logic functions. The logic network can be represented as a directed acyclic graph (DAG), with vertices corresponding to the modules and edges corresponding to two-terminal nets to which the original module interconnects are reduced.

Notice that a circuit behavior (i.e. a multiple output Boolean function) can be mapped to many equivalent structures. The lack of uniqueness is the main limitation of the the structural description. Given two circuit descriptions, checking their equivalence is not an easy task. On the other hand, there are Boolean function for which all known abstract descriptions have unmanageable size. For such functions, a structural representation is the only viable alternative. Moreover, structural descriptions are conceptually closer to the physical implementation, and are widely used for simulation and performance analysis.

2.1.2 Finite state machines

We formally define a finite state machine with binary inputs and outputs as a 6-tuple $(X, Z, S, s^0, \delta, \lambda)$, where $X = B^n$ is the input space, $Z = B^m$ the output space, S is a finite set of states, s^0 is the initial (reset) state, $\delta(x, s) : X \times S \rightarrow S$ is the next state function and $\lambda(x, s) : X \times S \rightarrow Z$ is the output function. FSMs are categorized in two classes [hart66, henn68, koha70]:

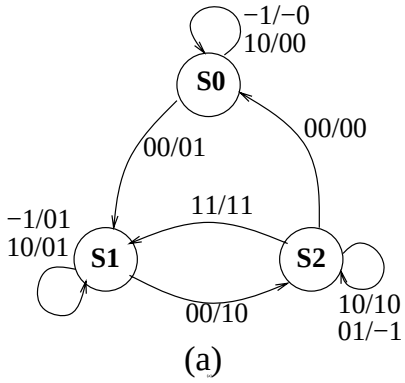

PS	In	NS	O
S0	−1	S0	−0
S0	10	S0	00
S0	00	S1	01
S1	−1	S1	01
S1	10	S1	01
S1	00	S2	10
S2	10	S2	10
S2	01	S2	−1
S2	11	S1	11
S2	00	S0	00

(b)

Figure 7: State transition graph and state table of a FSM

Definition 2.8 *A Moore machine is a FSM where* $\lambda(x, s) = \lambda(\cdot, s)$*, i.e. the outputs do not depend directly on the input value, but the depend only on the state. A Mealy machine is a FSM for which this property does not hold.*

Finite-state machines can be *incompletely specified*. An incompletely specified FSM is one where $\delta(x, s)$ and/or $\lambda(x, s)$ are incompletely specified Boolean functions. Notice that in the definition of FSM, the state set S is not defined as a Boolean space. In other words, the states are elements of a generic set, and they are uniquely identified by a symbol (a string or any other unique identifier). A FSM can be represented by a graph or, equivalently by a table. The two representations ale called *state transition graph* (STG) and *state transition table* (or state table, for brevity), respectively. The states of the STG are labeled with the unique symbolic state name, the edges are labeled with the inputs and output values. The state table is simply the list of edges of the STG. An example will better illustrate these definitions.

Example 2.1.3. Consider the FSM in Figure 7 (a), (b). Part (a) shows the STG of the FSM, while Part (b) shows the state table. The notation used in the STG for edge labeling is that the inputs are followed by the outputs. Each edge in the STG correspond to an entry in the state table. The fist two fields in the state table are respectively present state and input. The last two fields are next state and output. The FSM of Figure 7 is incompletely specified, because for present state S2 and input 01 the first output is not specified (i.e. it can be

either one or zero). The output is incompletely specified for the first transition in the table as well. □

Notice that both STG and state table completely define the input-output behavior of a FSM, but they do not provide any information about the circuit implementation. Hence, STG and state table are *behavioral* representations of the FSM. In order to obtain a representation which is closer the the circuit implementation, we need to introduce the concept of *state-encoding.*

Definition 2.9 *A state encoding is a one-to-one mapping from S to B^{N_s}, a function $E : S \rightarrow B^{N_s}$. N_s is the number of state variables.*

By specifying the state encoding function E, we associate each symbolic state to a particular binary vector of N_s elements, i.e. to a vertex in the N_s-dimensional Boolean space. The vertex is called *state code.* Notice that we have numerous degrees of freedom in the choice if E. The only important constraint for E is that B^{N_s} has enough vertices to assign a different one to each symbolic state, thus $N_s \geq \lceil log_2|S| \rceil$. Once we have specified N_s and E, the state of a FSM is completely expressed by N_s binary variables called state variables.

If we specify E, the output and next state functions become Boolean functions: $\delta(x, v) : B^n \times B^{N_s} \rightarrow B^{N_s}$, $\lambda(x, v) : B^n \times B^{N_s} \rightarrow B^m$, where $v = E(s)$. If the number of elements in B^{N_s} is larger than $|S|$, both $\delta(x, v)$ and $\lambda(x, v)$ become incompletely specified, since their value is not relevant for values of v that do not correspond to any valid state. For the sake of brevity, we will often use the notation $\delta(x, s)$ and $\lambda(x, s)$ even for FSM where E has been specified, with the convention that s is the state code of the symbolic state.

Once the state encoding has been specified, the structural model of FSM shown in Figure 8 can be used to represent the FSM. A (combinational) logic network implements δ and λ, while state elements (flip-flops) store the value of one state

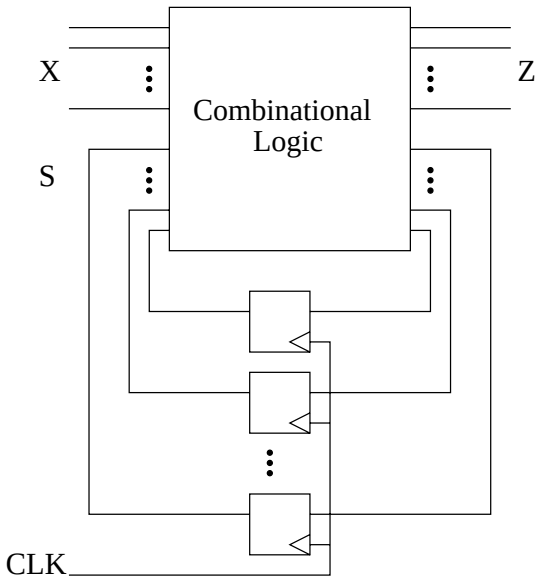

Figure 8: Structural representation of a FSM

variable. The structural model is called *sequential* or *synchronous* network. We assume that the flip-flops are triggered on the raising edge of the clock CLK (the triangular shape within each flip-flop symbol identifies the flip-flops as positive-edge-triggered). Numerous types of sequential elements and clocking styles can be used to implement real-life circuits, but it is useful to reason about a single implementation model.

The representation of Figure 8 is *structural*, because it refers to a particular circuit structure implementing the FSM. Notice that there are infinite structural representations for a single STG (they can be generated by changing N_s and E). The main reason why structural representations are useful even when developing algorithm or studying properties of FSMs is that they may be much more compact than the state-based representations.

Example 2.1.4. Consider a FSM with ten millions of states. If we represent each symbolic state with a string of characters from an alphabet with 32 symbols, we need at least 4 characters (minimum length identifiers) for each state. We want to estimate the memory needed to store the behavioral representation

of the FSM. Only storing the names of the states requires $10^6 * 4 * 5/8 \approx 25Mb$. In contrast, the minimum number of state variables needed to uniquely represent all states is $N_s = \lceil log_2 10^7 \rceil = 21$. Just 21 flip-flops are sufficient for encoding the 10^7 states. In other words, the STG of a relatively small sequential circuit with 21 flip-flops may already be unmanageably large. □

Although it is often convenient to reason about small-size sequential system using behavioral representations, structural representations are the only viable alternative for large sequential systems. Similarly to the case of combinational network, the main limitation of the sequential network representation is its lack of uniqueness. Additionally, checking the equivalence of two sequential networks is at least as hard as checking the equivalence of their combinational part.

2.1.3 Discrete functions

We have introduced the concept of Boolean functions and we showed how FSMs can be represented by Boolean functions. We now present a simple extension of Boolean functions.

Definition 2.10 *A discrete function $f : B^n \rightarrow V$ is a mapping from a Boolean space to a finite set V.*

Discrete functions encompass Boolean functions as a particular case. When $V = B = \{1, 0\}$, a discrete function is Boolean. Notice however that discrete functions are not more expressive than Boolean functions: since set V is finite, we can "encode" it with $N_e = \lceil log_2 |V| \rceil$ binary variable. Thus a generic discrete function f can be represented by a multi-output Boolean function and an encoding function. Despite this fact, discrete functions are an useful abstraction that will be employed in the development of algorithms for power minimization.

2.2 Implicit representation of discrete functions

Digital circuits may have unmanageably large abstract representations. The reason is that both Boolean functions and FSMs can be represented in tabular format, but the size of the tables is worst-case exponential in the number of inputs (and states, in the case of FSMs). One approach that mitigates this problem is to resort to structural representations. The main limit of structural representations is that they are not unique. A Boolean function can be represented by an infinite number of combinational networks, and a FSM can be represented by infinite sequential networks. Hence, it is hard to develop algorithms based on the properties of a Boolean function or a FSM when starting from a structural representation.

In this section we will describe a powerful data structure that allows the representation of Boolean functions and state machines in a canonical fashion (i.e. with a unique representation) which has in many cases manageable size, even when the tabular representation is excessively large.

2.2.1 Binary decision diagrams

Binary decision diagrams (BDDs) are a data structure developed for the compact representation of large Boolean functions. Several variants of BDDs have been developed by different groups of researchers (see, for instance, [brya86, brac90, madr88, mina90]). The differences are generally small. In our description we will follow [brya86] and [brac90], though with slightly different notation. We introduce the keys concept of the BDD representation by means of a simple example

Example 2.2.5.
Let us consider the following Boolean function:

$$f = abc + b'd + c'd.$$

A BDD for this function is given in Figure 9.

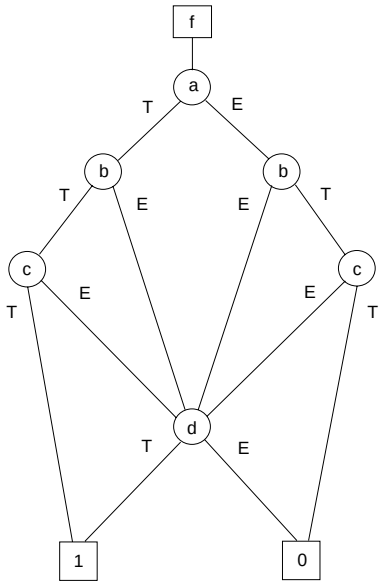

Figure 9: A Binary Decision Diagram.

If we want to know the value of f for a particular assignment to the variables a, b, c, and d, we just follow the corresponding path from the square box labeled f (this node is the *root* of the BDD) to one of the square boxes labeled 1 and 0 (these nodes are the *leaves* of the BDD). Suppose we want to determine the value of function f for the assignment $a = 1$, $b = 0$, $c = 1$, and $d = 0$. The first variable encountered from the root is a, whose value is 1. We then follow the arc labeled T (which stands for *then*). We then come across a node labeled b. Since the value of b is 0, we follow the arc labeled E (*else*). The next node is labeled d, which implies that for $a = 1$ and $b = 0$, the value of f does not depend on c. Following the E arc we finally reach the *leaf* labeled 0. This tells us that the value of the function is 0, as can be easily verified from the sum of products formula.

The BDD of Figure 9 is an *ordered* binary decision diagram, because the variables appear in the same order along all paths from the root to the leaves. The ordering in this case is

$$a \leq b \leq c \leq d.$$

The appearance and the size of the BDD depend on the variable ordering. This is illustrated in Figure 10, where a different BDD for f is given according to the following variable ordering:

$$b \leq c \leq a \leq d,$$

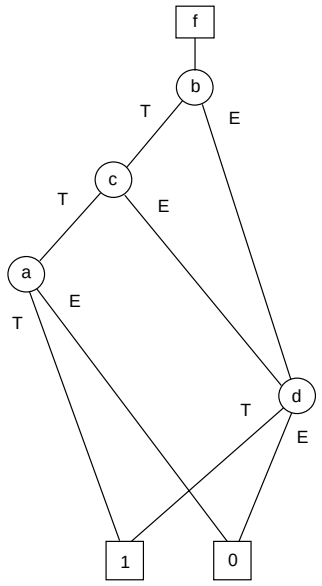

Figure 10: An Optimal BDD.

This is an optimal ordering, since there is exactly one node for each variable. We will assume that BDDs are ordered. □

The BDD of f constructed as shown in the example may not be reduced, that is, it may contain duplicated and superfluous nodes. However, a non-reduced BDD can be systematically transformed into a reduced one by iteratively applying:

- Identification of isomorphic sub-graphs;
- Removal of redundant nodes.

Given an ordering, the reduced graph for a function is unique. Hence, the Reduced Ordered BDD (ROBDD) is a canonical form, that is, two functions f_1 and f_2 are equivalent (i.e., $f_1 = f_2$) if and only if they have the same BDD. This is the first important characteristics of binary decision diagrams. Other interesting properties of BDDs are:

- The size of the BDD (the number of nodes) is exponential in the number of variables in the worst case; however, BDDs are well-behaved for many functions

that are not amenable to tabular representations (e.g., EXCLUSIVE-OR).

- The logical AND and OR of BDDs have the same complexity (polynomial in the size of the operands). Complementation is inexpensive (constant time).

- Both satisfiability (i.e. proving that a Boolean function has at least one satisfying assignment) and tautology (i.e. proving that a Boolean function is always **1**) can be solved in constant time. Indeed, f if satisfiable if and only if its BDD is not the terminal node 0, it is a tautology if and only if its BDD consists of the terminal node 1.

On the other side, BDDs have some drawbacks:

- BDD sizes depend on the ordering. Finding a good ordering is not always simple.

- There are functions for which the sum of products or product of sums representations are more compact than the BDDs.

- In some cases sum of products/product of sums forms are closer to the final implementation of a circuit. For instance, if we want to implement a PLA, we need to generate at some point a sum of products or product of sums form.

BDDs allow to compactly store and manipulated multiple Boolean function, since it is possible to share nodes in the BDD representations of two or more Boolean functions. As a limit case, notice that two equivalent functions fully share all nodes, i.e. they are represented by the same BDD (not just two identical BDDs).

Given that we are interested in reduced BDDs, instead of generating non-reduced BDDs and then reducing them, we guarantee that, at any time, there are no isomorphic sub-graphs and no redundant nodes in the multi-rooted DAG. This can be achieved by checking for the existence of a node representing the function we want to

add, prior to the creation of a new node. A straightforward approach would consist of searching the whole DAG every time we want to insert a new node. However, that would be far too inefficient. Instead, a hash table called *unique table* is created. The unique table contains all functions represented in the DAG. In other words, the table has one unique entry for each node.

BDDs are manipulated with recursive algorithms based on the *cofactor expansion* of Boolean functions f with respect to a variable:

$$f = x_i \cdot f_{x_i} + x_i' f_{x_i'}. \tag{2.9}$$

The usefulness of Equation 2.9 lies in the fact that after cofactor expansions, the two cofactors f_{x_i} and $f_{x_i'}$ are simpler functions. All Boolean operations defined in Section 2.1 can be efficiently carried out on the BDDs representing the functions on which they apply. The complexity of the computations is polynomial in the number of BDD nodes of the functions (more precisely, linear in the product of the number of BDD nodes of each operand).

BDD manipulation packages keep a cache of recently computed functions, called *computed table*, for efficiency reasons. The purpose of this table is different from that of the unique table. With the unique table we answer questions like: "Does there exist a node labeled v with children g and h?" On the other hand, the computed table answers questions like: "Did we recently compute the AND of f_1 and f_2?" We can ask this question before we actually know that the AND of f_1 and f_2 is a function whose top node is labeled v and whose children are g and h. Hence we can avoid recomputing the result.

2.2.2 Algebraic decision diagrams

Since discrete functions are a straightforward extension of Boolean functions, the intuition suggests that data structures similar to BDDs could be used to efficiently

manipulate them. Indeed, several "BDD-like" data structures have been developed to this purpose [clar93, lai94, baha95]. The one we adopt is the algebraic decision diagram (ADD) [baha95]. We do not describe the definition and the properties of ADDs since they are analogous the the ones we illustrated for BDDs: reduced and ordered ADDs are a canonical representation of discrete functions and all important operations with ADDs can be performed in polynomial time in the ADD size.

The main difference between BDDs and ADDs is in the terminal nodes. While all BDDs terminate in either the "0" or the "1" terminal nodes, ADDs have multiple terminal nodes. The terminal nodes (leaves) of an ADD are associated with the values of the discrete function it represents. Since operators on discrete functions are generalizations of Boolean operators, the ADD algorithms that implement such operators are very similar to the procedures used for BDDs. We review three important operators on ADDs that will be used in later chapters: ITE, APPLY, and ABSTRACT.

ITE takes three arguments: f, an ADD restricted to have only 0 or 1 as terminal values (called "0/1-ADD", and fully equivalent to a BDD), and g and h, generic ADDs. It is defined by:

$$\mathrm{ITE}(f, g, h) = f \cdot g + f' \cdot h \tag{2.10}$$

Intuitively, the resulting ADD has the same leaves as g when f is 1 and the leaves of h when f is zero.

APPLY takes one operator, *op* (e.g., $+$, $-$, $\times$), and two operand ADDs as arguments; it applies *op* to all corresponding elements of the two operands and returns the resulting ADD. Notice that APPLY generalizes the Boolean operators. For example, the APPLY of $*$ (multiplication) to two 0/1-ADDs degenerates to the Boolean AND operator.

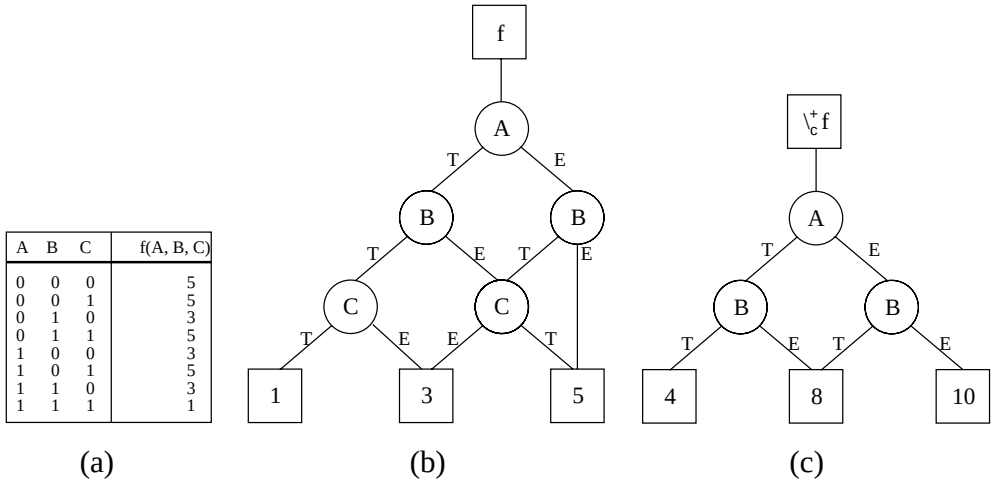

Figure 11: (a)-(b) A discrete function f and its ADD. (c) The ABSTRACT of f w.r.t c, $\setminus_c^+ f$.

ABSTRACT reduces the dimensionality of its argument function through existential arithmetic abstraction of some variables. Let x, y be the support of a pseudo-Boolean function $f(x, y)$, where x and y be two disjoint sub-sets of Boolean variables. The arithmetic existential abstraction of x from $f(x, y)$ with respect to the arithmetic sum is defined as:

$$\setminus_x^+ f(x, y) = \sum_x f(x, y). \tag{2.11}$$

This definition tells that, instead of taking the Boolean sum of all the the cofactors associated with the minterms of the x-variables, as in Boolean existential abstraction, the ABSTRACT operator computes precisely the arithmetic sum. Notice that the ABSTRACT operator eliminates x from the support (i.e $\setminus_x^+ f(x, y) = g(y)$). Similarly, the arithmetic existential abstraction of x with respect to the MAX operator is defined as:

$$\setminus_x^{MAX} f(u) = \max_x f(u). \tag{2.12}$$

Example 2.2.6. A discrete function f is given in tabular form in Figure 11 (a). The ADD of the function is shown in Figure 11 (b), with the

variable order $a \leq b \leq c$. The arithmetic existential abstraction of f with respect to variable c is shown in Figure 11 (c). As expected, $\backslash_c^+ f$ does not depend on c any more. □

2.3 Markov analysis of finite state machines

Power is a strongly pattern-dependent cost function, since it depends on the switching activity of a circuit, which in turn depends on the input patterns applied to the circuit. Hence, we need to specify some information about the typical input patterns applied to a circuit if we want to optimize or even only estimate its power dissipation. The most straightforward way to provide information about input patterns is to actually provide a long input stream representing a typical usage pattern together with the specification of the circuit.

This approach gives the most complete information, but it suffers from two serious drawbacks i) the input traces can be very large and cumbersome to manage, ii) in many cases only incomplete information about the environment may be available. A more synthetic description of the input streams can be provided by providing information about *input probabilities*. Given a sequential circuit, we may simply provide one real number for each input: the probability for the input to be one. This statistical parameter is called *signal probability*.

Obviously, signal probabilities express much less information than a complete input trace, for example they do not give any indication about correlation between successive input values (called *temporal correlations*) or between different inputs (called *spatial correlations*). Nevertheless, input probabilities are often used to synthetically describe the statistics of the input patterns.

Even if we assume that the input patterns can be described by signal probabilities with sufficient accuracy (i.e. spatio-temporal correlations are a second-order effect), it is not obvious how to estimate, in a FSM, the probability of a state transition, since

it depends not only on the inputs, but also on the state information. For example, if an FSM has a transition from state s_i to state s_j for all possible input configurations, we may think that this transition will happen with very high probability during the operation of the machine. This may not be the case: if state s_i is unreachable, the machine will **never** perform the transition, because it will never be in state s_i. Similarly, if the probability of being in state s_i is very low, a transition from state s_i to state s_j is very unlikely.

We model the stochastic behavior or a FSM by a Markov chain. A Markov chain is a representation of a finite state *Markov process* [triv82], a stochastic model where the transition probability distributions at any time depend only on the present state and not on how the process arrived in that state. The Markov chain model for the STG is a directed graph isomorphic to the STG and with weighted edges. For a transition from state s_i to state s_j, the weight $p_{i,j}$ on the corresponding edge represents the *conditional probability* of the transition (i.e., the probability of a transition to state s_j *given* that the machine was in state s_i). Symbolically this can be expressed as:

$$p_{i,j} = Prob(Next = s_j | Present = s_i) \tag{2.13}$$

Note that edges with zero conditional probability are never drawn in the graph representation of the Markov chain.

Definition 2.11 *The conditional probability distribution is the set of $p_{i,j}$ values.*

The conditional probability distribution is external input information. It does not depend on the structure of the Markov chain and we assume that it is known. Although conditional transition probabilities can be used as a rough approximation to the transition probabilities [roy93], we need to know the probability of a transition independent of the present state. These probabilities are called *total transition probabilities*, $P_{i,j}$, and can be calculated [triv82] from the *state probabilities*, where the

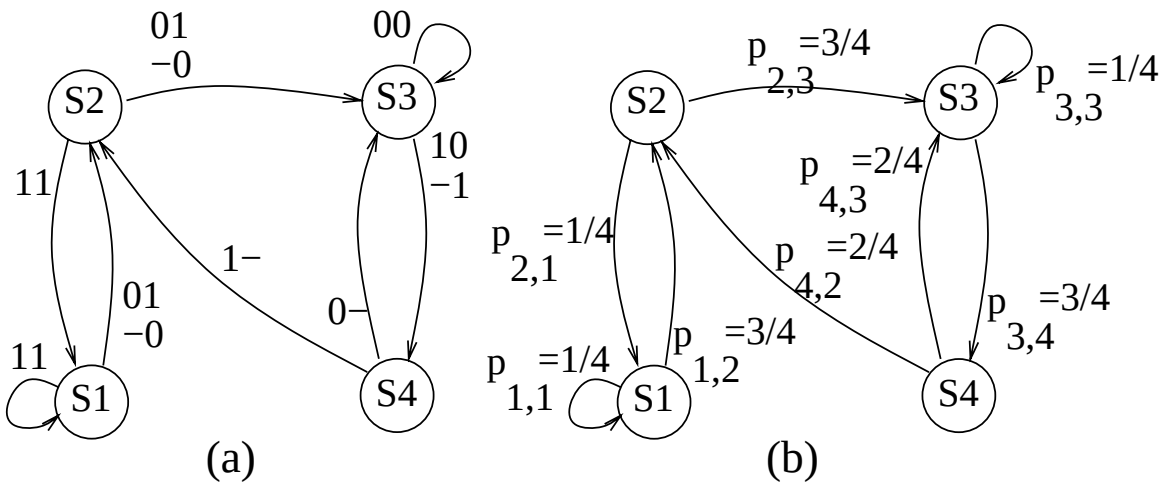

Figure 12: (a) A finite state machine (b) its Markov chain model

state probability, P_i, represents the probability that the machine is in a given state i.

$$P_{i,j} = p_{i,j} P_i \tag{2.14}$$

Equation 2.14 implies that, in order to have high total transition probability *both* the state probability *and* the conditional transition probability must be high. Using only the conditional transition probability can lead to incorrect estimates.

Example 2.3.7. Consider the FSM shown in Figure 12 (a) with two inputs, in_1 and in_2, and one output. Assume that the input probabilities are $Prob(in_1 = 1) = .5$ and $Prob(in_2 = 1) = .5$. The Markov chain model of the FSM is shown in Figure 12 (b). The edges of the Markov chain are labeled with the conditional transition probabilities of the patterns on the edges of the FSM. For instance, consider the transition between S2 and S1. Its conditional probability is $p_{2,1} = Prob(in_1 = 1) \cdot Prob(in_2 = 1) = .24 = 1/4$. Observe that the conditional transition probabilities are computed using only the input probability information, and they are generally different from the total transition probabilities. □

The next step is to show that it is possible to compute the state probabilities and, more importantly, to show that these values are not time-dependent. Intuitively, this implies that as the observation time increases, the probability that the machine is in

each of its states converges to a constant (stationary) set of real numbers. In other words, we must show that it is possible to compute a *steady state (or stationary) probability vector* whose elements are the stationary state probabilities.

It is quite easy to find STGs for which the stationary state probabilities do not exist, because, for example, their value is oscillatory. The general theory explaining the asymptotic behavior of the state probabilities is too involved to be described here, but it can be found in reference [triv82]. Here we just state an an important theorem that allows us define a large class of STGs whose corresponding Markov chains have a steady state probability vector.

Theorem 2.2 *For an irreducible, aperiodic Markov chain, with all states recurrent non-null, the steady state probability vector exists and it is unique*

An *irreducible Markov chain with all the states recurrent non null* is a chain where every state can be reached from any other state, and the greatest common divisor of the length of the possible closed paths from every state is one. For the sake of simplicity, we assume in the following that we deal only with FSMs for which the corresponding Markov chain satisfies all requirements of Theorem 2.2 for existence and uniqueness of the state probability vector. We will prove in a later chapter that the presence of a unique reset state is sufficient to ensure the existence of the steady state probability vector. Notice however that state probabilities can be computed in much more relaxed assumptions than those of Theorem 2.2 even for FSMs without a unique reset state [hama94].

In the next subsections we describe the basic methods for computation of the state probability vector i) for small-size FSMs that can be described in a behavioral style, ii) for large FSMs described in a structural fashion.

2.3.1 Explicit methods

The methods for computation of the state probability vector presented in this subsection are called *explicit* because they are based on the direct representation of the conditional transition probabilities with a matrix of size $|S| \times |S|$. Let $\mathbf{P}$ be the conditional transition probability matrix whose entries $p_{i,j}$ are the conditional transition probabilities, and $\mathbf{q}$ the steady state probability vector whose components are the state probabilities P_i (i.e $\mathbf{q} = [P_1, P_2, ..., P_{|S|}]^T$). Then we can compute the steady state probabilities by solving the $(n_s + 1)$ system of equations:

$$\mathbf{q}^T \mathbf{P} = \mathbf{q}^T \tag{2.15}$$

$$\sum_{i=1}^{n_s} P_i = 1 \tag{2.16}$$

The problem of finding the steady state probability vector is thus reduced to finding the left eigenvector of the transition matrix corresponding to the unit eigenvalue, and normalizing it in order to make the sum of its elements equal to unity [triv82]. The normalization condition (Equation 2.16) is required because matrix $\mathbf{P}$ is singular (since all its columns sum to one), and the Equation 2.15 has infinite solutions. The only valid solution is found by imposing that the sum of all the components of $\mathbf{q}$ is one, because the elements of $\mathbf{q}$ are probabilities of mutually exclusive events that cover the complete event space (i.e. the Markov chain is always in one and only one of its states).

Example 2.3.8. For the Markov chain of Example 7, the stationary state probabilities calculated solving Equation 2.15 are shown in Figure 13 besides the nodes in the chain. Obviously, the state probabilities sum to one, as enforced by the normalization condition. The figure shows also the total transition probabilities (the products $p_{i,j} \cdot P_j$) on the edges. Notice that the total transition probabilities are completely different from the conditional transition probabilities: while all conditional transition probabilities leaving a state sum to one, the sum of all total transition probabilities is one. □

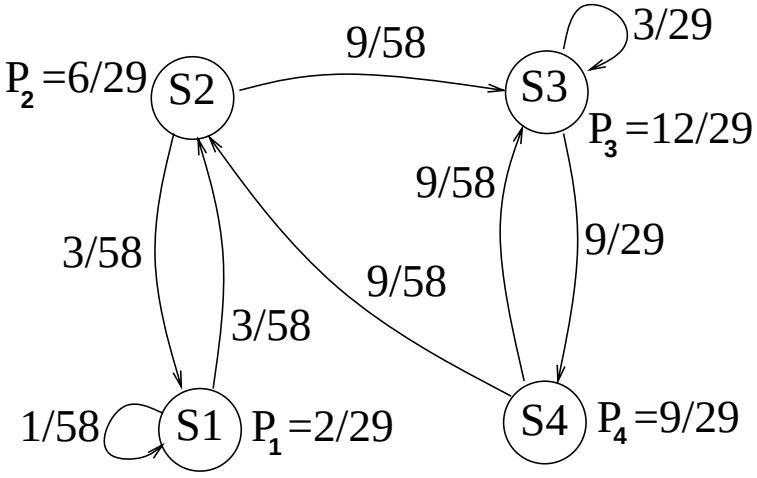

Figure 13: Stationary state probabilities and total transition probabilities

For sparse and large conditional transition probability matrices, the solution of System 2.15 can be carried out using iterative methods that do not require matrix inversion. One iterative method that is very simple and well-suited for state probability computations is the *power method*. With this approach, the state probability vector $\mathbf{q}$ can be computed using the iteration:

$$\mathbf{q}_{n+1}^T = \mathbf{q}_n^T \, \mathbf{P} \tag{2.17}$$

with the normalization condition $\sum_{i=1}^{|S|} P_i = 1$ until convergence is reached. The convergence properties of this method are discussed in [hama94]. The main advantage of the power method is that it can leverage well-developed techniques for the manipulation of large matrices for which the computation of matrix by vector product has complexity proportional to the number of nonzero elements of $\mathbf{P}$.

The main limitation of the methods presented in this section is that they are not applicable to Markov chains derived from large sequential circuits for which the state set large enough to make even the storage of matrix $\mathbf{P}$ a formidable task.

2.3.2 Implicit methods

When dealing with sequential circuits with thousands or even millions of states, specified by a structural description, it is very hard to extract and manipulate the transition probability matrix. Implicit methods allow the manipulation of large systems by representing the transition probability matrix with an ADD.

The STG of a finite state machine is implicitly represented by the BDD (or, equivalently, by a 1/0-ADD) of its *transition relation* [coud89]. The transition relation is a Boolean function $T(x, s, ns) : B^N \times B^{N_s} \times B^{N_s} \rightarrow B$. The support of the transition relation consists of: i) the input variables x, ii) the state variables s, iii) the *next state* variables ns. T has value 1 when the STG of the machine has a transition from state s to state ns with input x, zero otherwise.

The transition relation can be extracted directly from the next state function $\delta(x, s)$ with an iterative procedure of fixed point computation. Starting from an initial state (e. g. the reset state of the machine), the set of states that can be reached from it in one clock cycle is computed. The procedure then iterates computing all states reachable from the set of states reached in the previous iterations. The iteration stops a soon as no new states are reached in two successive iterations (i.e. a *fixed point* has been reached).

The fixed point computation can be carried out by operating directly on BDDs. The transition relation is computed without ever enumerating the states. BDD-based algorithms for the computation of $T(x, s, ns)$ have been able to completely explore the state spaces of machines with more than 10^{20} states, for which any enumerative algorithm would be completely impractical. The interested reader can refer to [some96] for a review of BDD-based procedures for transition relation computation.

Similarly, the input probabilities can be represented by an ADD. The ADD $PI(x)$ is extracted from the array of input probabilities, with the simple formula $PI(x) = \prod_{i=1}^{m} PI_i(x_i)$ where each $PI_i(x_i)$ is a single-node ADD, with two leaves with value p_i

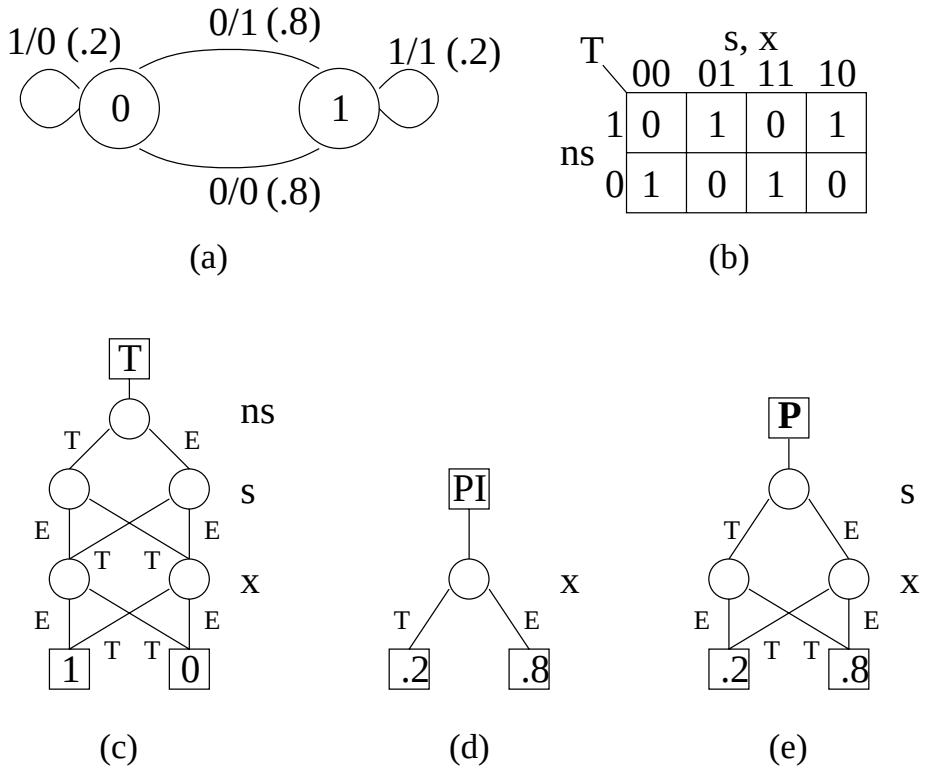

Figure 14: Symbolic computation of the conditional transition probability matrix

and $1 - p_i$.

Given T and PI, the implicit representation of matrix $\mathbf{P}$ can be obtained with the following symbolic formula

$$\mathbf{P}(x, s) = PI(x) \cdot \backslash_{ns}^{+} T(x, s, ns) \tag{2.18}$$

Equation 2.18 produces an ADD with leaves the conditional input probabilities of the transitions of the STG. Notice that the value of x and s are sufficient to identify every transition in the STG. Notice that the ADD of $\mathbf{P}$ can be exponentially smaller than the traditional matrix representation.

Example 2.3.9. The STG of a finite state machine is given in Figure 14 (a). Notice that each edge is labeled with input, output and conditional transition probability. The transition relation $T(x, s, ns)$ is shown in Figure 14 (b) in

the tabular format. The BDD (0/1 ADD) of T is shown in Figure 14 (c). The ADD of the conditional input probability is shown in Figure 14 (d). If we compute the ADD of matrix $\mathbf{P}$ using Equation 2.18, we obtain the result shown in Figure 14 (e). Although we used a small example for the sake of explanation, notice that symbolic representation based on ADD becomes useful when the STG and the truth table of T are unmanageably large. □

Once $\mathbf{P}(x, s)$ has been computed, the state probability vectors can be computed using the symbolic version of the power method. The matrix-by-vector multiplication required for the application of the power method (Equation 2.17) is implemented as an ADD operator, and the final result is $\mathbf{q}(s)$, the ADD whose leaves are the state probabilities. Notice that other implicit methods have been presented in the work by Macii et al. [hach94], as well as a detailed study of the convergence properties of symbolic algorithm for the calculation of $\mathbf{q}$ in the case of large FSMs that do not satisfy theorem 2.2.

2.4 Summary

In this chapter we covered the background material required for full understanding of the power optimization algorithms presented in the following chapters. The key concepts introduced so far are: Boolean and discrete functions, the quantification operators, BDDs, ADDs and Markov models for finite state machines. The BDD/ADD-based symbolic representation of Boolean functions, FSMs and Markov chains is a useful tool when dealing with systems with a large number of inputs and state variables.

Chapter 3

Synthesis of gated-clock FSMs

3.1 Introduction

In synchronous circuits, it is possible to selectively stop the clock in portions of the circuit where active computation is not being performed. As discussed in Chapter 1, local clocks that are conditionally enabled are called *gated clocks*, because a signal from the environment is used to qualify (gate) the global clock signal. Gated clocks are commonly used by designers of large power-constrained systems [sues94, schu94] as the core of dynamic power management schemes. Notice however that it is usually responsibility of the designer to find the conditions that disable the clock.

We consider sequential systems described by finite state machines and we target the reduction of the *useless switching activity* as defined in Chapter 1. We move from the observation that during the operation of a FSM there are conditions such that the next state and the output do not change. Therefore, clocking the FSM only wastes power in the combinational logic and in the registers. If we are able to detect when the machine is idle, we can stop the clock until a useful transition must be performed and the clocking must resume. The presence of a gated clock has a two-fold advantage. First, when the clock is stopped, no power is consumed in the

FSM combinational logic, because its inputs remain constant. Second, no power is consumed in the sequential elements (flip-flops) and the gated clock line.

Obviously, detecting idle conditions requires some computation to be performed by additional circuitry. This computation dissipates power and requires time. Sometimes it will be too expensive to detect all idle conditions. It is therefore very important to select a subset of all idle conditions that are taken with high probability during the operation of the FSM. We will show that idle conditions correspond to self-loops of Moore FSMs, and therefore it is relatively easy to detect them. Idle conditions in Mealy FSMs can also be detected, but with more effort.

We address the synthesis of the clock-stopping logic. More in detail, we formulate and solve a new logic synthesis problem, namely the choice of a minimum-complexity sub-function F_a of a given Boolean function f_a, such that its probability of being true is larger than a predefined fraction of the total probability of f_a. This is the main theoretical result in this chapter, and it is applicable to a variety of dynamic power management schemes, such as precomputation or guarded evaluation. From a practical point of view, our algorithm chooses a subset of all idle conditions such that the clock-stopping circuitry dissipates minimum power but stops the clock with high efficiency.

Experimental results will be presented for a number of benchmark circuits specified by state tables. Since state table specifications are suitable only for small sequential systems, the largest example we present has a few hundreds of states. One observation that could be made is that controllers specified as state table are responsible for a small fraction of the total power dissipation of a chip, therefore the impact of our technique is likely to be small. It is however important to notice that small FSMs control large data-paths and idle conditions for the controller are often idle for the data-path as well. Thus, detecting idle conditions on the controller leads to detecting (and exploiting) idle conditions for the controlled data-path, obtaining much larger

power savings. Moreover, in Chapter 4 we will introduce symbolic techniques that drastically enlarge the spectrum of applicability of automatic gated clock generation to sequential systems for which the behavioral description is unacceptably large.

We embedded our tool in a complete synthesis path from state-table specification to transistor-level implementation and we employed accurate switch-level simulation [salz89] to verify our results, because gate-level power estimation has limited accuracy. Since the clock-gating logic may add its delay to the critical path, particular care must be taken in detecting and eliminating timing violations that may arise when the cycle time closely matches the critical path of the original FSM. For some circuits more than 50% reduction in average power dissipation has been obtained, but quality of the results is strongly dependent on the type of finite-state machine we start with. In particular, our method is well suited for FSMs that behave as *reactive systems*: they wait for some input event to occur and they produce a response, but for a large fraction of the total time they are idle. Practical examples of such machines can be found for instance in portable devices such as pagers which are typical *reactive* systems, and for which power minimization in important.

The rest of the chapter is organized as follows. In Section 3.2 we describe the architecture of the gated-clock FSM and we discuss the detailed timing of the signals that control the clock. In Section 3.3 we formulate the problem of finding idle conditions for a FSM and we introduce a novel transformation that enables the extraction of such condition. Section 3.4 is dedicated to algorithms for the synthesis and optimization of the clock-stopping logic. Section 3.5 describes implementation details, experimental setting and results. Finally, in Section 3.6 we draw some conclusions.

3.2 Gated-clock FSMs

We will assume hereafter a single clock scheme with edge-triggered flip-flops, shown in Figure 15 (a). This is not a limiting assumption. We have indeed applied our methods to different clocking schemes in [beni94a] (where we used transparent latches and multi-phase clocks). The FSM model of Figure 15 (a) is different from the generic FSM structure we described in Chapter 2, where the primary inputs are not latched. The FSM structure without latched inputs is seldom used in the design practice. In a large system, control logic and data-path are always decomposed in interacting sub-units, for obvious reasons of complexity management. The interface between sub-units (interacting FSMs in our case) is usually composed by sequential elements [west92] (in our case, D-flip-flops). If such boundary does not exist, there is a combinational path between adjacent sub-units. This is seldom allowed in industrial design methodologies (it makes timing analysis harder and increases the risk of timing violations). Even if we consider a design that is simple enough to be described by a single FSM, flip-flops are usually inserted on the inputs to obtain better signal quality and synchronization.

From a more theoretical point of view, the FSM with latched inputs differs from the FSM without input latches because the outputs in the first model lag the outputs by one clock cycle. The input-output behavior of the two models is therefore equivalent modulo a translation in time of the output stream (assuming that the flip-flop on the inputs are reset at the same values taken in the first clock cycle by the primary inputs of the machine without input flip-flops).

A gated clock FSM is obtained modifying the structure in Figure 15 (a). We define a new signal called *activation function* (f_a) whose purpose is to selectively stop the local clock of the FSM, when the machine does not perform state or output transitions. When $f_a = 1$ the clock will be stopped. The modified structure is shown in Figure 15 (b). The block labeled "L" represents a latch, transparent when the

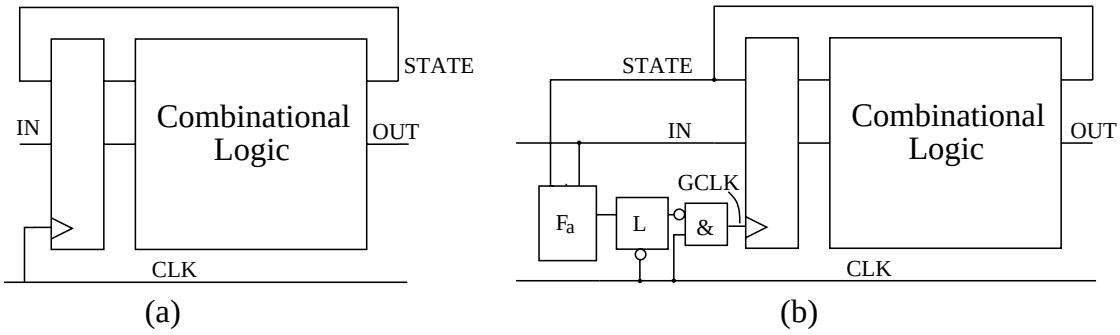

Figure 15: (a) Single clock, flip-flop based finite-state machine. (b) Gated clock version.

global clock signal CLK is low. Notice that the presence of the latch is needed for a correct behavior, because f_a may have glitches that must not propagate to the AND gate when the global clock is high. Moreover, notice that the delay of the logic for the computation of f_a is on the critical path of the circuit, and its effect must be taken into account during timing verification.

The modified circuit operates as follows. We assume that the activation function f_a becomes valid before the raising edge of the global clock. At this time the clock signal is low and the latch L is transparent. If the f_a signal becomes high, the upcoming edge of the global clock will not filter through the AND gate and therefore the FSM will not be clocked and GCLK will remain low. Note that when the global clock is high, the latch is not transparent and the inverted input of the AND gate cannot change at least up to the next falling edge of the global clock.

The activation function is a combinational logic block with inputs the primary input IN and the state lines STATE of the FSM. No external information is used, the only input data for our algorithm is the behavioral description of the FSM and the probability distribution of the input signals.

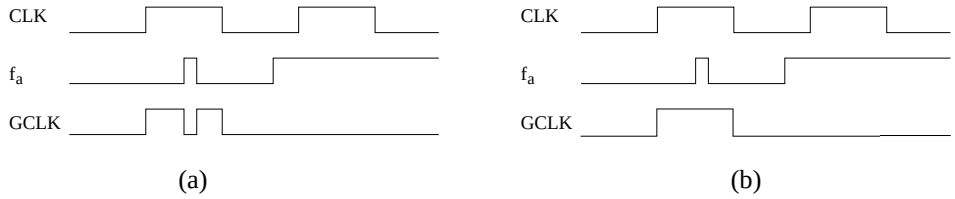

Figure 16: Timing diagrams of the activation function f_a, the global clock CLK and the gated clock GCLK when (a) a simple AND gate is used, (b) a latch and the AND gate are used.

3.2.1 Timing analysis

The activation function uses as its inputs the state and input signals of the FSM, therefore it is on the critical path of the circuit. In order to verify the correctness of the gated clock implementation, we need to make sure that the delay that the activation function adds to the delay of its inputs is less than the cycle time T of the circuit. We can test this condition performing static timing analysis on the network composed by the activation function and the logic that feeds its input (the combinational part of the FSM and the logic in the previous stages that computes the primary inputs). We call the critical path delay through this network T_{crit}.

If we collect the delays through the latch and the AND gate (Figure 15) and the setup time of the input flip-flops in one worst-case parameter T_{wc} we obtain the following constraint inequality for the activation function:

$$T_{crit} < T - T_{wc} \tag{3.19}$$

Moreover, the presence of a gate on the clock path usually implies increased clock skew. In a completely automated synthesis environment it should be possible for the designer to specify accurate skew control for the gated clock line, thus preventing possible races or timing violation involving the logic blocks in the fan-out of the FSM.

Finally, it should be noticed that the presence of the latch L is fundamental for the correct behavior of the proposed gated clock implementation. A simple combinational

AND gate is not acceptable because the activation function is not guaranteed to change when the global clock signal is low. If the activation function changes when the clock is high and it is not latched, it may create spurious pulses (glitches) on the local clock line. An example of this problem is shown in Figure 16. In part (a) the behavior of the gated clock line simply ANDed with f_a' is shown. The glitch on f_a produces a glitch on the gated clock line that will very likely produce incorrect behavior in the FSM. In contrast (Figure 16 (b)), when f_a is latched the glitch does not pass through the latch when the clock is high. Function f_a may also produce glitches when the clock is low , but in this case the AND gate itself will filter out the spurious transitions, because the global clock signal has the controlling value.

The presence of the latch could be avoided if we could guarantee that the activation function changes only after the falling edge of the global clock, or that the circuitry that implements the activation function is hazard free. These constraints may be acceptable in some particular examples, but the general solution that we have discussed has a small overhead (only one latch) and it does not require specialized techniques for the synthesis of f_a.

3.2.2 Mealy and Moore machines

The definitions of Mealy and Moore FSMs have been given in Chapter 2. Conceptually, Mealy and Moore machines are equivalent, in the sense that it is always possible to specify a Moore machine whose input-output behavior is equal to a given Mealy machine behavior, and vice versa [hart66]. Practically, however, there is an important difference. The Mealy model is usually more compact than the Moore model. Indeed the transformation from Mealy to Moore involves a state splitting procedure that may significantly increase the number of states and state transitions [hart66].

Example 3.2.1. In Figure 17 (a), a Mealy machine is represented in form of state transition graph (STG). It is transformed into the equivalent Moore

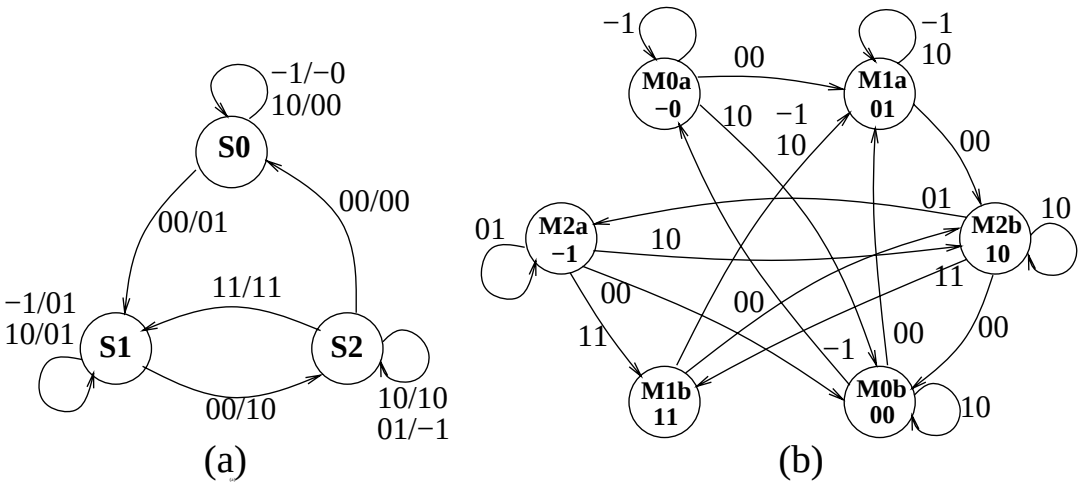

Figure 17: (a) STG of a Mealy machine. (b) STG of the equivalent Moore machine.

machine (using the procedure outlined in [hart66]) and the new STG is shown in Figure 17 (b). The STG of the Moore machine has the output associated with the states, while in the Mealy model the outputs are associated with the edges. The higher complexity in terms of states and edges of the Moore representation is evident. □

3.3 Problem formulation

Given the specification of the FSM and its probabilistic model (i.e. the Markov chain associated with it, with the conventions of Chapter 2), we first want to identify the idle conditions when the clock may be stopped. This is a simple task for Moore-type FSMs. For each state s_i we identify all input conditions such that $\delta(x, s_i) = s_i$. We define for each state s_i, $i = 1, 2, ..., |S|$, a *self-loop function* $Self_{s_i} : X \rightarrow \{0, 1\}$ such that $Self_{s_i} = 1 \ \forall x \in X \ where \ \delta(x, s_i) = s_i$.

We then encode the machine. After the encoding step every state s_i has a unique code e_i and $e_i = [e_{i,1}, e_{i,2}, ..., e_{i,|V|}]$, where V is the set of the state variables used in the encoding .

The *activation function* is defined as $f_a : X \times V \rightarrow \{0, 1\}$:

$$f_a = \sum_{i=1,2,\ldots,|S|} Self_{s_i} \cdot e_i \tag{3.20}$$

Example 3.3.2. For the Moore machine in Example 3.2.1, the self-loop function for state $M2a$ is $Self_{M2a} = in_0' in_1$ Similarly, all other self-loop state functions can be obtained. We encode the states using three state variables, v_1, v_2, v_3. The encodings are: $M0a \rightarrow v_1' v_2' v_3'$, $M1a \rightarrow v_1' v_2 v_3'$, $M2b \rightarrow v_1 v_2 v_3'$, $M0b \rightarrow v_1 v_2 v_3$, $M1b \rightarrow v_1' v_2 v_3$, $M2a \rightarrow v_1' v_2' v_3$. The activation function is therefore: $f_a = in_2 v_1' v_2' v_3' + in_2 v_1' v_2 v_3' + in_1 in_2' v_1' v_2 v_3' + in_1 in_2' v_1 v_2 v_3' + in_1 in_2' v_1 v_2 v_3 + in_1' in_2 v_1' v_2' v_3$. □

If the machine is Mealy-type, the problem is substantially more complex. The knowledge of the state and the input is not sufficient to individuate the conditions when the clock can be stopped. If only the next state lines and the inputs are available for the computation of the activation function, we do not have a way to determine what was the output at the previous clock cycle. This is a direct consequence of the Mealy model: since the outputs are defined on the edges of the STG, we may have the same next state for many different outputs. The important consequence is that, even if we know that the state is not going to change, we cannot guarantee that the output will remain constant as well, and therefore we cannot safely stop the clock.

Example 3.3.3. Consider the Mealy FSM in Example 3.2.1, and refer to Figure 15 for the implementation. If we use only the lines IN and STATE as inputs for the calculation of the activation function, we may for example observe state S2 on the next state lines, and input 10. Observing the STG, we know that for this state and input configuration the state will not change and the output will be 10 in the next clock cycle. Unfortunately, we do not have any way to know what is the output value in the current clock cycle (it could be either 10 or -1). The Moore model does not have this problem, since we know the output when we know what the state is. □

There are two ways to solve this problem. The simpler way is to use the outputs of the FSM as additional inputs to the activation function. The other approach is to transform the STG in such a way that the FSM will be functionally equivalent to the

original one, but it is possible to detect conditions where the clock can be stopped by observing only input and state lines.

In this chapter, we investigate the second method because our initial specification is in state table format. The state table is a behavioral, implementation-independent specification, therefore we still have the freedom to modify the number of states and the STG structure (this is not the case if we start from a synchronous network that is an implementation of the STG). In the next chapter, when we will assume a structural specification, the second method is not viable, since the initial circuit is given. We will then explore the first method.

The simplest transformation that enables us to use only input and state signals as inputs of the activation function f_a, is a Mealy to Moore transformation. The algorithm that performs this conversion is well known [hart66] and its implementation is simple, but it may sensibly increase the number of states and edges (correlated with the complexity of the FSM implementation). In the next subsection we propose a novel transformation that enjoys the advantage of the Mealy-to-Moore transformation (namely, it is sufficient to sample input and state signals to decide when the clock can be stopped), but does not suffer from the drawback (i.e. the excessive increase in number of states).

3.3.1 Locally-Moore machines

We now define and study a new kind of FSM transformation that enables us to use a Moore-like activation function without a large penalty in increased complexity of the FSM. We define a *Moore-state* as a state such that all incoming transitions have the same output. Formally, the subset of Moore-states of a Mealy machine is: $\{s \in S \mid \forall x \in X, \forall r \in S, \delta(x,r) = s \Rightarrow \lambda(x,r) = const\}$. States that are not Moore-states will be called Mealy-states.

Proposition 3.1 *A Mealy-state s with k different values of the output fields on the edges that have s as a destination can be transformed in k Moore-states. No other state splitting is required.*

We could transform the FSM by simply applying the Mealy to Moore transformations locally to states that have self-loops. The local Moore transformation has the advantage that it allows us to concentrate only on states with self-loops, avoiding the useless state splitting on the states without self-loops. The potential disadvantage is an increase in the number of states related to the number of different outputs on incoming edges of Mealy states (Proposition 3.1). We devised a heuristic strategy to cope with this problem. We split Mealy states with self-loops into pairs of states, where one is Moore-type with a self-loop that has maximum probability.

Thus, for each state we define the *maximum probability self-loop function* $MPself_s : X \rightarrow \{0,1\}$. Its *on set* represents the set of input conditions for a state that: (i) are on self-loops, (ii) produce compatible outputs (two outputs fields are compatible if they differ only in entries where at least one of the two is *don't care*), (iii) are taken with maximum probability.

The procedure that outputs $MPself_s$ is shown in Figure 18. Its inputs are: the state under consideration s, the self-loop function $Self_s$ (that includes all self-loops leaving state s) and the state transition graph STG of the finite-state machine. In the pseudo-code, SLO is a partition of the self-loops. An element of SLO consists of all self-loops from state s that have the *same* output (i.e. two self-loops with outputs differing only by *don't cares* will be in two different elements of SLO). The elements of SLO are mutually disjoint sets.

We then generate Q, a cover of the self-loops leaving state s. Initially Q is empty. In the first outermost iteration of the generation procedure, the first element of SLO becomes the first element of Q. Then, for each element of SLO, we check if it is compatible with any of the elements of Q. If this is the case, we incrementally modify

```
find_Mpself(s, Self_s, STG) {
  SLO = self_loop_const_out(s, Self_s, STG) ; /*Partition in classes with same output*/
  Q = ∅;
  foreach ( slo ∈ SLO ) {            /*Iterate on all self-loops classes in SLO*/
    compatible = 0;
    foreach ( q ∈ Q ) {          /*Iterate on all compatible classes of self-loops*/
      if ( is_compatible( slo, q ) ) {              /*increase compatible class*/
        q = q ∪ slo;
        merge_out_field( q );
        compatible = 1;
        break;
      }
    }
    if ( !compatible ) Q = Q ∪ {slo};            /*generate new compatible class*/
  }
  return( choose_max_prob_f( Q ) ); /*Choose the max.  probability compatible class*/
}
```

Figure 18: Algorithm for the computation of max. probability self-loop function $MPself_s$.

the elements of Q. Otherwise we create a new element.

The elements of Q are output-compatible, possibly overlapping sets of self-loops. Whenever we include an element of SLO in one of the elements in Q, we need to specify the *don't care* entries in the output field that are not always *don't cares* for all components of the set (this is done by procedure `merge_out_field` in the pseudo-code). This step is needed to guarantee pairwise compatibility. Notice that an element of SLO can be included in more than one element of Q. Finally, the procedure `choose_max_prob_f` selects the output-compatible set of self-loops with maximum probability. The input conditions corresponding to this set form the *on set* of $MPself_s$. In general, function $MPself_s$ *does not* include all self-loop leaving state s. Consequently, $MPself_s \subseteq Self_s$, with equality holding when there is a single output-compatible class. Notice that the probability of the output-compatible classes can be compared using only the conditional input probability, because they are collection of self-loops leaving the same state.

Example 3.3.4. In the Mealy machine of Example 3.2.1, if we consider state S2, we have two self-loops: $in_1 in_2'$ with output 10 and $in_1' in_2$ with output -1. The two output fields are not compatible, therefore we have two compatible classes (the same two functions). We will choose the class that is more probable. In this particular example, we assumed equi-probable and independent inputs and both functions have the same probability, therefore one of the two is randomly chosen. Assume now that $Prob(in_1 = 1) = .7$ and prob $Prob(in_2 = 1) = .5$. The probability of the first class is $p_1 = .7 * .5 = .35$, while the probability of the second class is $p_2 = .3 * .5 = .15$. In this case, the first class will be chosen. Observe that the probability of state S2 does not come into play, because state S2 is the tail of both self-loops, and the two total transition probabilities differ from the conditional probabilities only by the same scaling factor (i. e. the probability of S2). □

Once the $MPself_s$ functions have been found for all states with self-loops, the second step of our transformation algorithms is performed. A Mealy-state s with at least one self-loop is split in two states s_a and s_b. State s_b has the same incoming and outgoing edges as the original one, with just one important difference: the edges corresponding to the self-loops represented by $MPself_s$ become transitions from s_a to s_b.

The second state s_b is reached only from s_a and has a self-loop corresponding to $MPself_s$. All the outgoing edges that leave s_a are replicated for s_b, keeping the same destination. State s_b is now Moore-type, because, by construction, all edges that have s_b as head have the same output.

This procedure is advantageous for many reasons. First, the increase in the number of states is tightly controlled. In the worst case, if all states are Mealy-type and have self-loops, we can have a twofold increase in the number of states. Second, the self-loops with maximum probability are selected. Third, if we really want to limit the increase in the number of states, we may define a threshold: only the first k states in a list ordered for decreasing *total probability* of $MPself_s$ are duplicated.

We call the FSM obtained after the application of this procedure *locally-Moore* FSM, because in general only a subset of the states is Moore-type.

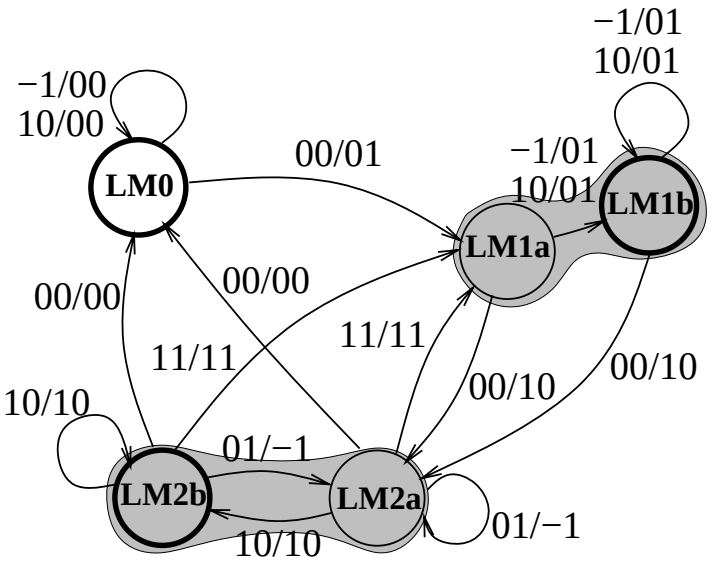

Figure 19: STG of the locally-Moore FSM

Example 3.3.5. The transformation of the Mealy machine of Example 3.2.1 produces the locally-Moore FSM shown in Figure 19. The shaded areas enclose states that have been split. The Moore-states with self-loops are drawn with thick lines. The number of states and edges of the locally Moore machine is smaller than those that we obtained with the complete Mealy to Moore transformation (state S0 has not been split).

The inputs are in_1 and in_2. Assume that we use three state variables for the encoding: v_1, v_2 and v_3. The state codes are LM0a $\rightarrow v_1'v_2'v_3'$, LM1a $\rightarrow v_1'v_2'v_3$, LM2a $\rightarrow v_1'v_2v_3'$, LM1b $\rightarrow v_1'v_2v_3$ and LM2b $\rightarrow v_1v_2'v_3'$. The activation function includes all self-loops leaving Moore-states: $f_a = in_2v_1'v_2'v_3' + in_1in_2'v_1'v_2'v_3' + in_2v_1'v_2v_3 + in_1in_2'v_1'v_2v_3 + in_1in_2'v_1v_2'v_3'$. □

Once the activation function has been found, we still need to solve the problem of synthesizing the clock-stopping logic in an optimal way. This problem will be addressed in the next section.

3.4 Optimal activation function

The most obvious approach to the synthesis of the activation function is use the complete f_a. This is seldom the best solution, because the size of the implementation of f_a can be too large, and the corresponding power dissipation may reduce or nullify the power reduction that we obtain by stopping the clock. Roughly speaking, it is necessary to be able to choose a function contained in f_a whose implementation dissipates minimum power, but whose efficiency in stopping the clock is maximum. We call such function $F_a \subseteq f_a$ a *subfunction*[1] of f_a.

An straightforward solution to this problem is the following. First, a minimum cover of f_a is obtained by a two-level minimizer. Then, the largest cubes in the cover are greedily selected until the number of literals in the partial cover exceeds a user-specified literal threshold. The rationale of this approach is that generally large cubes have high probability and the primes that compose a minimum cover are as large as possible. There are several weak points in this approach.

- There is no guarantee that choosing the largest cubes in a cover will maximize the probability of the cover, because in general the probability of a cube depends on the input and state probability distribution. Even if we assume uniform input probability distribution, the state probability distribution is in general not uniform.

- The function sought may not be found by looking only at a subset of cubes of the minimum cover of the original activation function. The number of possible subfunctions of f_a is much larger than the functions that we can generate using subsets of the cubes of the minimum cover.

[1] here, we exploit the isomorphism between set theory and Boolean algebra: Boolean function are seen as sets of minterms. A *subfunction* of f_a is therefore a function whose *on set* is contained in the *on set* of f_a.

- Even if we restrict our attention to the list of cubes in the minimum cover of f_a assuming uniform distribution for input and states, the cubes of the cover are in general overlapping (the minimum cover is not guaranteed to be disjoint). Finding the minimum-literal, maximum-probability subset of cubes becomes a set covering problem that certainly is not solved exactly by a greedy algorithm.

- The relation between the number of literals in a two-level cover of the activation function and the power dissipation of a multilevel implementation is not guaranteed to be monotonic.

In the next subsection, we will propose an algorithm that overcomes the first three limitations listed above. As for the last issue, we will assume that there is correlation between the number of literals of a two-level cover and the power dissipated in the final implementation, as suggested by experimental results presented in [land95]. We now formulate the problem that we want to solve in a more rigorous way.

Problem 3.1 *Given the activation function f_a, find $F_a \subseteq f_a$ such that its probability $P(F_a)$ is $P(F_a) \geq MinProb = \alpha P(f_a)$, (with $0 \leq \alpha \leq 1$) and the number of literals in a two level implementation of F_a is minimum.*

We call this problem *constrained-probability minimum literal-count covering* (CPML). Notice that we could as well formulate the dual problem, constrained literal count cover with maximum probability. The two problems can be solved using the same strategy, and are equivalent for our purposes. With the assumption of a good correlation between number of literals and power dissipation, we propose an exact solution to CPML and, by consequence to the problem of finding the best reduced activation function given a complete f_a to start with.

3.4.1 Solving the CPML problem

Apparently, the first source of difficulty comes from the fact that we are not constrained to completely cover f_a, therefore, the "algorithmic machinery" developed in the area of two-level minimization seems not useful. We first show that this is not true. Consider the set of primes of f_a, called $Primes(f_a)$. Consider the set Sub_{f_a} of all possible subfunctions of f_a. The set of primes of a generic subfunction $F_a \in Sub_{f_a}$ is called $Primes(F_a)$. We state the following theorem.

Theorem 3.1 *For every prime $p \in Primes(F_a)$ only two alternatives are possible.*

- $p \in Primes(f_a)$.
- *p is contained in at least one element q of $Primes(f_a)$ (consequently its literal count is larger than the literal count of q).*

  Proof: Assume that $p \in Primes(F_a)$, $(F_a \subseteq f_a)$. Two alternatives are possible: i) $p \in Primes(f_a)$, ii) $p \notin Primes(f_a)$. We will prove by contradiction that, if (ii) is true, there is always at least a prime $q \in Primes(f_a)$ such that $p \cdot q = p$ (in other words, p is contained in at least a prime of f_a). Assume that the assert is not true, therefore, p is not contained in any prime of f_a. Notice that p is an implicant of F_a therefore it is an implicant of f_a because $F_a \subseteq f_a$. By consequence, p is an implicant of f_a not contained in any prime of f_a. Therefore p is a prime of f_a by definition. This is not possible, because we assumed (ii) to start with. ♯

The important consequence of this theorem is that we do not need to generate all possible subfunctions of f_a. We can restrict our search to subfunctions that are formed by subsets of $Primes(f_a)$ if we want to find a minimum literal subfunction. Functions that belong to this class have all primes in the first category of Theorem 3.1.

Now that we have defined our search space ($Primes(f_a)$), we must find a search strategy that guarantees an optimum solution. The choice of a subset of $Primes(f_a)$

with minimum literal count satisfying the probability constraint cannot be done using a greedy strategy, because the primes are in general overlapping and a choice done in one step affects the following choices. An example will help to clarify this statement.

Example 3.4.6. Suppose that f_a is a function of four variables: a, b, c, d. The set of primes is $Primes(f_a) = \{a'b', a'c', bc', ab\}$. Assume for simplicity that all minterms are equi-probable ($Prob = 1/16$) and our probability constraint $MinProb$ (the minimum allowed probability of the subfunction) is $MinProb = 1/2$. All primes in this example are equi-probable (they have the same size). If we choose $a'b'$ first, the following choices are biased. Since $a'c'$ is partially covered by $a'b'$, it will not be the right next choice because we want to cover the largest number of minterms (remember that we are assuming equi-probable minterms). Consequently either bc' or ab must be chosen. □

CPML complexity is at least the same as two-level logic minimization, because CPML becomes two-level logic minimization for the particular case $\alpha = 1$. We describe here a branch-and-bound algorithm that has been shown to work efficiently on the benchmarks, even though its worst case behavior is exponential. Furthermore, the branch-and-bound can be modified to provide heuristic minimal solutions when the exact minimum is not attainable in the allowable computation time or memory space.

3.4.2 Branch-and-bound solution

Our algorithm operates in two phases. In the first phase, a heuristic solution is found in polynomial time (in the number of primes N_P). The second phase finds the global minimum cost solution using a branch-and-bound approach. The pseudo-code of the algorithm is shown in Figure 20.

We exploit the similarity of this problem with *knapsack* [gajo93]. We need to find the set of *items* (primes) with total *size* (probability) larger than or equal to the *knapsack capacity* ($MinProb$) minimizing the total *value* (number of literals). This formulation differs from knapsack in two important details. First, knapsack targets

```
FindFa (f_a, α)
{
  PrimeList = Generate_primes(f_a);
  MinProb = αP(f_a);
  CurBest = FindFa_PH1(PrimeList, MinProb);                    /* Phase 1 */
  CurPartial = ∅;
  FindFa_PH2 (PrimeList, CurBest, CurPartial, MinProb);        /* Phase 2 */
  return(CurBest);
}
```

Figure 20: Two-phases algorithm for the exact solution of CPML

the maximization of value given a constraint of the maximum allowed size (we face the opposite situation). Second, and most important, in knapsack the *size* of an item is a constant, while in our case the probability of a prime varies when other primes are selected. To clarify this statement, observe that primes may overlap and they contribute to the total probability of the reduced activation function only with minterms that are not covered by other already selected primes (Example 3.4.6). As a consequence, CPML is not solved in *pseudo-polynomial* time [gajo93] by dynamic programming. Notice however that CPML reduces to knapsack if all primes are disjoint (by complementing values and sizes).

In the first phase of our algorithm, we employ a greedy procedure that is reminiscent of an approximation algorithm for the solution of knapsack [mart90]. The solution obtained is heuristic and it is employed as a starting point for the second phase of the algorithm, that provides an exact solution.

The pseudo-code of first phase of the algorithm is shown in Figure 21. Let us call P_{ME} the total probability of minterms in p which are not covered by already chosen primes. We define *value density* $\mathcal{D}$ for a prime p the ratio $P_{ME}(p)/N_{lits}(p)$. We greedily select the primes with largest $\mathcal{D}$ until the constraint on $MinProb$ is satisfied. The selection is done by function `sel_prime_max`$P_{ME}N_{lits}$`ratio` in the pseudocode of Figure 21. We then check if there is a single prime whose probability satisfies the

```
FindFa_PH1(PrimeList, MinProb, CurBest)
{
  Selected = ∅; Pr = 0; ;
  while (Pr < MinProb ) {                          /* Greedy selection of primes */
    NewPrime = sel_prime_max P_ME N_lits ratio(PrimeList);
    Pr = Pr + Prob(NewPrime);
    Selected = Selected ∪ NewPrime;
    Compute P_ME (NewPrime, PrimeList);    /* Recompute P_ME for unselected primes */
  }
  MaxPrPrime = maxProb_prime(PrimeList);
  Pr1 = Prob(MaxPrPrime);
  if ( Pr1 ≥ MinProb && N_lits (MaxPrPrime) < N_lits (Selected) ) { /*Single-prime solution*/
    Pr = Pr1;
    Selected = MaxPrPrime;
    N_lits = N_lits (MaxPrPrime);
  }
  return(Selected);
}
```

Figure 21: First phase of CPML solution.

MinProb constraint and whose literal count is smaller than the total literal count of the greedily selected primes. If this is the case, the list is discarded and the single prime is selected.

The single prime solution is tested for two reasons. First, the same test is performed in the greedy algorithm for the heuristic solution of knapsack [mart90]. Second, and most importantly, it corresponds to a particular case that can be encountered in practice. Some machines have a *halt* state and a *halt* input value. If the machine is in *halt* and the inputs are fixed at the *halt* value, no output and state transitions are allowed. The cube of the activation function corresponding to the *halt* state and inputs may have a small value of $\mathcal{D}$, because even if its probability is high, so is the number of specified literals in the cube. When synthesizing the activation function we want to early detect the *halt* condition, that is indeed the most natural candidate for clock-gating. The single cube test helps in detecting such condition as soon as possible, before the time consuming exact search is started.

When the first phase of the algorithm terminates, it returns a feasible solution that is used as starting point for the branch-and-bound algorithm employed in the second phase. At the beginning of the second phase, we order the primes for decreasing ratio $P(p)/N_{lits}(p)$. The probability $P(p)$ of a prime is computed multiplying the conditional probability of the input part by the probability of the state part (remember that the probability of a transition is computed by multiplying the conditional input probability by the state probability), and it is computed once for all (contrasts with phase 1 of the algorithm, where P_{ME} that is recomputed whenever a new prime is chosen).

At the starting point of the branch-and-bound we have a *search list* corresponding to all primes. Moreover, we have a *current best* solution generated by the first phase. The *current partial* solution is initially empty. Each time the recursive procedure is invoked, all primes in the prime list are considered one at a time. If the prime being considered (together with the current-partial solution) yields more literals than the best solution seen so far, the prime is discarded and another prime is considered. Otherwise, a solution feasibility check is done (i.e. if the probability is larger than, or equal to $MinProb$). If this is the case, the current best solution is updated. Otherwise, a new recursive search is started, where the prime just being considered is kept as part of the current partial solution but the primes considered at the previous level of the recursion are discarded. The pseudo-code of the algorithm is shown in Figure 22.

Notice that the backtracking involved in the branch and bound is implicitly obtained in the pseudo-code. For each iteration of the inner loop, we generate a new partial solution adding to the original partial solution a single prime from the search list. In this way, each new iteration backtracks on the choice of the prime in the previous iteration. The algorithm terminates when all choices in the search list of the upper level of the recursion have been tried.

```
FindFa_PH2 (PrimeList, CurBest, CurPartial, MinProb)
{
  if(Bound(PrimeList, CurBest, CurPartial, MinProb)) return;    /* Bounding step */
  DoneList = ∅;
  foreach (Prime ∈ PrimeList) {                                  /* Branching step */
    DoneList = DoneList ∪ Prime;
    NewPartial = CurPartial ∪ Prime;
    if ( N_lits(NewPartial) < N_lits(CurBest) ) {
      if ( Prob(NewPartial) ≥ MinProb )
        CurBest = NewPartial;                                    /* New Best solution */
      else
        FindFa_PH2 (PrimeList − DoneList, CurBest, NewPartial, MinProb); /* Recursion */
    }
  }
}
```

Figure 22: Second phase of CPML solution.

The bound is based on the approximation algorithm for the solution of knapsack mentioned above. The greedy procedure guarantees a solution to knapsack within a factor of 2 from the optimum [mart90]. The optimum knapsack solution itself is an upper bound to the solution of our problem (it becomes the exact solution if all primes are disjoint). Intuitively, the bound eliminates the partial solutions that could not improve the current best solution even if all primes in the search list were mutually disjoint and not overlapping with primes in the current partial solution.

The bounding procedure (`Bound`) works on the search list. If the search list (`Primelist`) is empty, obviously the return value is 1. If the current partial solution (`CurPartial`) is empty, the return value is 0. In the general case, we select primes from the top of the search list until the sum of their literal count becomes larger than N_{lits}(`CurBest`) $-$ N_{lits}(`CurPartial`). We compute the sum of the probabilities of all selected primes (excluding the last selected one) and call it P_{tot}. We choose the maximum P_{max} between P_{tot} and P_{one}, where P_{one} is the largest probability value of a single prime in the search list whose literal count is less than N_{lits}(`CurBest`) $-$ N_{lits}(`CurPartial`).

Once P_{max} has been obtained, we can prune the partial solution if the following inequality is verified:

$$P_{max} < (MinProb - \texttt{Prob(CurPartial)})/2 \tag{3.21}$$

The rationale behind this bound requires further explanation. In the `Bound` procedure we are trying to discover if a selection of primes from `PrimeList` can increase the probability of the current partial solution by $\Delta P > MinProb - \texttt{Prob(CurPartial)}$ (an amount large enough to satisfy the bound on probability), without increasing the number of literals by more than `DeltaLits` (the difference between the number of literals in the best solution so far and the number of literals in the current partial solution).

If such a selection exists, its probability P_{exact} is $P_{exact} \leq P_{knap}$, where we obtain P_{knap} by assuming that all primes are disjoint (remember that primes can be overlapping, hence the inequality). An upper bound P_{max} for P_{knap} is obtained by the greedy algorithm described above, because finding P_{knap} requires the solution of a *knapsack* problem and the greedy algorithm provides an approximate solution $P_{max} \geq P_{knap}/2$ [mart90]. Thus, we have established the following chain of inequalities:

$$P_{exact} \leq P_{knap} \leq 2P_{max} \tag{3.22}$$

If $2P_{max} < \Delta P$, the same will hold for P_{exact}, thus proving the correctness of the bound.

Example 3.4.7. Assume that we have a current best solution that satisfies the constraint on the probability ($MinProb = .4$) with a cost of $Nlits = 40$. Assume that the current partial solution has cost $Nlits' = 36$ and probability `Prob(CurPartial)` $= .35$. Suppose that the first two element of the unselected prime list are $a'b'$ with probability .01 and $a'c'$ with probability .012. The maximum probability prime with at most 4 literals has probability .015. P_{max}

```
Bound(PrimeList, CurBest, CurPartial, MinProb);
{
  if ( PrimeList == ∅ ) return(1);
  if ( CurPartial == ∅ ) return(0);
  Selected = ∅; N_lits = 0; Pr = 0; exit = 0;
  DeltaLits = N_lits(CurBest) − N_lits(CurPartial);
  while ( !exit ) {                              /* Greedy selection of primes */
    NewPrime = sel_max_PNratio(PrimeList);
    if ( N_lits + N_lits(NewPrime) > DeltaLits ) exit = 1;
    else {
      Pr = Pr + Prob(NewPrime);
      Selected = Selected ∪ NewPrime;
      N_lits = N_lits + N_lits(NewPrime);
    }
  }
  MaxPrPrime = maxProb_prime(PrimeList);
  Pr1 = Prob(MaxPrPrime);
  if ( Pr1 ≥ Pr && N_lits(MaxPrPrime) < DeltaLits ) {      /*Single-prime solution*/
    Pr = Pr1;
    Selected = MaxPrPrime;
    N_lits = N_lits(MaxPrPrime);
  }
  if ( Pr < .5 (MinProb − Prob(CurPartial)) ) return(1);            /*Bound test*/
  else return(0);
}
```

Figure 23: Bounding function.

is therefore $P_{max} = max\{.015, .012 + .01\} = .022$. This branch of the search tree is pruned, because $P_{max} < (MinProb - \texttt{Prob(CurPartial)})/2 = .025$. Notice that the two primes are partially overlapping, therefore the actual increase in probability for the current solution if we select the two primes would be smaller than the estimated one. □

The bound can be made even tighter if after selecting a new prime in a partial solution, the probabilities of the remaining primes are reduced accordingly to the overlap with the chosen prime. Notice that the computation of this second bound requires the re-calculation of all probabilities of the currently unselected primes (and the reordering of the search list). As a consequence, the second bound should be computed only after the first has been unsuccessful in pruning the search tree.

We want to point out that there are two possible sources of complexity explosion

in our algorithm. First, the number of primes for a Boolean function is worst case exponential in the number of the function inputs. Second the branch-and-bound algorithm has a worst case exponential complexity in the number of primes that form the candidate list.

The double source of exponential behavior may seem worrisome. Nevertheless, the structure of our algorithm is flexible enough to generate fast heuristic solutions if the execution time and/or memory requirements exceed some user-defined limit. The problem of the large number of primes can be avoided if we apply the algorithm to a reduced set of primes. The most natural candidate is obviously a prime and irredundant cover of the function, obtainable using two-level minimizers that can provide optimum or near-optimum covers for single output functions with a large number of inputs [mcg93].

If either the branch-and-bound is interrupted or a reduced set of primes is used, the exact minimality of the last solution found is not guaranteed, but we will have in general a good quality heuristic solution. Notice that the first phase of our algorithm finds a feasible solution in polynomial time, and we could even completely skip the branch-and-bound if we consider it too expensive.

3.4.3 The overall procedure

We can now briefly outline the full procedure used for the synthesis of the low-power gated-clock FSMs. Our starting point is a FSM specified with a transition table or a compatible format. The synthesis flow is the following.

- The Mealy machine is transformed to an equivalent locally-Moore machine
- The complete activation function f_a is extracted from the Moore-states of the locally-Moore machine.
- The probability of the complete f_a is computed.

- The prime set $Primes(f_a)$ is generated.
- The branch-and-bound algorithm finds the minimum literal count solution F_a whose probability is a pre-specified fraction α of the probability of f_a
- F_a is used as additional *don't care set* for optimizing the combinational logic of the FSM.

The last step can sensibly improve the quality of the results, in particular if F_a is large. Unfortunately, it is hard to foresee the effects of F_a used as *don't care* set. Sometimes it may be convenient to choose a F_a that is not minimal in the sense discussed above, if it allows a large simplification in the combinational part of the FSM. Our heuristic approach is to try different F_a that range from the complete f_a to a much smaller subfunction, in an attempt to explore the trade-off curve.

This iterative search strategy raises the problems of choosing appropriate values of the parameter $\alpha \leq 1$ used to scale down the probability of f_a when the reduced activation functions are generated. The approach that we adopted is to generate a set of reduced activation functions $Cand_F$ using different values of α, in such a way that the possible range of solutions is uniformly sampled. We have devised a heuristic procedure that generates suitable α values and we briefly outline it.

Initially, the user specifies the number of candidate solutions N_{cand} that should be generated by the tool. Then, the values of α are generated by uniformly dividing the interval $(0, 1)$:

$$\alpha_i = i/N_{cand} \quad i = 1, 2, ..., N_{cand} \tag{3.23}$$

It may be the case that for two or more consecutive values α_i the algorithms generates the same solution. This happens for example when eliminating even a single prime from a solution generated for $i + 1$ causes a decrease in the $P(F_a)$ in the

solution generated for i larger than $P(f_a)/N_{cand}$. In this case our algorithm adaptively select new values of α such that the new candidates will have a probability between those of solutions generated with two consecutive values of α that have maximum literal cost difference.

Obviously, if large N_{cand} are used, the computational time required to generated $Cand_F$ increases. Notice however that only the last two steps in the overall procedure describe before need to be iterated, and usually a small number of different values of α is sufficient to find a satisfying solution.

One more point is worth noting. Although our procedure for the synthesis of a constrained probability minimum literal cover of F_a is exact, the overall synthesis path is heuristic. As a consequence, finding an exact solution to CPML may not be essential, because the approximation introduced may cause large errors that we do not control. Nevertheless, the strength of our approach lies in its flexibility: our algorithm offers the possibility of exploring the search space with a fine granularity, and it can find heuristic solutions at a very low computational cost.

3.5 Implementation and experimental results

We implemented the algorithms as a part of our tool-set for low-power synthesis. The tool reads the state transition table of the FSM. The first step is the transformation of the Mealy machine to a locally-Moore machine and the extraction of the self-loops from the Moore-states.

An input probability distribution must be specified by the user. For our experiments we set the input probabilities to .5 for all inputs, since we did not have any information on the environment where the FSMs are embedded. Moreover, we assumed that every input line has a maximum of one transition per clock cycle. This

is an optimistic assumption, because multiple input transitions (high transition density) may increase the power dissipated in the activation function logic (but not in the FSM logic because the input are guarded by flip-flops). If inputs with high transition activity are present, smaller activation function should be allowed.

The power method is applied to compute the exact state probabilities given a conditional input probability distribution. Notice that this step can be modified to use the exact and approximate methods described in [hama94, mont94, marc94] that have been demonstrated to run on very large sequential circuits. Presently, our procedure employs sparse matrix techniques and it has been able to process all MCNC [mcnc91] benchmarks provided in state transition table format in a small time (less than 10 sec. on a DECstation 5000/240 for the largest example `s298`).

We then state assign both the original machine and the locally-Moore FSM using JEDI [lin89]. Once the state codes have been assigned, our probabilistic-driven procedure for the selection of the activation function can start. First, all primes of the activation function are generated using symbolic methods [coud92], then the probability of the minimized cover (obtained with ESPRESSO [sent92]) of the complete activation function f_a is computed. The number of literals of the complete minimized cover is used as initial literal cost limit in the branch-and-bound algorithm.

The user specifies the number of activation functions that the procedure should generate, and the branch-and-bound algorithms solves the CPML as many times as it is requested. Surprisingly, for all MCNC benchmarks this step has never been the bottleneck, the CPU time being in the order of 30 seconds maximum. This is certainly due to the fact that the majority of the FSM MCNC benchmarks do not have a large number of self-loops (in particular the larger ones). Nevertheless, even if difficult cases are found, our algorithm stops the search when a user specified CPU time limit has been reached. The solution becomes then suboptimal, but there are other sources of inexactness in the overall procedure. Therefore the search for an

exact optimum solution of CPML is not of primary practical importance.

The combinational logic of the locally-Moore FSM is then optimized in SIS [sent92] using the additional *don't care set* given by the activation function. This step is repeated for all activation functions generated in the preceding step, and alternative solutions are generated. The *don't care*-based minimization of the combinational logic using the activation functions is the main bottleneck of our procedure. In our tool the user has the possibility to specify a CPU-time limit for each minimization attempt. This of course limits the possible improvements obtainable on large FSMs.

The activation functions are also optimized using SIS, then the alternative solutions are mapped with CERES [mail91], and the gated clock circuitry is generated. Again the same optimization and library binding programs are used for both the original Mealy machine and the locally-Moore gated clock machines. We employed a simple target library which includes two, three and four input gates. Our flip-flops have a master-slave structure, and their cost (in terms of area and input load capacitance) is approximatively equivalent to 2 three-input logic gates.

Finally the alternative gated clock implementations and the implementation of the original Mealy FSM are simulated with a large number of test patterns using a switch level simulator (IRSIM [salz89]) modified for power estimation.

The quality of the results strongly depends on two factors. First, how much state splitting has been needed to transform the machine to a locally-Moore one. Second, for what percentage of the total operation time the FSM is in a self-loop condition (this depends on the FSM structure and on the input probability distribution). For machines with a very small number of self-loops or a very low-probability complete activation function, the chance of improvement is limited or null. This is the case for many MCNC benchmarks for which the final improvement is negligible. As for the first problem, it may be worth to investigate if, in case the state duplication is too high, using an activation function with the outputs of the FSM as additional inputs

Circuit	Original		Locally-M.		Gated		%	F_a Size	α
	Size	P	Size	P	Size	P			
bbara	330	67	422	72	408	34	49	74	1
bbsse	640	121	742	137	736	119	2	140	1
bbtas	142	56	138	57	164	44	21	34	.93
keyb	721	128	754	132	820	114	10	62	.91
lion9	188	60	226	60	248	52	13	8	.25
s298	7492	899	7496	900	7502	810	10	14	1
s420	544	132	544	132	602	108	18	44	.75
scf	3222	437	3222	437	3169	400	8	26	1
styr	1474	159	2468	230	2534	208	0	560	.75
test	348	73	442	76	374	32	56	64	.88

Table 1: Results of our procedure applied to MCNC benchmarks. Size is number of transistors. P (power) is in μW.

may lead to better results.

Example 3.5.8. The Mealy machine of Example 3.2.1 has been synthesized without any gated clock. The number of states is 3, the mapped implementation has 124 transistor and a total nodal capacitance of 2.32 pF. The average power dissipation is 52 μW.

Using our algorithm, the minimum power implementation (obtained with the complete activation function in this case) of the equivalent locally-Moore gated clock machine has 178 transistors and a total nodal capacitance of 3.14 pF. The average power dissipation is 42 μW. Notice that the efficacy of the activation function in stopping the clock allows substantial power savings (24%) even if the total capacitance is larger (35%). This is due to the fact that the locally-Moore machine has 5 states, and its combinational logic is more complex. In contrast, with a complete Moore transformation the minimum power implementation has 196 transistors and total nodal capacitance of 3.39 pF. Its power dissipation is 48 μW. □

Table 1 reports the performance of our tools on a subset of the MCNC benchmarks. The first six columns show the area (number of transistors) and the power dissipation of the normal Mealy FSM, the locally-Moore FSM without gated clock and the locally-Moore machine with gated clock. The last three columns show the percentage power

reduction (computed as $100(P_{mealy} - P_{gated})/P_{mealy})$), the size (in transistors) of the activation function and the α factor used in the solution of CPML leading to the best result. Notice that, if there is no power improvement the improvement is set to 0.

The tool is able to process all benchmarks, but in the table we list examples representative of various classes of possible results. The benchmarks `bbara` and `test` are reactive FSMs. The high number and probability of the self-loops allow an impressive reduction of the total power dissipation, even if the area penalty can be not negligible. For this class of FSMs our tool gives its best results.

In contrast, for `bbsse` and `styr` there is no power reduction or even a power increase. The `bbsse` benchmark is representative of a class of machines where the number and probability of the self-loops is too small for our procedure to obtain substantial power savings. The `styr` benchmark has many self-loops, but they all have low probability. Moreover, the transformation to locally-Moore machine has a too large area overhead in this case, therefore, even if there are power savings with respect to the locally-Moore implementation without clock, the smaller Mealy implementation has the lowest power consumption.

For all other examples in the table the power savings vary between 10% and 30%. For some of these machines (`s420` and `scf`), there is no area overhead for the locally-Moore transformation. This happens when all states with self-loops are already Moore states in the original FSM. We included some of the larger examples in the benchmark suite (`s298` and `scf`) to show the applicability of our method to large FSMs.

From the analysis of the results, it is quite clear that several complex trade-offs are involved. First, the transformation to locally-Moore machine can sometimes be very expensive in terms of area overhead. Second, the choice of the best possible activation function is paramount for good results. In fact, for many examples, the complete activation function was too large, and reduced activation functions gave

Circuit	$P^{Comb}_{Gated}/P^{Clk}_{Gated}$	$P^{Comb}_{Loc\_M}/P^{Clk}_{Loc\_M}$	$P^{Comb}_{Gated}/P^{Comb}_{Loc\_M}$	$P^{Clk}_{Gated}/P^{Clk}_{Loc\_M}$
bbara	1.2777	2.7006	0.3624	0.7660
bbsse	1.5317	2.5386	0.7601	1.2597
bbtas	1.2242	1.8715	0.6861	1.0488
keyb	2.4024	3.2242	0.8185	1.0985
lion9	2.0734	2.2749	0.8937	0.9806
s298	17.7560	17.9872	0.9887	1.0016
s420	1.3517	1.5251	0.8126	0.9169
scf	2.8988	2.7368	0.9274	0.8755
styr	4.2330	4.3990	0.8969	0.9320
test	1.1751	2.8957	0.3048	0.7512

Table 2: Partition and comparison between power dissipation in clocking logic and FSM logic for locally-Moore and gated-clock FSMs

better results. Notice however that for some examples the efficiency of the activation function in stopping the clock was such that the power was sensibly reduced even with large area overhead.

Having discussed *how much* power is saved, we address now the problem of *where* the power is saved. In our approach the FSM clock is stopped only when the next state variables and the outputs are not going to change in the upcoming clock cycle. It may be possible to think that power is saved only in the flip-flops and the clock line. This intuitive observation is deceiving, because power is also saved in the combinational logic, as it is shown in Table 2. We have compared in the table the power dissipation of the locally-Moore implementation with and without gated clock. We compare to the locally-Moore FSM because its STG is isomorphic to those of the gated-clock FSM. Hence, all modifications are due only to the insertion of the activation function. The comparison with the Mealy machine is less explicative because the locally-Moore transformation modifies the STG and consequently the next state and output function, making impossible to distinguish how the clock-gating circuitry alone affects the power dissipation.

In the first two columns of the table, for the two implementations, we compare the ratio of the power dissipated in the combinational logic (flip-flops outputs, all nodes in the FSM logic and outputs) and the power dissipated in the clock-related circuitry (activation function, clock lines, NAND gate, latch, inputs and internal nodes of the flip-flops). In the last two columns we show the power ratio for the combinational logic and the power ratio for the clock-related circuitry for the two implementations.

First, notice that the ratio P^{Comb}/P^{Clk} is almost always smaller for the gated-clock FSMs. This result is quite intuitive, because P^{Clk} in the gated-clock FSM includes the power dissipation of the activation function. The results of columns 3 and 4 are somewhat counterintuitive, because they show that *there is consistently higher power saving in the combinational logic than in the clock-related circuitry.* This result is due to three factors. First, the reduced switching activity on the outputs of the flip-flops, that are generally highly loaded. Second, the absence of propagation to internal nodes in the FSM logic of input transitions when the FSM is in a self-loops. Third, and most importantly, the simplification in the FSM's logic that is obtained using the *on set* of the activation function as additional controllability *don't care set.*

We want to point out that our methodology attains consistent power savings not only when the clock line is heavily loaded and large flip-flops are used, but also for very small FSMs with optimized flip-flops. It is however important to remark that the full extent of the possible savings is obtained only if the combinational logic is re-optimized with the increased *don't care* set previously described. Moreover, for classes of FSMs such as synchronous counters, or more generally, FSM without self-loops, our methodology is ineffective in reducing power consumption.

In summary, the power savings depend on the fraction of the total operation time that the FSM spends in idle condition. Don't care optimization is very helpful when the FSM is small and the idle time is a relatively small fraction of the total, because it helps in reducing the overhead of the clock-gating circuitry. For large FSMs the

impact of *don't cares* is generally less relevant. Even if the power savings are basically decided by the initial structure of the FSM, it is important to have an automated synthesis procedure such ours, so as to avoid unnecessary effort from designers in trying to manually design clock-stopping logic.

3.6 Summary

In this chapter we have described a technique for the automatic synthesis of gated clocks for Mealy and Moore FSMs.

From the practical point of view, we want to emphasize that our method is part of a complete procedure, starting from FSMs state-table specification to fully mapped network, and it has been tested with accurate power estimation tools. The quality of our results depends on the initial structure of the FSM, but we obtain important power reductions for a large class of finite-state machines, where the probability of being in a self-loop (idle) is high. Even if our tool cannot fully replace the knowledge of the designer in finding idle conditions at the architectural level, it may enable design exploration for cases where it is not clear if clock gating may produce sizable power savings.

From the theoretical point of view, this chapter makes two contributions. First, we presented a transformation for Mealy FSMs that makes them suitable for gated-clock implementation, allowing for greater flexibility in the choice of clock-stopping functions with small support and lower complexity. Second, we have proposed a logic optimization problem, called "constrained probability minimum literals" problem, and we have described its exact and heuristic solutions. Our solver has large applicability, and can improve the performance of any power management scheme that relies on optimized combinational logic that stops the clock with maximum efficiency.

In this chapter we did not address how the presence of the clock-control circuitry

affects the testability of the gated-clock FSM. This is an important practical issue that will be addressed in Appendix A. Probably the main limitation in our approach is its applicability to relatively small sequential system (with a few hundred states) specified with state tables. In the next chapter we will take a step towards extending the basic ideas and principles introduced so far to larger sequential circuits described by synchronous networks.

Chapter 4

Symbolic gated-clock synthesis

4.1 Introduction

In the previous chapter we proposed and effective way for obtaining power savings on a design whose initial specification is given as a state transition graph (STG). More specifically, the strategy adopted to save power is based on the concept of *clock gating*. Given the STG of the circuit to be synthesized, conditions under which the next state and the output signals do not change are identified. In presence of such conditions, the clock is disabled, since no useful computation is performed by the circuit, thus avoiding node switching that causes useless power dissipation. We described techniques for calculating the conditions under which the clock can be stopped, as well as exact and approximate algorithms for synthesizing the FSM with embedded clock gating mechanisms.

We now investigate two directions of improvement. First, the algorithms and data structures described in the previous chapter can effectively handle only FSMs described by state transition tables. Controllers which are automatically synthesized from high-level specifications may have millions of states; explicitly enumerating all of them in a state transition table, as required by the algorithms described in the

previous chapter, may thus be simply unacceptable. Second, the computation of the clock gating conditions is performed without considering the controller as a piece of a more complex system but, rather, as a component running in isolation. This implies an inevitable loss of information which could have been exploited to achieve a more effective global optimization.

In this chapter we address both the critical issues pointed out above. The problem of optimizing larger controllers is tackled in two ways. First, by resorting to symbolic data structures, that is, BDDs and ADDs, to simplify the representation of the clock gating conditions as well as the calculation of the probability of the *activation function* (i.e., the set of clock gating conditions). Second, by employing a new and efficient algorithm for the search of the optimal activation function that is able to dynamically estimate the savings, in terms of power consumption, that different realizations of the clock gating logic produce on the circuit.

For what concerns the calculation of the activation function, in the previous chapter it was computed by assuming that the FSM is as a self-standing computing element. We implicitly assumed equiprobable input statistics, because environmental information were not available. Control-dominated systems are usually interacting with other controllers and/or data-paths; this may pose some constraints on the signals that appear at the circuits I/O interfaces. One way of properly modeling the influence of the environment on the behavior of a design is through non-equiprobable primary input statistics. In addition, even when the circuit's primary inputs are totally independent from the other components, there may be cases in which assuming a 0.5 input transition probability is not realistic (think, for example, to the external reset signal of a microcontroller). We therefore propose to use non-equiprobable primary input probability distributions in the computation of the activation function. Such distributions can be determined from the knowledge of the specific functionalities associated with the various input signals or, alternatively, by performing system-level

simulation over a large number of clock periods.

We present experimental results that show the feasibility and the effectiveness of the proposed techniques. Power savings of up to 36% have been obtained on some of the mid-sized circuits belonging to the `Iscas'89` suite [isca89]). Moreover, experimental data show the impact that an accurate knowledge of the primary input statistics can have on both the total probability of the activation function and the power savings obtainable through implementation of the gated clock architecture.

The rest of the chapter is organized as follows. In the next section we briefly review some background material (refer to Chapter 2 for a more complete treatment). In Section 4.3 we illustrate how idle conditions can be detected for sequential circuits using symbolic methods. Section 4.4 describes BDD-based algorithms for the synthesis the activation function. Section 4.5 and 4.6 discuss the optimization of the activation function the sequential circuit. Section 4.7 describes an enhancement to the synthesis of the activation function that allows more idle conditions to be detected. Finally, in Section 4.8 we report the experimental results.

4.2 Background

We assume the reader to be familiar with the basic concepts of Boolean functions and with the data structure commonly used for the symbolic manipulation of such functions, that is, the binary decision diagrams (BDDs). Background material on this subject has been given in Chapter 2. Recall from Chapter 2 that given a single-output Boolean function, $f(x_1, x_2, \ldots, x_n)$, the *positive and the negative cofactors* of f, with respect to variable x_i, are defined as: $f_{x_i} = f(x_1, \ldots, x_{i-1}, 1, x_{i+1}, \ldots, x_n)$ and $f_{x_i'} = f(x_1, \ldots, x_{i-1}, 0, x_{i+1}, \ldots, x_n)$; the *existential* and the *universal abstraction* of f with respect to x_i are defined as: $\exists_{x_i} f = f_{x_i} + f_{x_i'}$ and $\forall_{x_i} f = f_{x_i} \cdot f_{x_i'}$.

4.2.1 Sequential Circuit model

We assume the same clocking scheme as introduced in the previous chapter. All flip-flops are controlled by the same clock, and are all resetable to a given state. Associated with a sequential circuit is an encoded, Mealy-type, finite-state machine (FSM) that describes the behavior of the circuit. An FSM, M, is a 6-tuple $(X, Z, S, s_0, \delta, \lambda)$, where X is the input alphabet, Z is the output alphabet, S is the finite set of states of the machine, s_0 is the reset (initial) state, $\delta(x, s)$ is the next state function ($\delta : X \times S \rightarrow S$), and $\lambda(x, s)$ is the output function ($\lambda : X \times S \rightarrow Z$). Boolean functions δ and λ have multiple outputs: they implicitly define the state transition graph (STG) of the given FSM.

Elements $x \in X$ are encoded by vectors of n Boolean variables, $x_1, \ldots, x_n$, called input variables. Similarly, present states $s \in S$ are encoded by k Boolean variables, $s_1, \ldots, s_k$, called present-state variables, elements $z \in Z$ are encoded by vectors of m Boolean variables, $z_1, \ldots, z_m$, called output variables, and next states $t \in S$ are encoded by k Boolean variables, $t_1, \ldots, t_k$, called next-state variables.

4.2.2 Symbolic Probabilistic Analysis of a FSM

The ADD-based representation of discrete functions has been introduced in Chapter 2 as well as the most important operators for efficient ADD manipulation: ITE, APPLY, and ABSTRACT. Remember that the probabilistic analysis of a FSM is performed studying the Markov chain associated with it. Given the STG of the FSM representing the circuit and the conditional input probability distribution, we showed in Chapter 2 that it is possible to compute the vector $\mathbf{p}$ whose entries p_s are the steady-state probability of the FSM to be in state s. Unfortunately, the extraction of the STG from a sequential circuit with many flip-flops is a difficult task, and the storage of the STG itself (using traditional data structures such as adiacency lists or

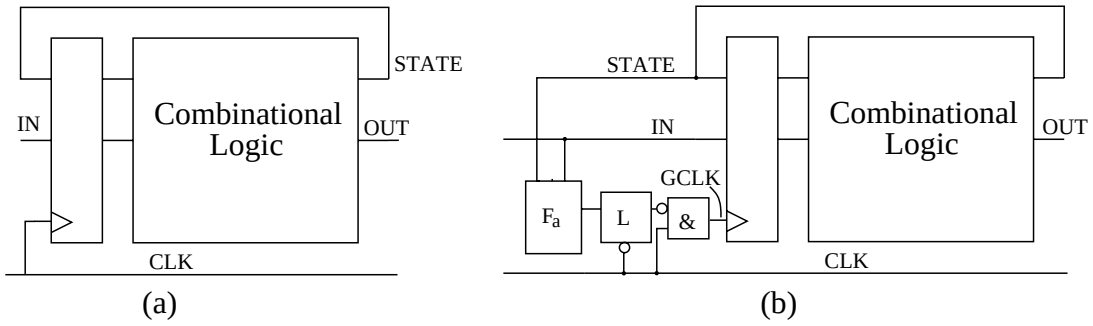

Figure 24: (a) Single Clock, Flip-Flop Based Sequential Circuit. (b) Gated-Clock Version.

matrices) is extremely memory demanding.

ADD-based procedures enable the computation of the state probability vector for very large FSMs (transition graphs with up to 10^{27} states can be successfully handled). Note that the the state probability vector is represented by an ADD, and explicit state enumeration is never required. Complex primary input probability distributions can be specified and efficiently represented with ADDs in order to have more detailed hardware modeling options. We rely on the performance of these algorithms to overcome some of the limitations which appeared in the implementation of the optimization methods proposed in the previous chapter.

4.3 Detecting idle conditions

We refer to the FSM implementation with latched inputs introduced in the previous chapter and reproduced in Figure 24 for the reader's convenience. Given the gate-level description of the circuit and its probabilistic model, we first want to identify the idle conditions when the clock may be stopped. A gate-level netlist is the implementation of a sequential circuit that can be represented by a finite-state machine. In the following we will refer to the FSM associated with the netlist to clarify some important points. First, remember that identifying idle conditions is a simple task for circuits

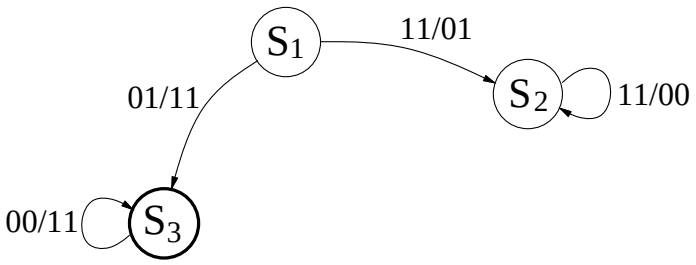

Figure 25: Fragment of a Mealy FSM. S_2 is Mealy-State while S_3 is a Moore-State.

implementing Moore-type FSMs. When the present state and the inputs are such that the next state does not change, the Moore FSM is idle; in symbols: $\delta(x, s) = s$ (i.e., the self-loops). We have shown that this property does not hold for Mealy FSMs.

Consider for example the fragment of a Mealy FSM shown in Figure 25. State S_2 has a self-loop, but we cannot stop the clock when we observe the code of S_2 and inputs 00 on the state and input lines. The reason is that the self-loop does not change the next state, but it *changes the output* if the previous transition was $S_1 \rightarrow S_2$. Intuitively, the self-loop on S_2 becomes an idle condition only if it is taken for two consecutive clock cycles. In contrast, the self-loop on S_3 is an idle condition, because every incoming edge of S_3 has the same output and knowing that the next state is S_3 provides enough information to infer the output value.

This observation has been formalized in the previous chapter where the states of a Mealy-type FSM have been divided into two classes. States like S_2 where self-loops are not idle conditions (unless taken twice), are called *Mealy-states*, while states like S_3 are called *Moore-states*. For Mealy-states it is not possible to stop the clock of the circuit just by observing the state and input lines. Hence, we formulated an algorithm that operates on the STG of the FSM to transform Mealy-states into Moore-states, thus allowing the exploitation of more self-loops as idle conditions where the clock can be stopped.

Our starting point is now completely different: we are *not* given the STG (or the

state table) of the FSM and we want to *extract* the idle conditions available in the synchronous network implementing the FSM. It is generally computationally infeasible to extract the STG representation for large sequential circuits. As a consequence, the transformation from Mealy-states to Moore-states is not practically applicable and we must restrict ourselves to the Moore-states of the Mealy FSMs. In other words, while in the previous chapter we could *increase* the number of idle conditions by transforming the STG of the FSM, we will now momentarily assume that only the self-loops leaving Moore-states of the original FSM can be selected as clock-gating conditions. This assumption will be relaxed later.

4.3.1 Activation Function

Given an FSM implemented by a synchronous network, we want to find the self-loops of Moore-states. Such self-loops are uniquely identified by the present-state and input values and represent the set of idle conditions that may be exploited to stop the clock. For example, for the FSM fragment in Figure 25, the only useful idle condition is the self-loop on S_3 (identified by input value 00 and state value S_3).

The *complete activation function* $F_a(x, s)$ is defined by the union of all self-loop conditions for Moore-states (x and s are respectively the input and state variables). The set of all self-loops in the FSM includes F_a, because it contains also the self-loops of Mealy-states.

The identification of the Moore-states can be performed implicitly (i.e., without extracting the STG) by a procedure that requires a single *unrolling* of the sequential circuit, i.e., duplicating the combinational logic to represent two consecutive time frames, as shown in Figure 26. There are two cascaded logic blocks: the inputs of the first combinational block are x and s, representing respectively primary and state inputs. The outputs are z and t. The next state outputs t of the first block are fed into the state inputs of the second block. The primary input values in the second

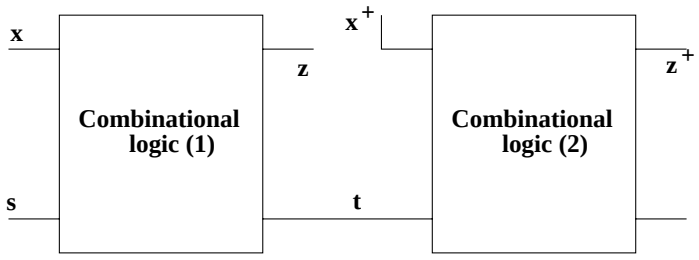

Figure 26: Unrolling of a FSM.

block are represented by x^+, while the output of the second block are z^+ and the next state outputs.

With this model, finding the Moore-states is quite simple. For a Moore state t, the following property holds: if in the second combinational logic block the state transition is a self-loop (i.e. $\delta(x^+, t) = t$), for each state transition $s \rightarrow t$ in the first block, the output $z = \lambda(x, s)$ and $z^+ = \lambda(x^+, t)$ are the same. Intuitively, this property expresses the requirement that every incoming edge for state t has the same output value, but we are interested only in states with self-loops, because otherwise no idle conditions are available. Finding all states for which the condition is true is equivalent to finding all Moore-states with self-loops, but no STG extraction is required. This procedure lends itself to an elegant symbolic formulation that will be described in the next section.

4.4 Symbolic Synthesis of the Clock Gating Logic

In this section we describe a symbolic algorithm to generate the clock gating circuitry and we discuss the issues related to the global optimizations that are enabled by the presence of the new logic into the circuit. The expression giving the activation

function F_a in symbolic form is the following:

$$F_a(x^+,t) = \prod_{i=1}^{k} \left(\delta_i(x^+,t) \equiv t_i\right) \cdot \forall_{x,s} \left(\prod_{i=1}^{m} \left(\lambda_i(x,s) \equiv \lambda_i(x^+,t)\right) \; + \; (\prod_{i=1}^{k} (\delta_i(x,s) \equiv t_i))' \right) \tag{4.24}$$

We analyze each term of the seemingly complex Equation 4.24 in greater detail.

- The term $\prod_{i=1}^{m}(\delta_i(x^+,t) \equiv t_i)$ imposes the condition that, in the second frame of the unrolled circuit, the machine has a self-loop. This is expressed by having each present-state variable t_i identical to the next state function $\delta_i(x^+,t)$.

- The term $\prod_{i=1}^{m}(\lambda_i(x,s) \equiv \lambda_i(x^+,t))$ describes the constraint on the output values. Since we are detecting Moore-states, we require that the output values of the incoming edge and the self-loop are the same. Notice that the unrolling implies the use of different variables for the two frames of the unrolled circuit.

- The term $(\prod_{i=1}^{m}(\delta_i(x,s) \equiv t_i))'$ is ORed with the second term to express the fact that the equality of the outputs in two frames does not need to be enforced for transitions not in the next state functions of the FSM.

The universal quantification on the inputs x and the state variables s enforces the condition for all states and input values. Is is important to notice that we do not use the transition relation of the FSM to compute F_a. This implies that we are considering all states as reachable, even if this is not generally true. Fortunately, this assumption does not lead to incorrect implementation.

To justify this claim, consider the following situation. Assume that state s_0 is unreachable, and for input i_0, $F_a(s_0,i_0) = 1$, in other words, the clock would be stopped when the state is s_0 and the input is i_0. However, since s_0 is unreachable, the state lines will never hold that state value, therefore the point s_0, i_0 in the *controllability don't care set* of F_a.

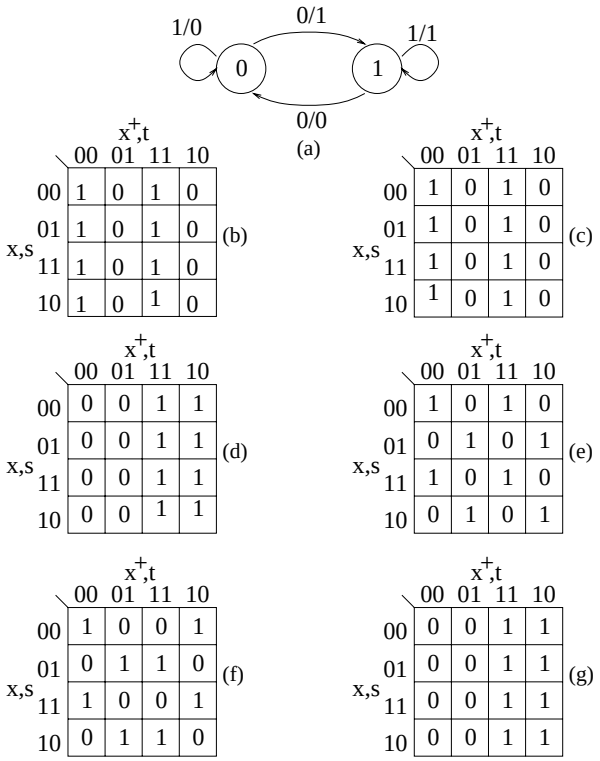

Figure 27: Example of symbolic computation of F_a.

The activation function F_a produced by Equation 4.24 is expressed in terms of the auxiliary variables (x^+, t) for convenience, and can be easily re-expressed as a function of the inputs x and present states s by variable renaming.

Example 4.4.1. Consider the FSM of Figure 27 (a). The next state function $\delta(x^+, t)$ and output function $\lambda(x^+, t)$ of the FSM are shown in Figure 27 (b) and (c), respectively. We represent Boolean functions using truth tables, which are conceptually equivalent to BDDs but more human-readable. The functions $\delta(x, s)$ and $\lambda(x, s)$ can be obtained by simply rotating the truth tables of $\delta(x^+, t)$ and $\lambda(x^+, t)$ by 90 degrees (clockwise), and are not shown.

The truth table of the first term in Equation 4.24 ($\prod_{i=1}^{m}(\delta_i(x^+, t) \equiv t_i)$) is shown in Figure 27 (d). The truth table of the second term ($\prod_{i=1}^{m}(\lambda_i(x, s) \equiv \lambda_i(x^+, t))$) is shown in Figure 27 (e), while the third term (i.e. $(\prod_{i=1}^{m}(\delta_i(x, s) \equiv t_i))'$) is shown in Figure 27 (f).

The truth table of the activation function $F_a(x^+, t)$ is shown in Figure 27 (g). The reader can verify the correctness of the result by observing that the F_a is

one in both self-loops of the STG. This is correct, since both states of the FSM are Moore-states. □

4.5 Optimizing the Activation Function

Direct application of Equation 4.24 yields, in the general case, functions whose power dissipation may partially mask off the potential power savings. Therefore, it is mandatory to develop a systematic method to reduce the power consumption of the implementation of F_a, while keeping as high as possible the probability of its ON-set.

The reader should notice that this is exactly the same problem discussed in Chapter 3 where we formulated an exact procedure for the minimization of a sum-of-product implementation of F_a. The two main limitations of such procedure were i) its high computational cost, ii) the fact that we are interested in minimizing power dissipation of F_a, thus minimizing the number of literals is only a rough approximantion.

In this section we address both limiations: the algorithms presented in this section are highly efficient because they operate directly on the BDD representation of F_a, moreover they explictly target the power minimization of a multi-level implementation of F_a.

First, we build a pseudo-Boolean function, P_{F_a}, which implicitly represents the probability of the minterms in the ON-set of F_a. Then, we iteratively remove from F_a some of its ON-set minterms until a given cost criterion breaks the loop. Clearly, both the minterm removal and the stopping condition must be guided by a combination of the size improvement in the implementation of F_a and the probability decrease of the ON-set of F_a. We have devised several heuristics that help in keeping together these two requirements.

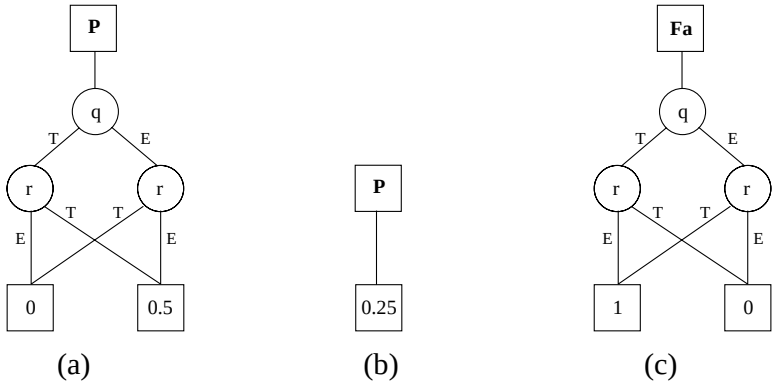

Figure 28: The ADD of a two-input probability distributions.

4.5.1 Computing P_{F_a}

Let us assume the pseudo-Boolean functions of the primary input probabilities, $P_{inputs}(x)$ and of the state occupation probabilities, $P_{states}(s)$, to be available (for the details on how these two functions can be computed implicitly using ADDs the reader may refer to Chapter 2). The probability P_{F_a} can be simply obtained as:

$$P_{F_a}(x,s) = P_{inputs}(x) \cdot P_{states}(s) \cdot F_a(x,s). \tag{4.25}$$

Obviously, P_{F_a} is stored as an ADD, whose paths from the root to the leaves give the probability of all the minterms in the ON-set of F_a. The total probability of the ON-set of F_a, (i.e., a real number) can then be computed by applying the ABSTRACT operator: $PROB(F_a) = \backslash^{+}_{x,s} P_{F_a}(x,s)$.

Notice that the ADD representation of the input probabilities $P_{inputs}(x)$ is complete and accurate. The ADD represents a discrete function that may theoretically have as many leaves as different values of x. Hence, we can represent exactly any generic input probability distribution where the inputs have arbitrarily complex correlations.

Example 4.5.2. Consider a circuit with two inputs q and r. Assume that the inputs can assume only the values 00 and 11 and that the occurrences of such patterns are equally probable. The probability the first input is $PROB(q =$

1) = .5 and the probability of the second input is $PROB(r = 1) = .5$. If we now consider an input probability distribution where all input patterns 00, 01, 10, 11 are equally probable, we still have $PROB(q = 1) = .5$ and $PROB(r = 1) = .5$, but the input streams associated with the two distributions are completely different.

Assume that $F_a = qr' + q'r$ (we neglect state variables for the sake of simplicity). We want to compute $PROB(F_a)$. If we exploit only the information on $PROB(p = 1)$ and $PROB(q = 1)$ we obtain $PROB(F_a) = .5(1 - .5) + (1 - .5).5 = .5$ for both input probability distributions. This is obviously incorrect, since $PROB(F_a) = 0$ for the first distribution, $PROB(F_a) = .5$ for the second.

The ADD representation allows us to capture the difference and to correctly estimate $PROB(F_a)$ in both cases. The ADDs of $P_{inputs}(x)$ for the two input probability distributions are shown in Figure 28 (a) and (b), respectively. The 0/1 ADD (i.e the BDD) of F_a is shown in Figure 28 (c). Multiplying the 0/1 ADD of F_a by $P_{inputs}(x)$ and applying the ABSTRACT operator lead to the correct $PROB(F_a)$ value in both cases. □

4.5.2 Iterative Reduction of F_a

Given the activation function, F_a, and its probability function P_{F_a}, the reduction algorithm iteratively prunes some of the minterms of F_a until an acceptable solution is found. The pseudo-code of the procedure is shown in Figure 29.

As mentioned earlier, the objective of procedure `Reduce_Fa` is to determine a new activation function, F_a^{Best}, which is contained into the original F_a, has a high global probability, and is less costly (in terms of both power and area) if compared to F_a. Three main routines are called inside `Reduce_Fa`:

- `Prune_Fa` eliminates some of the minterms of F_a producing a function whose *on set* is strictly contained into that of the origial F_a

- `Compute_Cost` evaluates the power cost of the implementation of the current F_a. It can be designed to take into account different cost metrics such as area and timing.

```
procedure Reduce_Fa(F_a, P_Fa) {
    F_a^Best = F_a; P_Best = P_Fa;
    F_a^Current = F_a; P_Current = P_Fa;
    Best_Cost = Compute_Cost (F_a^Current);
    while (not Stop_Test(F_a^Best,P_Best)) {
        F_a^Current = Prune_Fa (F_a^Current);
        Curr_Cost = Compute_Cost (F_a^Current);
        if (Curr_Cost ≤ Best_Cost) {
            F_a^Best = F_a^Current;
            P_Best = P_Current;
            Best_Cost = Curr_Cost;
        }
    }
    return (F_a^Best);
}
```

Figure 29: The `Reduce_Fa` Algorithm.

- `Stop_Test` is the exit condition. It returns one when it estimated that further reduction of the *on set* of F_a cannot improve the circuit's power dissipation.

The algorithm in Figure 29 is a simple greedy procedure that decreases the size of the activation function until the point of diminishing returns. The quality of the optimization depends on the implementation of the three routines `Prune_Fa`, `Compute_Cost` and `Stop_Test`. We discuss them in this order.

4.5.3 Pruning of F_a

We have experimented with two different pruning heuristics. The first one is based on the idea of removing from the ON-set of F_a the minterms whose probability is smaller than a relative, user-selected threshold, $\alpha \in [0, 1]$. Given the probability function $P_{F_a}(x, s)$, we first compute the maximum value of its leaves:

$$Max = \setminus_{x,s}^{MAX} P_{F_a}(x, s).$$

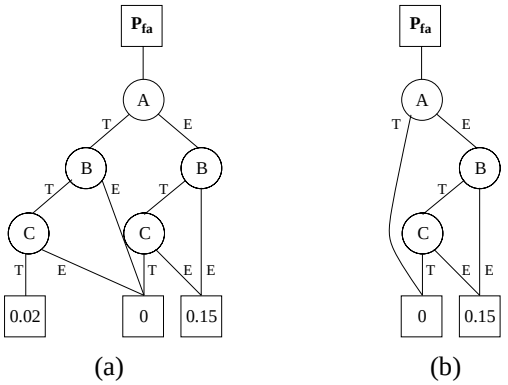

Figure 30: Pruning the activation function.

Then we set to 0 all the leaves of the $P_{F_a}(x,s)$ ADD whose values are smaller than αMax, and we set to 1 the remaining leaves. This is accomplished through an ad-hoc ADD operator called THRESHOLD; we denote as $\tilde{P}_{F_a}$ the so obtained ADD. Finally, the current activation function is computed by application of the ITE operator:

$$F_a^{Current} = \text{ITE}(\tilde{P}_{F_a}, F_a, 0).$$

Preserving a high probability for F_a is essential. However, it is equally important to keep the area of the clock gating circuitry under control. It is well known that reducing the number of minterms in the *on set* of a function does not guarantee that the size of the corresponding (optimized) circuit decreases. On the other hand, if some *on set* minterms are moved to the *don't care set* instead of the *off set*, then the final realization of the circuit can always be better optimized than the original function. To take this aspect into account, we need to generate the *don't care* function, $DC_{F_a}^{Current}$, associated with F_a, which can be computed as:

$$DC_{F_a}^{Current} = F_a \oplus F_a^{Current}. \tag{4.26}$$

Clearly, $DC_{F_a}^{Current}$ can be used to optimize $F_a^{Current}$ at each iteration of the reduction process.

Example 4.5.3. Consider the ADD of P_{F_a} shown in Figure 30 (a). The paths in the ADD leading to leaves of with non-zero value are minterms of F_a. Thus, the sum of products description of the full activation function is $F_a = ABC + AB + AB'C$, with empty *don't care* set. We now apply the pruning procedure, with $\alpha = .2$. The maximum leaf of the ADD has value .15, therefore, the THRESHOLD operator will prune all leaves with value smaller than $.15\alpha = .03$.

The ADD of $F_a^{Current}$ after pruning is shown in Figure 30 (b). Now the sum of products description of the reduced activation function is $F_a^{Current} = AB + AB'C$. The *don't care* set is $DC_{F_a}^{Current} = ABC$. □

In the rare cases where a large fraction of minterms of F_a has the same probability, we propose a solution based on the concept of BDD *subsetting* [ravi95]. We retain only the "dense" subset of minterms with probability p, in the hope that to a small ADD for the probability function corresponds a compact logic circuit realizing the reduced F_a. Experimental evidence has proved this choice to be effective.

The reduction technique outlined above uses as primary pruning criterion the probability of the minterms to be added to the don't care set. An alternative heuristic is reminiscent of the strategy presented in [alid94], and it is based on the key observation that reducing the number of variables in the support of F_a may cause a reduction in the size of its implementation, since the number of circuit inputs decreases accordingly. The second heuristic selects a variable x_i to be eliminated from the support of F_a based on the probability of the universal abstraction $q_i = \forall_{x_i} F_a(x)$. Variables with the highest $P(q_i)$ are eliminated, one at a time, until a user-selected cost requirement (which accounts for both the total probability of the reduced F_a and the size of its implementation) is met. Also in this case, the reduced activation function can be further optimized at each iteration of procedure `Reduce_Fa` by using the *don't care* information that can be computed using Equation 4.26.

4.5.4 Computing the Cost of Function F_a

The pruning heuristics described in the previous section use, as driving criterion, the total probability of the reduced activation function as well as the size of its implementation. However, the ultimate objective of the optimization algorithm is the reduction of the dissipated power of the overall design. Therefore, the cost function we employ to decide whether the current solution is acceptable considers power as primary target. We have considered three different options of increasing accuracy and computational cost.

1. $Curr\_Cost = \text{POWER}(Circuit)(1 - PROB(F_a^{Current})) + \text{POWER}(F_a^{Current})$.
   This is the simplest cost function; POWER(*Circuit*) is the average power dissipation of the original circuit, computed through Monte-Carlo or symbolic simulation. POWER($F_a^{Current}$), on the other hand, is the average power dissipation of an optimized multi-level implementation of $F_a^{Current}$. The first term of the summation represents an estimate of the expected power dissipation of the circuit when clock gating is present. The second contribution is the additional power consumed by the activation function. The biggest source of approximation is in the assumption that the power of the gated-clock circuit (excluding the activation function) scales linearly with the probability of $F_a^{Current}$. The advantage of this cost function stands in its limited computational requirements, since POWER(*Circuit*) is calculated once and for all before starting the F_a reduction process. The negative side is, obviously, that the possibly beneficial effects of simplifying the logic of the overall circuit using $F_a^{Current}$ as external *don't care set* are not accounted for. In contrast, POWER($F_a^{Current}$) is clearly recomputed for each new activation function, that is, at each iteration of the `Reduce_Fa` algorithm.

2. $Curr\_Cost = \text{POWER}(F_a^{Current} + Circuit)$.

   This is a more accurate cost function. Each $F_a^{Current}$ is first synthesized and optimized, and then connected to the original circuit as in Figure 24-b. The power dissipation of the overall network is then estimated. The improved accuracy of this cost function stems from the fact that it does not assume that the power saved in the FSM is proportional to the probability of the activation function. On the other hand, the complexity of the computation is increased because a power estimation of the FSM and the activation function is required at each iteration.

3. $Curr\_Cost = \text{POWER}(\text{OPTIMIZE}(F_a^{Current} + Circuit))$.

   This is the most accurate cost function. Each $F_a^{Current}$ is first synthesized and optimized, then it is connected to the original circuit, and the so obtained global network is optimized using standard techniques which exploit $F_a^{Current}$ as additional external *don't care set*. Notice that the complexity of this cost function is much higher than the previous two. In this case, the computationally intensive logic minimization of the FSM logic is performed for each cost evaluation. In fact, using this cost function is equivalent to generating a set of solutions and estimating the power savings for each one.

We choose the first cost function for the final implementation, because its (relative) low computational cost allowed us to generate and evaluate a much larger number of reduced activation functions. However, the second activation function may be the preferred choice for a conservative version of our algorithm. The first cost function may lead to incorrectly predicting power savings for cases where actually there is power increase. For some circuits the power savings in the FSM logic and flip-flops may grow less than linearly with the probability of the activation function. If this is the case, the first cost function will bias the algorithm toward excessively complex

(and power consuming) high-probability activation functions.

In contrast, the second cost function is strictly conservative because it assumes that the clock gating logic is added to the original circuit (i.e. it is fully redundant), then, power is estimated for the full gated-clock implementation. Compared to the third cost function, the second one is only more conservative, because it does not estimate the possible additional power reductions obtainable by optimizing the combinational logic of the FSM using F_a as *don't care set*. As a result, using the second activation function may lead to convergence on excessively small activation functions (with almost no power savings), but it will never lead to circuits with increased power consumption compared to the initial implementation without gated-clock.

The third cost function was not used because of its excessive computational cost, since the time spent in the optimization of the FSM logic completely swamps the time spent in all other parts of the optimization procedure. Including this expensive step in the inner loop of the optimization procedure would intolerably slow town the search.

4.5.5 The Stopping Criterion

As in any gradient-based refinement procedure (where the iterations continue as long as there are improvements, and stop as soon as the cost function starts increasing again), we reduce the *on set* of F_a at each iteration and we exit the reduction loop the first time the cost function starts increasing, i.e., $Curr\_Cost > Best\_Cost$. This choice is based on following observation. The reduction of the activation function is such that the newly generated F_a is contained into the one generated at the previous iteration, and therefore once a minimum is hit, it is difficult to hit another one. This argument is plausible as long as the circuitry implementing F_a and the original circuit are kept separated (this is the assumption made by the first two cost functions). In fact, in this case, a smaller activation function improves the power dissipation only

by reducing the consumption in the clock-gating circuitry. A size reduction of F_a that increases the power implies that the power not saved in the circuit is larger than the power saved in the clock-gating circuitry, and using an even smaller activation function will only make this situation worse.

However, reality is more complex. If we use the most accurate cost function, this line of reasoning may no longer be correct. This is because a complex F_a with a large ON set may enable drastic optimizations in the logic of the FSM. Remember that the ON set of F_a is used as *don't care set* for the optimization of the FSM logic. It is clear then that, due to the complexity of the third cost function, finding a direct relationship between such function and the optimality of the computed solution is not an easy task. Moreover, the computational complexity of the third cost function prevents its use for any large scale example. We therefore chose to trade off some loss in optimality of results for the applicability of our method to large circuits.

4.6 Global Circuit Optimization

The result produced by procedure `Reduce_Fa` is a gate-level specification of the activation function, F_a, which is expected to reduce power dissipation when appropriately connected to the original sequential design.

After the logic is included in the circuit in the way shown in Figure 24-b, some global optimization can be performed. Notice that the activation function is functionally redundant. Since we employed redundancy removal procedures targeting area minimization rather than power minimization, the optimizer may remove the clock-gating logic in its entirety, thus producing a circuit which is very similar to the original one. This is most likely to happen when F_a is used as external *don't care set* for each primary and state output and redundancy removal methods are used for the optimization. Clearly, this is something we must avoid.

The solution we have adopted to overcome this problem consists of adding to the circuit an extra output pin to make function F_a directly observable. With this artifact, redundancy removal procedures can be applied to the circuit. This type of optimization has highly beneficial effects on the gated-clock circuits: not only it may reduce the power dissipation, it also increases the testability of the system, because it eliminates the untestable faults in the combinational logic generated by the insertion of the redundant clock-activation logic [fava96]. Testability issues regarding gated-clock FSMs are addressed in more detail in Appendix A

4.7 Covering Additional Self-Loops

If a sequential circuit is an implementation of a Mealy FSM with no Moore-states, the activation function obtained by Equation 4.24 is the null function **0**. In this section we discuss generalizations of the procedure used to find the initial F_a that allow the exploitation of different kinds of idle conditions.

We target self-loops on Mealy states. As discussed above, these self-loops are not idle conditions because we cannot guarantee that output transitions will not be required, even if the next state does not change. While in Chapter 3 we solved the problem by transforming the STG, we now investigate the alternative solution: the outputs of the sequential circuit are taken as inputs of the activation function as well as the state and primary inputs.

The gated-clock architecture can be modified as shown in Figure 31. If all outputs are taken as inputs of the activation function, *all self-loops can be exploited to stop the clock*. As an example, consider again Figure 25: if we are allowed to observe the output values, then a state value of S_2, an input value 00, and an output value 11 uniquely identifies the self-loop in S_2. Observing these values we can stop the clock because: i) the FSM is in a self-loop, ii) the output is not going to change in the next

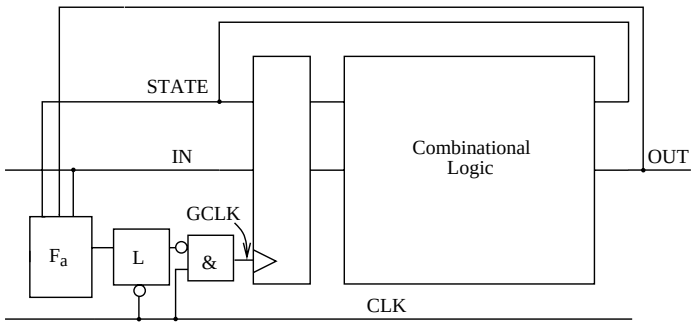

Figure 31: Modified Gated-Clock Architecture to Take into Account Circuit Outputs.

clock cycle.

The expression of the activation function including output values is very similar to the one presented in Equation 4.24:

$$F_a(x^+, t, z^+) = \prod_{i=1}^{k} (\delta_i(x^+, t) \equiv t_i) \cdot \forall_{x,s} \left(\prod_{i=1}^{m} \lambda_i(x^+, t) \equiv z_i^+) \ + \ (\prod_{i=1}^{k} (\delta_i(x, s) \equiv t_i))' \right) \tag{4.27}$$

Notice that the support of F_a has been extended to include the output variables z^+. The term $\prod_{i=1}^{m}(\lambda_i(x^+, t) \equiv z_i^+)$ expresses the condition that the observed output value must be equal to the output that would be computed if we clocked the machine when traversing a self-loop. If this is true, we do not need to clock the FMS, hence, $F_a = 1$. This term is the main difference between Equation 4.24 and Equation 4.27: since we have increased the input support of F_a, we now possess additional information for stopping the FSM more frequently.

We observed in Chapter 3 that the number of outputs in a sequential circuit is often very large, thus, the size of the activation logic may increase too much if we include all outputs in its support. However, it is often the case that we do not need to use *all outputs* as inputs of F_a. For example, referring to Figure 25, to exploit the self-loop on S_2 it is sufficient to sample the second output, because the first output does not change on all transition reaching S_2. Formula 4.27 can be modified so that

only a subset of the outputs becomes part of the support of F_a. We have:

$$\begin{aligned} F_a(x^+,t,z^+) &= \prod_{i=1}^{k}(\delta_i(x^+,t)\equiv t_i)\ \cdot \\ &\quad \forall_{x,s}\left(\prod_{i=1}^{w}(\lambda_i(x^+,t)\equiv z_i^+)\cdot \prod_{i=w+1}^{m}(\lambda_i(x,s)\equiv\lambda_i(x^+,t))+\right. \\ &\quad \left.(\prod_{i=1}^{k}(\delta_i(x,s)\equiv t_i))'\right) \end{aligned} \tag{4.28}$$

where w is the number of circuit outputs we want to include in the support of the activation function. Equation 4.28 can be seen as a compromise between Equation 4.24 and Equation 4.27. The smaller w is, the closest the activation function is to the one computed by Equation 4.24.

There is clearly a trade-off between the additional self-loops that can be included in the activation function by adding one or more outputs to its support and its size (and power dissipation). We have devised the following heuristic procedure to perform the selection of an optimal subset of outputs for inclusion in the support of the activation function.

- For each output, z_i^+, we first compute $F_a(x^+,t,z_i^+)$ and we determine the value of its probability. Notice that $F_a(x^+,t,z_i^+)\geq F_a(x^+,t)$, therefore $P_{F_a(x^+,t,z_i^+)}\geq P_{F_a(x^+,t)}$.

- We build $F_a(x^+,t,z^+)$ incrementally by adding to the previously computed activation function the new activation function obtained by inserting one more output in its support. The outputs are picked in order of decreasing $P_{F_a(x^+,t,z_i^+)}$. In symbols:

$$F_a^{(0)} = F_a(x^+,t) \tag{4.29}$$

$$F_a^{(k)} = F_a^{(k-1)} + F_a(x^+,t,z_1^+,z_2^+,...,z_k^+) \tag{4.30}$$

The first activation function $F_a^{(0)}$ is the one computed by Equation 4.24.

The rationale behind the procedure is that we want to increase the support of F_a by adding first the outputs that contribute more to increasing the total probability of F_a. After each new $F_a^{(k)}$ is generated, we optimize the activation function with the algorithm described in Section 4.5. The best optimized activation function is chosen. To reduce the computational burden we stop the generation of new $F_a^{(k)}$ as soon as increasing k by one leads to a new activation function that, after optimization, performs worse than the last computed one.

4.8 Experimental Results

The power optimization algorithms of this chapter have been implemented within the SIS [sent92] environment, and their effectiveness benchmarked onto some examples taken from the literature.

The original synchronous circuits have been optimized for area through the SIS script `script.rugged` and mapped for speed using the SIS command `map -n 1 -AFG`. These mapped circuits have been used as the starting point for our experiments. The logic for the reduced activation function has been computed through procedure `Reduce_Fa` and connected to the original circuit as indicated in Figure 24-b. The functional specification of F_a has then been added as external *don't care set* for each circuit output, and the circuit optimized for area through `script.rugged`.

The library we used for the experiments had NAND and NOR gates with up to four inputs, and buffers and inverters with 3 different size/drive options. Power values of the initial and final circuit implementations were obtained using Irsim [salz89]. All the experiments were run on a DEC-Station 5000/240 with 64 MB of memory.

Tables 3 and 4 summarize our results obtained on some `Iscas'89` synchronous networks [isca89]. In particular, columns *PI*, *PO* and *FF* of Table 3 show the characteristics of the circuits. Column *Gates*, *Delay* and *Power* tell the number of gates,

Circuit	*PI*	*PO*	*FF*	*Before Optimization*			*After Optimization*		
				Gates	*Delay*	*Power*	*Gates*	*Delay*	*Power*
`s208.1`	10	1	8	90	11.00/10.98	75	95	11.07/ 11.05	49
`s298`	3	6	14	131	19.26/19.24	89	140	19.90/19.88	72
`s386`	7	7	6	148	14.94/14.92	63	160	15.97/15.95	58
`s400`	3	6	21	168	20.81/20.79	90	185	21.14/21.12	63
`s420.1`	18	1	16	171	16.42/16.40	106	185	17.61/17.59	67
`s444`	3	6	21	199	20.31/20.29	101	217	22.12/22.10	76
`s510`	19	7	6	289	25.62/25.60	95	306	27.31/27.29	81
`s526`	3	6	21	206	18.24/18.22	119	230	19.83/19.81	114

Table 3: Results for Some `Iscas'89` Circuits.

the rise and fall delays (in *nsec*), and the power dissipation (in μW), before and after optimization. Columns *Variation* in Table 4 give the percentage of gate count and delay increase and power reduction obtained on each example. Finally, column F_a *Time* reports the CPU time (in *sec*) required by procedure `Reduce_Fa` to determine the simplified activation function.

The cost function used for the the experiments is the first one introduced in Section 4.5.4. We have tested both pruning heuristics for the generation of the optimal F_a, but the quality of the results did not change sensibly (for the results in the table we report the best obtained savings).

The size (and the number states, exponentially related to the number of flip-flops) of the circuits considered in our experiments is such that the application of the techniques presented in Chapter 3 would be impractical, because of the complexity of the STG extraction procedure. In contrast, our symbolic algorithms easily deal with these examples, even with the limited memory available on our machine. To our knowledge, these are the largest sequential circuits for which gated clocks have been automatically generated. For some examples the power savings are sizable (25%-35%), while for others almost no advantage is given by gating the clock. The area

Circuit	*Variation*			F_a *Time*
	Gates	*Delay*	*Power*	
s208.1	+5%	+1%	−34%	7.3
s298	+7%	+3%	−19%	17.8
s386	+8%	+7%	−8%	69.9
s400	+10%	+2%	−30%	80.1
s420.1	+8%	+7%	−36%	150.3
s444	+9%	+9%	−25%	51.0
s510	+6%	+6%	−15%	301.3
s526	+11%	+9%	−4%	120.2

Table 4: Variations in area delay and power, and runtime for some Iscas'89 Circuits.

Circuit	*PI*	*PO*	*States*	*Power Savings*	
				Symbolic	*Explicit*
bbara	4	2	10	45%	49%
bbtas	2	2	6	12%	21%
keyb	7	2	19	26%	11%
lion9	2	1	9	10%	13%
s420	19	2	18	24%	18%

Table 5: Comparison to the Results of the previous chapter on the Mcnc'91 FSMs.

and the delay are kept under control (8% and 5%, increase, on average).

4.8.1 Comparison with the explicit technique

In Table 5 we compare the power savings achieved by the symbolic method to those obtained in the previous chapter for some of the small, Mcnc'91 FSMs [mcnc91] (chosen among those for which the explicit algorithm produced the largest savings). From the results we can conclude that the symbolic approach is not much worse than the explicit approach, even for FSMs of small size.

The comparison reveals that in some cases the Locally-Moore transformation described in the previous chapter performs better than the output inclusion technique of Section 4.7, but this is not always true. This fact can be explained by observing that the Locally-Moore transformation increases the complexity of the FSM logic itself, while the output inclusion technique has more controllable effects, since it modifies only the structure of the activation function.

4.8.2 Effect of input statistics

Since the reactive nature of a controller typically depends on the external environment, it is likely to happen that idle conditions are exercised when the circuit is interacting with the components in its neighborhood. We mentioned before that such interaction may be modeled through non-equiprobable primary input distributions. Since the computation of the activation function depends on the input probabilities, we expect the size and the probability of F_a to be affected by the use of non-equiprobable input distributions.

We consider, as an example, the `minmax3` circuit [coud89], a sequential circuit that finds the maximum and the minimum of a stream of numbers. The circuit has 3 inputs: *clear*, used to reset the maximum and minimum values, *enable*, whose function is to prevent the circuit from analyzing some data and the input data port. We plot the value of $PROB(F_a)$ for varying values of the probability of the `enable` (active high) and `clear` (active low) control inputs (see Figure 32).

For a fixed value of the probability of `clear`, $PROB(F_a)$ increases as the probability of `enable` decreases, and it goes up as the probability of `clear` increases. This is reasonable, since a high probability of both `enable` and `clear` to be active drives the circuit into the hold states, corresponding to the traversal of the self-loops of the STG.

To show how the knowledge of the primary input statistics impacts the synthesis

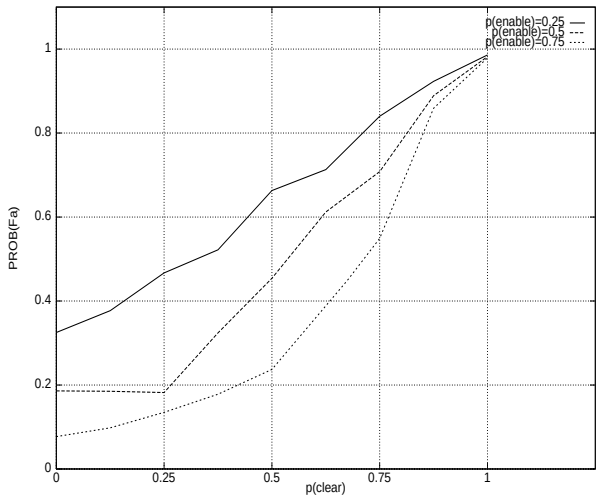

Figure 32: Case Study: The `minmax3` Circuit.

and the refinement of the activation function, and thus the power savings achievable with our optimization technique, we present results for the same circuits of Table 3 in which the probability of some of the inputs has been set to values different from 0.5.

Since no information was available for both the circuit functionalities and the environment in which the controllers are supposed to operate, we have chosen to modify the statistics of the primary inputs belonging to the support of the activation function calculated for the equiprobable case. More specifically, we have set the input probabilities so as to emphasize the reactivity of the benchmarks. As expected, power savings have gone up sensibly.

The results of Table 6 confirm that power is a strongly pattern-dependent cost function. It is therefore important to formulate algorithms for power minimization that can take input statistics into account with the highest possible accuracy. We showed in Section 4.5 that the ADD-based input statistic characterization is much more accurate than the simple information provided by input probabilities. As a consequence, our gated-clock generation algorithm is very flexible and effective even

Circuit	*Equiprobable Inputs*				*Non-Equiprobable Inputs*			
	$PROB(F_a)$	*Power*			$PROB(F_a)$	*Power*		
		Orig.	*Opt.*	*Savings*		*Orig.*	*Opt.*	*Savings*
s208.1	0.314	75	49	34%	0.831	64	17	73%
s298	0.241	89	72	19%	0.902	53	10	81%
s386	0.110	63	58	8%	0.642	52	18	65%
s400	0.249	90	63	30%	0.809	67	15	77%
s420.1	0.311	106	67	36%	0.829	90	21	76%
s444	0.249	101	76	25%	0.811	69	19	72%
s510	0.140	95	81	15%	0.670	81	45	44%
s526	0.244	119	114	4%	0.798	88	43	51%

Table 6: Results for Different Input Probability Distributions.

for complex input statistics with strong correlation between inputs.

4.9 Summary

In this chapter, we presented a fully symbolic approach to the automatic generation of clock-gating logic for control-oriented sequential circuits. Our methodology starts from synchronous networks and does not require the extraction of the STG, a very computationally expensive operation. We leverage the BDD-based representation of Boolean and pseudo-Boolean functions to extend the applicability of clock-gating techniques to classes of sequential systems of size unattainable by previous methods based on explicit algorithms.

The generality of our symbolic formulation enables the application of the synthesis procedure to activation functions with extended support (including some of the circuit outputs). The compactness and expressive power of ADDs allow us to accurately compute the probability of the activation function, and to formulate algorithms that control the optimization of the global power dissipation with superior accuracy,

compared to previous methodologies.

Our power optimization strategy also relies on an integrated synthesis methodology that aims at reducing the overhead of the redundant clock-gating logic by effectively exploiting the additional *don't care* conditions in the combinational logic. The results are promising, since we obtain power reductions as high as 36%.

Further investigation on this subject will focus on several directions. First, approximate algorithms for FSM probabilistic analysis need to be developed to further enhance the scope of applicability of this technique. This is because the real bottleneck of the symbolic approach is the ADD-based calculation of the exact state occupation probabilities, which becomes infeasible when the circuits contain more than 50 registers. Constructing and pruning the activation function, on the other hand, is neither computationally intensive nor too memory demanding. Second, the problem of estimating the impact of the activation function as additional *don't care set* has to be factored into an efficiently computable cost function.

Chapter 5

FSM decomposition for low power

5.1 Introduction

In the previous chapters we demonstrated that clock gating is an effective technique for minimizing wasted power. Sizable power reduction are obtained for reactive FSMs that are idle for a large fraction of the operation time. In this chapter we investigate a more aggressive approach: we attempt the minimization of the useful power dissipation. In other words, we focus on reducing power consumption in sub-systems that may be idle for a small fraction of the operation time. For such systems, the clock-gating techniques presented so far are not effective.

The fundamental intuition behind the optimization techniques presented in this chapter is that a sequential circuit may be decomposed into a set of small interacting blocks. During operation, only one block is active at any given time and controls the input-output behavior. In the remaining blocks, the clock can be stopped and, consequently, the total power consumption is reduced. Obviously, a decompostion approach allows us to save power even for systems that are never idle.

Unfortunately, in many cases the behavior of the system is specified without any

consideration for *power-efficient decompositions*. Hence, we need to develop procedures for the detection of such decompositions and the synthesis of a hardware architecture where unused parts of the system can be shut down without compromising the correctness of the global input-output behavior.

We propose a procedure for the automatic synthesis of a network of interacting FSMs starting from a single state-table specification (or an equivalent format). We call *decomposed FSM* the interacting FSM implementation. The straightforward single-machine implementation is called *monolithic FSM*. The monolithic finite-state machine can be decomposed into smaller sub-machines that communicate through a set of interface signals. *Usually, one single sub-machine is clocked* at any given time and it controls the outputs values while all other sub-machines are idle: they do not receive the clock signal and dissipate little power. When a sub-machine terminates its execution, it sends an *activation signal* to another sub-machine which takes control of the computation, then it de-activates itself. This transition is characterized by a single cycle for which both sub-machines are clocked.

There is full cycle-by-cycle equivalence between the input-output behavior of the decomposed and monolithic implementation. It the FSM is embedded in a larger system, the decomposed implementation can replace the monolithic one and the beahvior of the system remains unchanged.

Given the state transition graph (STG), or equivalently, the state table of the FSM, our procedure decomposes the STG into a set of smaller STGs. Each component is then synthesized using standard FSM synthesis algorithms. The resulting sequential circuits are then connected and dedicated clock-control circuitry is synthesized, which allows selective clocking of the sub-FSMs. The final result is a circuit that is functionally equivalent to the original specification but has reduced power dissipation and increased speed compared to an monolithic implementation of the specification.

The total area of the interacting FSM implementation is larger than that of the monolithic counterpart. Notice however that the increase in area is accompanied by more hierarchical structure: the interacting FSMs implementation consists of small and loosely coupled blocks instead of one large highly coupled block. This characteristic can be very useful during synthesis and the placement and routing phase: small blocks are more effectively synthesized, placed and connected. Consequently the improved power and performance of our implementation will not be damaged by excessive wiring even if it has area overhead. Accurate power and timing estimation shows that the decomposed implementation achieves on average 31% power reduction and 12% speed improvement at the price of a 48% increase in the number of standard cells. Since our method trades off power reduction and speed increase for area usage, it is well-suited for high-performance VLSI systems where speed and power are the primary concerns.

It is important to notice that our technique is compatible with sequential power minimizations such as state assignment [hahe94, tsui94] (see also Chapter 6) and retiming [mont93], as well as power optimization of the combinational logic [iman96, baha95, rofl96]. Indeed, after FSM decomposition, the power minimization techniques can be applied to its components.

5.1.1 Previous work

Finite-state machine decomposition has been extensively studied for several decades. Its theoretical foundations were laid down by Hartmanis and Stearns [hart66] in the sixties. Hartmanis and Stearns defined several flavors of decomposition and formulated numerous decompostion procedures. More recent work [geig91] reports experimental result on the implementation of the decomposition procedures described in [hart66].

A different viewpoint on the problem was proposed in recent years by Ashar,

Devadas and Newton [asha91] who presented numerous algorithms for the automatic decomposition of FSMs specified by an monolithic state transition graph (STG). In this work, the authors introduced the concept of *factorization* (an efficient algorithm to detect and exploit decomposition opportunities) as well as exact and heuristic solutions to the problem of two-way FSM decomposition for minimum-area two-level implementation. The work by Hartmanis and Stearns is based on an algebraic model of FSMs rooted in lattice theory. By contrast, Ashar et al. rely on Boolean algebra as the underlying theoretical framework.

More recent work is based on graph theory [royn93, kuo95]. The STG of the FSM is decomposed using graph partitioning algorithms. Our approach has several points in common with [royn93]. Most notably, our approach and [royn93] both focus on a partitioning strategy, where the initial FSM is decomposed in sub-modules that are never performing useful computation at the same time. However, we target the minimization of power consumption and we rely on a different assumption on the hardware implementation (i.e. gated clock versus single clock).

The algorithms mentioned so far target area minimization, or the optimization of area-related cost functions (i.e. number of input and outputs, connectivity). Although sizable area reductions can be achieved, the average effectiveness of decomposition techniques for area is not impressive, mainly for two reasons. First, the majority of real-life FSMs do not have a simple decomposition, and some replication is almost always required. Second, the computational requirements of the exact decomposition algorithms are too high on large examples (where the potential savings are substantial), and heuristic solutions fail to find good decompositions.

We believe that the potential impact of decomposition techniques for low power and high performance is much higher. This conjecture is confirmed in [hasa95], where

decomposition techniques have reported very promising delay reductions on multi-level logic implementation. The experimental results presented in this chapter provide convinging evidence on the effectiveness of the tecompositon approach for power minimization.

5.2 Interacting FSM structure

Let $F = (X, Y, S, s_0, \delta, \lambda)$ be an monolithic Mealy-type FSM specification, where X is the input set, Y the output set, S the set of states, $s_0 \in S$ the reset state. The next state function is $\delta : X \times S \rightarrow S$ and the output function is $\lambda : X \times S \rightarrow Y$.

Assume that a *partition* Π on S is given [hart66]. A partition is defined as a collection of n disjoint subsets of S whose set union is S, i.e $\Pi(S) = \{P_1, P_2, ..., P_n\}$, such that $P_i \cap P_j = \emptyset$ for $i \neq j$, and $\bigcup_{i=1}^{n} P_i = S$. We call *partition blocks* the subsets P_i.

Given the monolithic F and $\Pi(S)$ we proceed to the formal definition of the decomposed FSM. The decomposed FSM Φ is a set of n FSMs $\Phi = \{F_1, F_2, ..., F_n\}$. We call *sub-machines* the FSMs $F_i \in \Phi$. A generic sub-machine F_i is defined as $F_i = (X_i, Y_i, S_i, s_{0,i}, \delta_i, \gamma_i)$, where:

- $s_{0,i}$ is the reset state of F_i.
- S_i, the state set of F_i is $S_i = P_i \cup \{s_{0,i}\}$.
- The input set X_i is $X_i = X \cup GO_{-,i}$. We define $GO_{-,i}$ as follows. For each transition from a state $t \in P_j$ to a state $s \in P_i$ in the monolithic FSM F, a new signal $go_{t,s}$ is created which is an input for F_i and an output for F_j. The set $GO_{-,i}$ is the set of all *go* signals which are inputs for F_i. In symbols: $GO_{-,i} = \{go_{t,s} \mid \delta(\cdot, t) = s,\ s \in P_i,\ t \in P_j,\ P_i \neq P_j\}$

- The output set Y_i is $Y_i = Y \cup GO_{i,-}$. The set $GO_{i,-}$ is the set of all *go* signals which are outputs for F_i: $GO_{i,-} = \{go_{t,s} \mid \delta(\cdot,t) = s,\ s \in P_j,\ t \in P_i,\ P_i \neq P_j\}$

- The next state function $\delta_i(x, go_{q,t}, s)$ is defined as follows:

$$\delta_i(x, go_{q,t}, s) = \begin{cases} \delta(x,s) & if\ s \in P_i\ and\ \delta(x,s) \in P_i \\ s_{0,i} & if\ s \in P_i\ and\ \delta(x,s) \in P_j,\ P_i \neq P_j \\ t & if\ s = s_{0,i}\ and\ go_{q,t} = 1,\ q \in P_j,\ t \in P_i,\ P_i \neq P_j \\ s_{0,i} & if\ s = s_{0,i}\ and\ \forall go_{q,t} \in GO_{-,i}\ go_{q,t} = 0 \end{cases} \tag{5.31}$$

  The definition means that every transition between states s and t in the monolithic FSM does not change its source and destination if the two states belong to the same block P_i (this case is shown in Figure 33 (a) and (b)). A transition from s to t belonging to different partition blocks, respectively P_i and P_j, becomes: i) a transition from s to the reset state of machine F_i; ii) a transition from the reset state to t for machine F_j. When a sub-machine F_i is in reset state, it exits from it only when one of the *go* signals is set to one.

- The output function $\lambda_i(x, go_{q,t}, s)$ takes values on the new output set Y_i that includes the original outputs of the monolithic FSM and the *go* outputs. We represent the output value with the notation (x, go).

$$\lambda_i(x, go_{q,t}, s) = \begin{cases} (\lambda(x,s), \mathbf{0}) & if\ s \in P_i\ and\ \delta(x,s) \in P_i \\ (\lambda(x,s), go_{s,t} = 1) & if\ s \in P_i\ and\ \delta(x,s) = t \in P_j,\ P_i \neq P_j \\ (\mathbf{0}, \mathbf{0}) & otherwise \end{cases} \tag{5.32}$$

  We used the shorthand notation $(x, \mathbf{0})$ to indicate that all *go* outputs or are held at value 0. Similarly, the notation $(\mathbf{0}, \mathbf{0})$ is used to indicate that all original outputs in set X and all *go* signals are held at value 0. The notation $go_{s,t} = 1$ is used to indicate that only one *go* output has non-zero value, namely $go_{s,t}$.

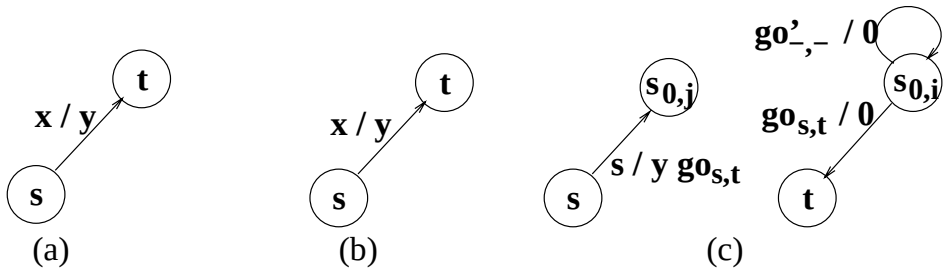

Figure 33: Pictorial representation of the definitions of δ_i and λ_i

The definition of λ_i means that whenever there is a transition between two states belonging to the same P_i, the output of sub-machine F_i is the same as in the monolithic FSM. A transition toward the reset state has the output value corresponding to the transition in the monolithic FSM between state s in S_i and state t in S_j, and asserts the $go_{s,t}$ output. All outputs are zero for the self-loop on $s_{0,i}$ and all transitions leaving $s_{0,i}$.

The definition of the sub-machines F_i completely defines our decomposition strategy. To better understand the definitions of δ_i and λ_i refer to Figure 33. Part (a) shows a transition in the monolithic FSM. Part (b) shows the transition in the decomposed FSM when its source and destination state both belong to the same partition block P_i (the transition is unchanged). Part (c) shows the case when the source and destination state belong to different partition blocks. For each transition leaving a state sub-set P_i in the monolithic FSM, the sub-FSM F_i associated with P_i performs a transition to its reset state. On the other hand, a transition entering a sub-set P_i from $P_i \neq P_j$ corresponds to a transition exiting the reset state in the sub-FSM F_i. A sub-machine can exit the reset state only upon assertion of a *go* signal by another submachine. At any given clock cycle only two situations are possible: i) one sub-machine is performing state transitions and all other sub-machines are in reset state, ii) one sub-machine is transitioning toward its reset state, while another one is leaving it.

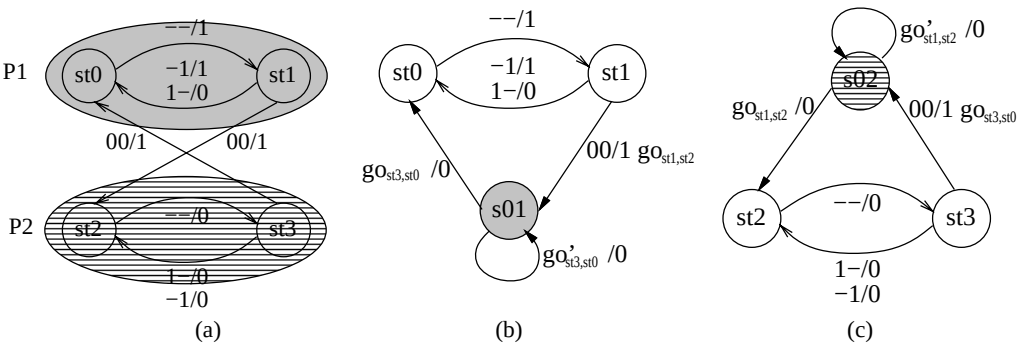

Figure 34: Decomposition of the monolithic FSM

All inputs and outputs of the monolithic FSM are inputs and outputs of the sub-machines. The *go* signals are new, additional inputs and outputs. If an edge $s \rightarrow t$ of the original machine has head and tail state included in sub-machine F_i, the edge is replicated in F_i, with the same input and output fields. Edges in the global FSM connecting states which belong to different partitions are associated with edges representing transitions to and from the reset states of the corresponding sub-FSMs. These transitions are labeled as follows: i) edges toward reset have the same input field as the original edge, assert an additional output $go = 1$ and have the same output field as in the original transition edge of the monolithic FSM. ii) Transitions leaving reset have only one specified input *go* and all outputs set to zero. The outputs of a sub-machine blocked in reset state are zero.

Example 5.2.1. Consider the FSM in Figure 34 (a). We assume that the state partition is $\Pi(S) = \{P_1, P_2\} = \{\{st0, st1\}, \{st2, st3\}\}$. The two sub-machines created by the decomposition procedure are shown in Figure 34 (b) and (c). The additional reset states are shaded. P_1 originates sub machine (b) and P_2 originates sub machine (c). Notice that the "go" signals are shown only on the transitions from and to the reset states. A sub-machine asserts a "go" signal only when transitioning to the reset state, in all other cases the signal has value zero. Similarly, a submachine is sensitive to input "go" signals only when it is in reset state. The "go" inputs are not observed for all other transitions. □

After describing our decomposition strategy, we now focus on how to reduce the

total power dissipation of the interconnection of sub-FSMs.

5.2.1 Clock gating

In the interacting FSM system, most of the machines F_i remain in state $s_{0,i}$ during a significant number of cycles. If we stop their clock while they stay in reset state, we would save power (in the clock line, the flip-flops and in the FSM combinational logic) because only a part of the system is active and has significant switching activity. To be able to stop the clock, we need to observe the following conditions.

- The condition under which F_i is idle. It is true when F_i reaches the state $s_{0,i}$. We use the Boolean function $is\_in\_reset_i$ that is 1 if F_i is in state $s_{0,i}$, 0 otherwise.

- The condition under which we need to resume clocking, even if the sub-FSM is in reset state. This happens when the sub-FSM machine receives a *go* signal and must perform a transition from s_{0i} to any other state.

We can derive $F_{a\,i}$, the *activation function* (in negative logic). The clock to F_i is halted when $F_{a\,i} = 1$. Namely:

$$F_{a\,i} = is\_in\_reset_i \wedge \overline{(\bigvee_{q \in F_i, p \in F_j \neq F_i} go_{p,q})} \tag{5.33}$$

The first term $is\_in\_reset_i(s)$ stops the clock when the machine reaches $s_{0,i}$. The second term ensures that clock is not halted when one of the $go_{p,q}$ is asserted and the sub-FSM must exit the reset state. This activation function allows the newly activated sub-FSM to have its first active cycle during the last cycle of the previously active FSM. The two sub-FSMs make a transition in the same clock cycle: one is transitioning to its idle state, and the other from its idle state. The local clocks of

F_i and F_j are both active. We call *transitions of control* the cycles when a sub-FSMs shuts down and another activates.

Each local clock of the FSMs F_i is controlled by a clock-gating circuit. The circuit implements the activation function F_{ai}. We could use F_{ai} directly as *enable* signal on the flip-flops, but this scheme would let the clock lines active and consume power, therefore we choose an aggressive implementation: the clock itself is stopped when a submachine is inactive. The power savings on the clock are sizable because the clock line is heavily loaded and switches with high frequency. We use a low-level sensitive latch for F_{ai}, in order to avoid spurious transitions on the clock line that would result in incorrect behavior. Refer to Chapter 3 for a detailed description of the clock-gating circuitry.

The clocking strategy discussed so far has two important functions: reducing power dissipation and keeping the sub-FSM in lock-step. We now address the issue of ensuring cycle-by-cycle equivalence between the monolithic FSM and the decomposed implementation. The outputs of the gated-clock sub-machines are connected to n-way OR gates, one for each primary output. The output equivalence between the decomposed machine and the specification is guaranteed by the fact that, at any given clock cycle, only the active sub-machine is controlling the output value, and all inactive sub-FSMs have their output forced to zero. During the transitions of control, when a machine stops and another resumes execution, the value of the output is controlled by the machine terminating execution.

Example 5.2.2. The gated-clock implementation of the interacting FSMs of Figure 34 is shown in Figure 35. Notice how the external output is obtained by OR-ing the outputs of the sub-FSMs. Figure 35 also shows the clock waveforms, the "in_reset" signals and the "go" signals. Notice that there is a clock cycle for which both local clocks are enabled. The waveforms show how sub-FSM 1 is deactivated and sub-FSM 2 activates thanks to the assertion of the $go_{st1,st2}$ signal. □

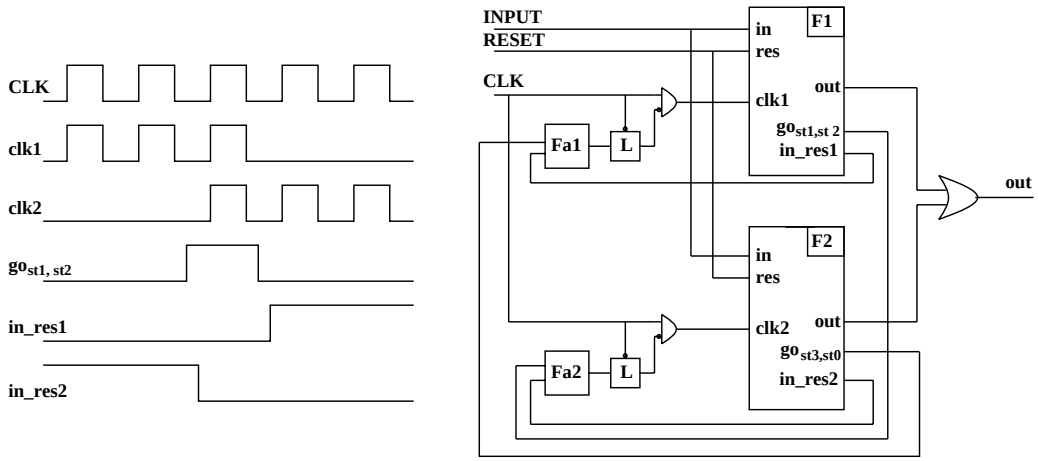

Figure 35: Gated-clock implementation of the interacting FSMs

The startup of the decomposed FSM is obtained by disabling F_a for all sub-FSMs when a synchronous RESET is asserted (this can be done by inserting a AND gate controlled by RESET on the output of F_a). When the RESET signal is high, all sub-machines receive the clock signal. Notice that only the sub-FSM containing the original reset state of the monolithic FSM is actually set to the corresponding state code. All other machines are put in reset state $s_{0,i}$ and they stop and wait for an external *go* signal.

5.3 Partitioning

The power savings in the interacting FSM implementation strongly depends on the quality of the partition $\Pi(S)$. A good partition is characterized by loose interaction between sub-FSMs and small communication overhead. We analyze these requirements in detail.

The ideal mode of operation for the interactive FSM circuit is one of minimum transition of control between different sub-FSMs. When a sub-FSMs disables itself and another one takes control, both machines are clocked for one cycle, the *go* signals

involved in the control transfer change value, and the clock control circuitry switches as well. As a result, transitions of control are power consuming and should be avoided as much as possible.

Minimizing the number of *go* signals is another important objective. The generation of such signals requires additional hardware, that increases power dissipation. Moreover, the *go* signals increase the coupling between sub-machines, complicating the placement and routing of the circuit. On the other hand, if we reduce the number of *go* signals to zero, i.e. we do not decompose the FSM, no power savings are achieved.

In summary, we should look for a partition $\Pi(S)$ which maximizes the locality of the computation and minimizes the hardware overhead for communications between sub-FSMs. We formally describe this problem in the next subsection.

5.3.1 Partitioning as integer programming

In the following discussion we assume that the probability of occupancy of every state in the original FSM has been computed. This task can be performed by simulating the behavioral description of the FSM or by an analysis based on a Markov chain model, as seen in Chapter 2.

The problem of finding an optimal partition $\Pi(S)$ can be formalized as an Integer Programming (IP) problem [nehm88]:

Given:

a_i, the probability to be in state i,

b_{ij}, the probability to transition from state i to j,

n_{max}, the maximum number of blocks in the state partition.

A set of binary decision variables $\{x_{ip},\ i = 1, 2, ..., |S|,\ p,\ p = 1, 2, ..., n_{max}\}$ such that $x_{ip} = 1$ if state i in partition block p and 0 otherwise.

Minimize:

$$\sum_{p=1}^{n_{max}} K_p \times Prob(F_p) \tag{5.34}$$

With constraints:

$$\sum_{p=1}^{n_{max}} x_{ip} = 1, \forall i \tag{5.35}$$

i.e. every state has to be assigned to exactly 1 partition.

The formulation of the cost function requires further discussion. The cost of the interacting FSM implementation can be expressed as the summation over all sub-FSMs of the cost of each sub-machine (K_p) weighted by its probability to be active ($P(F_p)$). The cost of a sub-machine is expressed by a linear combination of the number of states of the machine and the number of possible transitions from and to the sub-machine (meaning extra I/O). This is can be expressed by the following equation:

$$K_p = \left(1 + \sum_i x_{ip}\right) + \alpha \left(\sum_{p_1 \neq p} \sum_i \sum_j \lceil b_{ij} \rceil x_{ip_1} x_{jp} + \sum_{p_2 \neq p} \sum_i \sum_j \lceil b_{ij} \rceil x_{ip} x_{jp_2}\right) \tag{5.36}$$

The first part of the formula is simply the number of states in partition block p. The second part of the formula accounts for the transitions connecting states in p with states in other partition blocks. The term $\lceil b_{ij} \rceil x_{ip_1} x_{jp}$ is 1 if the transition probability from state i to state j is $b_{ij} > 0$, with i in partition block p_1 and j in p. It is zero otherwise. By summing over all edges (a sum over i and j) and all partition blocks p_1 different from the one under consideration, we obtain the total number of transitions into p. Similarly, the term $\lceil b_{ij} \rceil x_{ip} x_{jp_2}$ holds value 1 only for transitions with non-null probability from a state in partition block p to a state in another partition block.

The rationale behind the cost function is that we look for a decomposed implementation with minimum interface cost. The first part of the formula penalizes implementation with excessively coarse granularity, while the second part penalizes implementations where the interface overhead is high. The coefficient α expresses the relative weight that should be given to minimizing the additional gates and wires needed to implement the interface between sub-FSMs (i.e. the *go* signals and the logic generating them) with respect to the number of states of each sub-FSM (i.e. the granularity of the decomposition).

The probability that a particular machine F_p is powered, $Prob(F_p)$ is equal to the total state occupancy probability for states in F_p plus the total probability of transition to F_p. From other partition blocks. In symbols:

$$Prob(F_p) = \sum_i a_i x_{ip} + \sum_{p_1 \neq p} \sum_i \sum_j b_{ij} x_{ip_1} x_{jp}. \tag{5.37}$$

Notice that it is important to consider the probability of the incoming edges for each partition because they mark transitions of controls. During transitions of controls *two sub-machines are powered on at the same time.* Therefore, the summation of $Prob(F_p)$ over all sub-machines F_p is larger than one, accounting for the cycles when two sub-machines are enabled. The formalism used for the IP formulation will be clarified through an example.

Example 5.3.3. Consider the FSM specified by the STG in Figure 34 (a), reproduced in Figure 36. We assume equiprobable and independent inputs for the sake of simplicity. From the input probability distribution and the STG, the state probabilities are computed: $[1/4, 1/4, 1/4, 1/4]^T$. The transition probabilities are computed from state probabilities and input probabilities. They are collected in the transition probability matrix:

$$\begin{bmatrix} 0 & \frac{1}{4} & 0 & 0 \\ \frac{3}{16} & 0 & \frac{1}{16} & 0 \\ 0 & 0 & 0 & \frac{1}{4} \\ \frac{1}{16} & 0 & \frac{3}{16} & 0 \end{bmatrix}$$

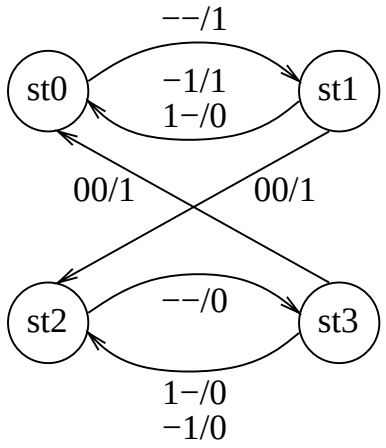

Figure 36: STG of the example FSM

We assume a 2-way partition of the states, where `st0` and `st1` are assigned to block 0 and `st2` and `st3` to block 1 . The partition is expressed by the matrix of x_{ip}:

$$\begin{bmatrix} 10 \\ 10 \\ 01 \\ 01 \end{bmatrix}$$

Notice that this matrix is constrained by the fact that every row sums up to 1, since every state is assigned to exactly one partition. We calculate the cost for partition block P_1. The first term is $1 + \sum_i x_{ip} = 3$, which counts the 2 states of block P_1, `st0, st1` and the reset state the sub-machine goes into when it is powered down. The second term in the cost function consists of two contributions: i) incoming edges, ii) outgoing edges. There is only one incoming edge, namely for $i = 3, j = 0, p_1 = 1$, and one outgoing edge, for $i = 1, j = 2, p_2 = 1$. The cost for P_1 is therefore $3 + \alpha(1 + 1)$.

The probability to be in P_1 is 1/2. We know from the cost calculation that there is 1 possible transition into this partition, for $i = 3, j = 0, p_1 = 1$. The probability of this transition is $b_{30} = \frac{1}{16}$. Note that the probability of transitioning out of the partition equals the probability of transitioning into it. We only have to count one of both. Hence, the total probability is for P_1 to be powered is $\frac{9}{16}$.

The total cost function for this example is given by the scalar product of the matrix of costs for each partition and the matrix of the probabilities for each partition to be powered. Considering the symmetry of the example and choosing $\alpha = 1$, we get $5\frac{9}{16} + 5\frac{9}{16} = \frac{45}{8}$. □

Several techniques have been proposed solve the IP problem exactly and heuristically [nehm88]. The exact solution of IP requires algorithms with above-polynomial worst-case complexity since IP is NP-complete [nehm88]).

5.3.2 Partitioning algorithm

In our case, exact minimization is unnecessarily computationally expensive because the cost function is only an approximate measure of the quality of a partition $\Pi(S)$, which is dependent on the power dissipation of the decomposed implementation. We implemented a heuristic solution based on a *genetic algorithm* [gold89] (GA) which still leverages the IP formulation of the problem. Some properties of the problem made it well suited for this approach. First, the solution space is easily representable as a set of bit-strings: a chromosome is encoded as a set of $|S|$ blocks of $\lceil log_2 n_{max} \rceil$ bits. Each block is associated with a state and represents the number identifying the partition block to which the state belongs. The length of the chromosome in bytes is $|S| \cdot \lceil log_2 n_{max} \rceil / 8$. This is a very compact encoding and if n_{max} is chosen as a power of two, every chromosome represents a valid solution.

Second, the crossover operator is meaningful. If in a given generation the genetic search finds a set of states which are good candidates for clustering, thanks to the crossover operator, the substring representing the set of states will be replicated with high probability in successive generations.

Third, and more importantly, the cost function can be efficiently evaluated, and its computation is $O(|E|)$ where $|E|$ is the number of edges in the STG of the original machine. The compact encoding (with no invalid solutions) and the inexpensive computation of the cost function allow us to take very large populations (in the order of 10^6 individuals).

To efficiently evaluate the cost function, the state probability vector and the transition probability matrix of the monolithic FSM are stored once for all at the beginning

```
foreach (state i) {                          /* Compute partition probabilities */
  Cost[partition(i)] ++;
  probability[partition(i)] += StateProbability(i);
}
foreach (edge i → j) {                /* Compute cost of transitions of control */
  if (partition(i) ≠ partition(j)) {
    probability[partition(i)] += TransitionProb(i→j)
    Cost[partition(i)] += α
    Cost[partition(j)] += α
  }
}
TotalCost = 0;
foreach (partition p) {                                  /* Compute total cost */
  Cost[p] ++;
  TotalCost += Cost[p] * probability[p]
}
```

Figure 37: Algorithm for the computation of the cost function

of each GA run. Other inputs parameters are the relative cost of the I/O overhead (parameter α in Equation 5.36) and the maximum number of partitions to consider n_{max}. The simplified pseudo-code for the evaluation of the cost function in the genetic algorithm is shown in Figure 37.

There are three loops in the algorithm. The first iterates over all the states to compute the first part of the cost function ($\sum_i x_{ip}$) and the cumulative probability of the states in each partition. The second loop computes the second part of the cost function (i.e. the cost of the interface signals) and the probability of the transitions of control. Finally, the third loop iterates on the partitions and computes the final value of the cost function (i.e. the weighted sum of Equation 5.36). The worst case complexity is $O(|E|)$ because, for non-sparse STGs, the number of edges is of the order of $|S|^2$. The second loop usually dominates the execution time.

It is important to notice that our optimization strategy not only tries to find an optimal partition, but also automatically searches for an optimal *number of blocks* in the partition. In particular, if the circuit is not decomposable in a favorable way, the GA run will produce a degenerate partition consisting of a single block containing

all states of the original FSM. The only constraint on the partition is the n_{max}, the maximum number of allowed blocks.

Concluding this section, we point out that our optimization strategy is based on a cost function which is not directly proportional to the actual power dissipation. However, the experimental results confirm that our cost measure is very informative in the *relative* sense (i.e. it can be used to compare the power dissipation of two alternative decomposed implementations). If one partition has much better locality and lower interface cost than another one, the power dissipation of the first will be usually much smaller than the second one. This is because our gated clock implementation guarantees that only a small part of the system is active at any given cycle, therefore a system with few transitions of control and few *go* signals dissipates less power than a system with poor locality and high interface overhead.

Notice also that our technique can be biased by increasing the relative cost of the interface overhead in the cost function. Changing the value of coefficient α the user can control the likelihood of the generation of a decomposed implementation. Moreover, by controlling n_{max} the user can set a lower limit to the granularity of the partition.

5.4 Refined model for partitioning

In the previous sections we have assumed that every transition between states of two different partition blocks corresponds to an additional interface signal in the interacting FSM implementation. This is a safe but conservative assumption. In many cases the number of interface *go* signals can be highly reduced.

The reduction in the number of *go* signals is based on the following observation. When the control is transferred from one sub-FSM to another, the only information that the newly activated machine needs is the destination state to which it has to

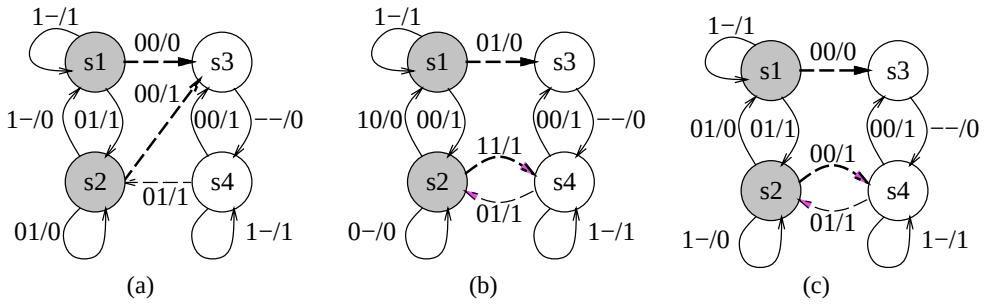

Figure 38: Decomposition of the monolithic FSM

transition. Assume that there are two incoming edges from states in block P_i to states in block P_j of the state partition. If the two edges are directed to the same state in P_j, there is no need to have two different *go* signals, because sub-machine F_j should transition to the same state when it is activated by submachine F_i. The output values during the transfer of control are not a problem, because they are set by F_i, which can distinguish between the two transitions, since they are originating from two different states.

Even if the two edges go to different states in P_j, we might be able to use the input signals that caused the transitions to discern between the destination states. If the input value labeling the transitions are different, we can use them in sub-machine F_j to direct the transition from its reset state towards the right destination. The only case when we need to implement more than one *go* signal between two sub-FSMs is if there are transitions to multiple states in F_j which are not distinguishable by their input fields.

Example 5.4.4. Consider the STGs of three monolithic machines shown in Figure 38. In each FSM, states $s1$ and $s2$ belong to the same partition block, states $s3$ and $s4$ belong to another. The edges drawn with thick dashed lines represent transitions of control in the decomposed implementation from the first to the second sub-machine, while the edges drawn with thin dashed lines are transitions of control from the second to the first sub-machine. We focus on the transitions of control from the first to the second sub-machine. Figure 38 (a) shows a case where two edges between partition blocks do not require two "go"

```
if( list of edges from partition(i) to partition(j) == NULL ||
    ( list of edges from partition(i) to partition(j)
      contains an edge going to a different state &&
      being triggered by the same input &&
      doesn't contain an edge to this state for which a signal was added)) {
  Cost[partition(i)] += α
  Cost[partition(j)] += α
}
add (i,j) to list of edges from partition(i) to partition(j);
```

Figure 39: Improved computation of the cost function

signals in the interacting FSM implementation, because they are both directed towards the same state. Figure 38 (b) shows another case that requires only one "go" signal, since the input field in the two edges allows to distinguish the destination state. The situation shown in Figure 38 (c) requires two "go" signals. The input on the edges cannot be used to distinguish the destination state when, in the decomposed implementation, the sub-machine containing $s3$ and $s4$ is activated by the sub-machine containing $s1$ and $s2$. □

Reducing the number of interface signals gives us much more freedom in the choice of the partition. Moreover, many controllers have STG that cannot be partitioned without cutting numerous edges. For these controllers the basic technique proposed in the previous section would not find any acceptable partition but the trivial one (i.e. the unpartitioned state set), while the improved partitioning technique leads to effective decompositions.

Since our improved decomposition technique can greatly reduce the number of *go* signals required in the interface of the sub-FSMs, the cost function used during the GA to evaluate the quality of a partition is modified accordingly. In the cost function, the number of outgoing and incoming edges is replaced by the actual number of output and input signals to be added to the machine. This is calculated using the pseudo-code of Figure 39, which replaces lines 8 and 9 in the original algorithm.

5.5 Experimental results

We specifically designed the FSM decomposition tool for seamless embedding into pre-existing synthesis-based design flows. The tool consists of two programs: the *partitioner* and the *netlister*. The partitioner reads in the STG of the monolithic FSM and finds an optimal partition $\Pi(S)$. The frame for the genetic algorithm implemented in the partitioner is provided by the Genesis package [gref90]. The netlister reads in the partition $\Pi(S)$, the STG of the specification and produces the decomposed FSM. One important task of the netlister is the reduction of the number of *go* signal, which is performed following the approach outlined in Section 5.4.

The input of our tool is a simple state table description (in Berkeley `kiss` format or in the similar Synopsys `state table` format) and a file containing the state and input signal probabilities. The output is a set of state tables, one for each partition of the decomposition and a synthesizable Verilog description of the clocking circuitry, containing empty modules corresponding to the sub-machines. Thanks to this simple interface, the user can just read the Verilog code and the state tables in the logic synthesis tool of choice and proceed to the logic-level optimization of the full hierarchical design.

We also implemented a program for the computation of the state probabilities given the input probability distribution based on Markov analysis (see Chapter 2). This is a simple utility that can be used when the state probabilities are not known. Alternatively, the user can just simulate the behavioral description of the FSM and collect information on the state occupancy probability. We do not rely on any limiting assumption on state or input probability distribution, our decomposition algorithm simply assume that this data is externally provided.

The time spent in decomposition strongly depends on the effort that the user want to dedicate to the search of an optimal solution. This is controlled by a parameter file

that is specified once for all by the user and is used to set-up the GA run and control the parameters in the cost function. The file contains: i) parameters for the GA run (population size, number of cost function evaluations, probability of cross-over and mutation, and other secondary parameters); ii) the values of n_{max} and α for the control of the cost function. In our experiments we wanted to explore the maximum optimization achievable, therefore we specified large population sizes (from 10^5 to 10^6) and large numbers of cost function evaluations (from 10^6 to $5 * 10^7$). Our GA runs were scheduled for overnight runs on SGI Indy machines with 64Mb of memory.

The parameters for the control of the cost function have been the subject of careful study. With our technology library, $\alpha \approx 1$ gave the best results. If pre-layout estimates of the interface cost are considered too optimistic, the value of α can be set to a constant larger than one. Also, α is technology dependent and could change with the technology library used for mapping. The maximum number of partition blocks n_{max} was always set $n_{max} = 8$, since initial exploratory analysis with larger n_{max} showed that solutions with more than 8 sub-machines were never included among the best individuals of the GA runs.

Table 7 shows the results on a number of benchmarks. The first three examples are controllers of data-path small full-custom chips implemented in a class project. The remaining FSMs are standard MCNC benchmarks [mcnc91], with the exception of the last one which is a modified version of MCNC benchmark `s298` (we reduced the number of states because the commercial tool we used for FSM synthesis could not optimize the monolithic implementation with the memory resources available on our machines).

The decomposed and monolithic implementation were both optimized with Synopsys `Design Compiler` running on a Sun SPARC10 workstation, using the same optimization script targeting minimum delay. The circuit power was estimated by

Name	# of states	# of partitions	Original # of std cells	Original power	Original crit. path	Partitioned # of std cells	Partitioned power	Partitioned crit. path
test1	24	4	67	804	3.81	118 (+76%)	679 (−16%)	3.01 (−21%)
test2	18	3	58	930	2.83	89 (+53%)	642 (−31%)	2.98 (−5%)
test6	80	4	252	2115	7.09	336 (+33%)	1209 (−43%)	5.92 (−17%)
bbsse	13	4	112	1146	4.21	145 (+29%)	847 (−26%)	3.60 (−14%)
dk512	14	2	61	1138	3.29	88 (+44%)	853 (−25%)	2.79 (−15%)
keyb	18	3	157	1688	4.15	262 (+67%)	1387 (−18%)	4.69 (+13%)
planet	48	4	360	4967	6.76	503 (+40%)	3241 (−35%)	5.85 (−13%)
s1488	48	4	433	2743	6.68	642 (+48%)	1717 (−37%)	5.82 (−13%)
s820	25	3	191	1717	5.01	238 (+25%)	1171 (−32%)	3.83 (−24%)
s832	25	3	211	1889	4.61	274 (+30%)	1244 (−34%)	3.72 (−19%)
sand	32	4	429	3395	7.86	471 (+10%)	2554 (−25%)	6.78 (−14%)
scf	112	8	672	3719	7.07	988 (+47%)	2280 (−39%)	5.36 (−24%)
test13	166	8	681	7006	7.38	1610 (+137%)	4124 (−41%)	7.57 (+3%)

Table 7: Power, area and speed of the decomposed implementation versus the monolithic one

`PPP`[bogl96], an accurate full-delay gate-level power estimator. The critical path timing was estimated after technology optimization by the static timing analysis tool within `Design Compiler`. Our technology library is a subset of the Berkeley *Low-Power CMOS library* [burd94]. Interestingly, for all larger examples in the table, the run time of the synthesis tool was much decreased for the decomposed implementation.

The differences in area, power and speed between the partitioned machine and the original unpartitioned design is given in Table 7 between parentheses in the last three columns. The average power reduction is 31%. There is also an increase in speed of 12%. The number of standard cells increases on average by 48%. The results listed are only for machines that actually are successfully partitioned. Some designs do not have an effective partitioning, and they are left monolithic by our tool. For example, in the MCNC benchmark suite, the FSMs `bbara`, `bbtas`, `dk16` and `donfile` are not decomposed. Notice that, with the values of P_{max} and α we chose, the tool never produced partitioned machines with power consumption larger than the original one. This indicates that i) our technique is conservative ii) more aggressive settings (for example, $\alpha < 1$) could lead to the decomposition of more machines, but the uncertainty on the quality of the results would increase.

Notice also that the increase in area is marked on all the examples. The main reason for this phenomenon is the overhead due to additional flip-flops. We specified minimum-length state encoding in all our experiments. This encoding style implies that the number of flip-flops in the monolithic machine increases only logarithmically with the number of states. When the machine is decomposed, the number of states in each sub-machine is decreased by a factor of two if the partition is balanced. In this case each sub-machine has just one flip-flop less than the original machine and the total number of flip-flops is almost doubled. If the partition is unbalanced, the number of flip-flop is generally increased by the flip-flops required in the smaller

machine. Obviously the sequential overhead is larger for N-way partitions, with $N > 2$. We could have performed our tests specifying *one-hot* encoding. In this case, the sequential overhead would have been null. However, we feel that the comparison with minimum-length encoding is fairer towards the monolithic implementation.

It can be observed that the increase in area may translate after layout in increase in power and delay. However our implementations are more modular, because they consist of small and loosely connected blocks. This characteristic may actually improve the quality of the layout. Moreover, the power savings are quite large and unlikely be completely swamped during layout.

5.6 Summary

We have described an algorithm for finite-state machine decomposition for low power consumption. We leverage clock-gating techniques to produce an interacting FSM implementation in which only one or two sub-machines are clocked at any clock cycle, while the others are inactive and dissipate small power. Our tool integrates easily in synthesis-based design methodologies and can be seen as a pre-processing step on the state table specification of the original FSM. Standard synthesis tools (or the techniques illustrated in previous chapters) can then be used for optimizing the sub-FSMs and additional power reductions can be obtained.

Our partitioning algorithm takes into account the overhead imposed by the interface signals required for the interaction of the sub-machines and automatically chooses not only how to partition the state set of the original specification, but also how many partition blocks will be generated. The algorithm is based on conservative assumptions and avoids the generation of decomposed FSMs if the expected power savings are not high. An important byproduct of our technique is the increase in speed of the interacting FSM.

The search for an optimal decomposition is based on a Genetic Algorithm and it is therefore heuristic in nature. However, the compact encoding scheme and the efficient computation of the cost function allow us to search effectively the solution space by selecting large population sizes. The results achieved by our algorithm are very promising: on average, 31% power reduction, 12% speed increase at the price of a 48% area increase are observed for FSMs that are decomposed.

Several extensions of the decomposition approach are possible. First, deterministic graph-based algorithms can be used for improving the quality of the partition, since the genetic algorithm is a randomized general-purpose technique that does not exploit information on the particular structure of the optimization problem. Tailored heuristics may outperform the GA both in speed and quality of results. Moreover, it is possible to extend the decomposition technique to deal with large sequential systems for which the state table is not available (or too large to be handled). This can be accomplished by leveraging implicit state-space decomposition algorithms such as those presented in [cho94] and the ADD-based approach introduced in Chapter 4.

Chapter 6

State assignment for low power

6.1 Introduction

As seen in previous chapters, the behavioral specification of a finite-state machine is typically in the form of a state transition graph, where each state is represented symbolically. In Chapter 2 we defined *state assignment* as the synthesis step where binary codes are assigned to the symbolic states. The designer (or the synthesis tools) is free to decide the length of the code words (i.e. the number of state variables) and the encoding of each state. Such degrees of freedom can be exploited to obtain an optimized implementation of the FSM.

Earlier approaches to state assignment have targeted area and performance both for two-level and multi-level logic implementation ([dmc86] [esch92], [asha91] and [dmc94] are good surveys of previous work). In this chapter we investigate state assignment algorithms targeting low power dissipation.

Compared to the approaches described in previous chapters, state assignment does not require any manipulation of clock-related circuitry. However, it has similarities with the decomposition techniques presented in Chapter 5. Indeed, FSM decomposition can be seen as a flavor of state assignment, where the binary codes assigned to

the symbolic states are chosen so as to enable a decomposed implementation of the combinational FSM logic. In contrast to the clock-gating techniques introduced in Chapters 3 and 4, state assignment and FSM decomposition both reduce the *useful* switching activity, namely the switching that is required for the correct operation of the system.

The main theoretical contributions of this chapter are in the formulation of a cost function and in the study of a new class of algorithms for the search of optimal and suboptimal solutions to the problem of finding a state assignment that gives low power dissipation. It is important to notice that the choice of an adequate cost function implies a difficult trade-off between its accuracy and the complexity of its evaluation.

The power dissipation on state lines and in the flip-flops can be modeled with a clean mathematical formulation. The key intuition is that power is minimized when the switching activity on the state lines is reduced. This target can be achieved by selecting state codes that minimize the number of bit differences between states with high transition probability. In other words, when a transition between two states is very likely, we should try to assign codes as similar as possible to the states.

Unfortunately, minimizing the switching activity on the state lines in a FSM by itself does not guarantee reduced total power dissipation, because the power consumed in the combinational part is not accounted for. We discuss this problem and propose a more accurate cost metric that also factors in the complexity of the combinational logic.

We tested our state assignment algorithms on several benchmark FSMs (from the MCNC suite [mcnc91]), obtaining a 34% average reduction in switching activity of the state variables, a 16% average reduction of the **total** switching activity of the implemented circuit with a corresponding 14% average area increase. Although our solution is heuristic, and does not guarantee the minimum power dissipation, these results demonstrate that our approach leads to a reduction in the power dissipated

in the complete circuit, not just in the part used for the computation and the storage of the state information. Moreover, the proposed algorithms can be used to explore the complex tradeoff between area and power dissipation.

The rest of the chapter is organized as follows. In Section 6.2 we give some theoretical results on the effectiveness of the probabilistic approach for describing the switching behavior of FSMs defined by state transition graphs. In Section 6.3 we formalize the state assignment problem targeting power dissipation in state lines and flip-flops and present an exact algorithm for its solution. We implemented heuristics based on the exact algorithm, which we describe in Section 6.4, along with extensions to control the effect of state assignment on the combinational logic of the FSM. In Section 6.5 we present some experimental results on the application of the previously described algorithms. In Section 6.6 we investigate some interesting relationships between state assignment and the techniques presented in the previous chapters.

6.2 Probabilistic models

As discussed in Chapter 2, given the input probability distribution, it is possible to calculate the probability of the state transitions in a FSM. This information can be used to find an encoding that minimizes the switching probability of the state variables. We showed in Chapter 1 that in CMOS circuits power consumption is proportional to switching activity. We defined the *average switching activity* as the average number of signal transitions. The *switching probability* is the limit value of the average switching activity as the observation time goes to infinity [ghos92].

Here, we target the minimization of the average switching activity in a sequential circuit. This is a complex problem because the specification is at a high level of abstraction. Thus, we concentrate on the state assignment problem whose solution determines the register configuration. Note again that the state assignment strongly

affects the size and the structure of the FSM's combinational component.

Given the state transition graph (STG) of a finite-state machine, we want to compute the transition probabilities. The input probability distribution can be obtained by simulating the FSM in the context of its environment, or by direct knowledge from the designer. As discussed in Chapter 2, transition probability information for each edge in the STG can be determined by modeling the FSM as a Markov chain.

Remember that transition probabilities are strongly dependent upon the initial state. For example, if an FSM has a transition from state s_i to state s_j for all possible input configurations, we may think that this transition will happen with very high probability during the operation of the machine. This may not be the case: if state s_i is unreachable, the machine will *never* perform the transition, because it will never be in state s_i. Similarly, if the probability of being in state s_i is very low, a transition from state s_i to state s_j is very unlikely. Our state assignment algorithm targets the reduction of the switching activity by assigning similar codes to states with very high transition probability. We must therefore compute the correct value of the transition probabilities before applying the optimization procedure.

Consider a FSM with n_s states, described by an STG with state set $S = \{s_1, s_2, ..., s_{n_s}\}$ and a edge set representing the set of transitions from one state to another. The Markov chain model for the STG is directed graph isomorphic to the STG and with weighted edges. For a transition from state s_i to state s_j, the weight $p_{i,j}$ on the corresponding edge represents the *conditional probability* of the transition (i.e., the probability of a transition to state s_j *given* that the machine was in state s_i). In Chapter 2 we called the set of all conditional probabilities the *conditional probability distribution*. The total transition probabilities $P_{i,j}$ can be computed from the state probabilities P_i and the conditional input probabilities: $P_{i,j} = p_{i,j}P_i$.

In Chapter 2 we discussed several methods for the computation of the state probabilities. Such methods rely on a fundamental assumption: the probability that the

machine is in each state converges to a constant (stationary) set of real numbers as the running times goes to infinity. It is quite easy to find STGs for which this property and the stationary state probabilities do not exist, because, for example, they are oscillatory. Considerable attention has been devoted in the literature to such "pathologic" STGs and several methods have been proposed to deal with them [hach94].

We claim that, for the vast majority of practical sequential circuits, stationary state probabilities do exist. More in detail, a sufficient condition for their existence is the presence of a "reset" signal with non-null probability of being active. In other words, if a FSM is resetable to an initial state, and the reset operation is performed sometimes, we can guarantee that P_i exists and are well defined.

To prove this claim we first refer to the fundamental theorem of Markov chains theory introduced in Chapter 2. The theorem states that: *for an irreducible, aperiodic Markov chain, with all states recurrent non-null, the stationary probability vector exists and it is unique* [triv82]. Remember that an *irreducible Markov chain with all the states recurrent non null* is a chain where every state is recurrent non null and can be reached from any other state. A state is recurrent non null when the greatest common divisor of the length of the possible cycles from the state is one.

We define the *reset state* of a FSM, s_0, as a state such that there is a transition (with non-zero probability) to it from every state in the STG. A *resetable STG* is defined as an STG where all unreachable states (from the reset state) in the original STG have been eliminated. With these definitions, we can state the following theorem:

Theorem 6.1 *The Markov chain corresponding to a resetable STG with reset state s_0 and known conditional transition probabilities is irreducible, aperiodic, with all states recurrent non null.*

> **Proof:** First, we prove that the Markov chain is irreducible. Since every state has a transition to the reset state s_0, and every state is reachable

t

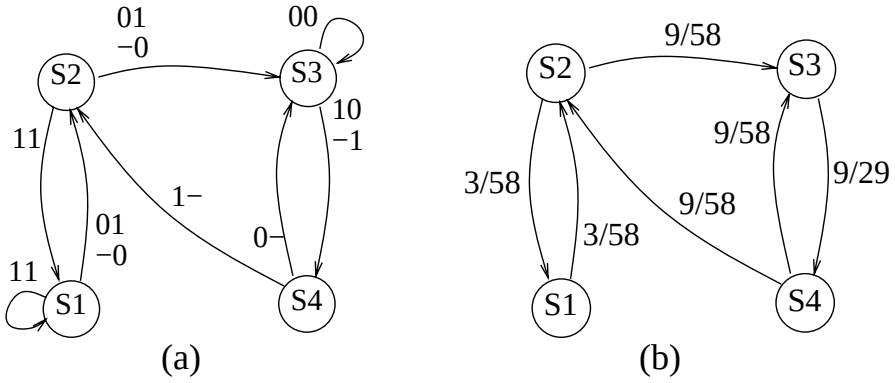

Figure 40: (a) The STG of a FSM with four states and two input signals. (b)

from s_0, we can always reach a state from any other state using a path through s_0.

Second, we need to show that the chain is aperiodic. The reset state is aperiodic, because it can be reached from every other state and from itself in one step. It is possible to show that, if a Markov chain is irreducible and one of its states is aperiodic then all its states are aperiodic [triv82], therefore the aperiodicity of the chain is proven.

Finally, all the states are recurrent non null because they are reachable and from every other state including themselves with probability greater than zero. ♯

Note that this theorem is only a *sufficient* condition, i.e. there are STGs without a reset state for which we can successfully compute the transition probabilities.

Example 6.2.1. Figure 40 (a) shows the STG for a simple FSM with two inputs. The example is taken from Chapter 2. We use this STG throughout the chapter as an example for the application of our algorithms.

The stationary state probabilities (calculated with the methods introduced in Chapter 2) are shown in Figure 40 (b) besides the nodes in the STG. Recall that the matrix $\mathbf{P}$ of conditional input probabilities is initially known. The figure shows the total transition probabilities (the products $p_{i,j}P_j$) on the edges. Note that the probabilities for self-loops are not shown only because we are not interested in edges that do not imply any state transition. Note also that

although our STG does not have a reset state, its stationary probability vector can be calculated. □

6.2.1 Transformation of the STG

Once the total transition probabilities have been calculated, we can transform the original STG into a weighted graph which preserves the relevant information needed for state assignment. For each pair of connected states, we only need to know the probability of a transition from one state to the other and vice-versa. Therefore, all input-related information and self-loops can be eliminated.

The transformations of the STG can be summarized as follows:

- Eliminate all unreachable states, if any.
- Calculate the state stationary probability vector and, from that, calculate the total transition probabilities.
- Remove any self-loops and label each remaining edge with a weight representing its *total* transition probability (the weights are normalized to integers for notational simplicity).
- Collapse all multiple directed edges between two states into a single undirected edge with weight $w_{i,j}$ equal to the sum of the directed edges probabilities. Note that this step can be performed only if the weights are computed from total transition probabilities.

The STG is thus transformed into a weighted undirected graph $G(S, E, W)$, called *reduced graph*, where the weights on the edges are proportional to the total probability of a transition (in either direction) between the two states connected by the edge. This will be the starting point for the state assignment algorithms.

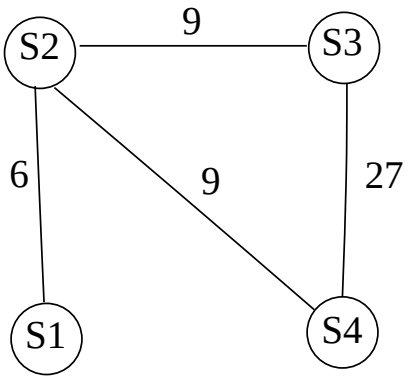

Figure 41: The reduced graph used as a starting point for the state assignment.

Example 6.2.2. The transformation of the STG is illustrated in Figure 41. Note that an edge with high conditional probability (like $s_1 \leftrightarrow s_2$) can have a weight (proportional to the *total* transition probability) equal or even smaller than an edge with small conditional probability (like $s_4 \leftrightarrow s_2$). □

As a concluding remark for this section, we observe that the calculation of the total transition probability requires solving a system of equations of size proportional to the number of states. This can become a computational problem for large systems whose state graph is extracted from an existing synchronous network, because the number of states is exponential in the number of storage elements used. In this case symbolic techniques described in Chapter 2 can be employed, allowing calculation of the steady state probabilities for very large sequential circuits [hama94].

6.3 State assignment for low power

The main idea in our approach to this problem is to find a state assignment which minimizes the number of state variables that change their value when the FSM moves between two adjacent states in the reduced graph. Ideally, if we can guarantee that each state transition results in a single state variable change, we will have optimally reduced the switching activity associated with the registers in the given STG. We

now give some examples of possible specific solutions for restricted classes of STGs, then we discuss the general problem and its exact solution.

Given an STG representing a counter, a state assignment that gives the minimum switching activity in the circuit is a Gray encoding of the states (an encoding used for binary numbers that guarantees that two successive numbers always have adjacent codes [mccl86]). Gray encoding is a solution only for this particular form of STG, for which the problem is quite trivial (note that in a counter inputs are irrelevant, and all transitions are equiprobable).

Given a STG of arbitrary structure, good performance in terms of reduced switching activity results from using a 1-Hot encoding [dmc94] of the states. 1-hot encoding guarantees that exactly two state variables will switch for every state transition, thus achieving good results with no algorithmic effort. However, the number of state variables needed is equal to the number of states. It has been shown that shorter codes correlate to smaller area for both two-level [dmc86] and multi-level [du91] implementations and larger areas often lead to higher power dissipation. In addition, with 1-hot encoding, two state variables switch for every state transition, while other codes can lead to a change of a single state variable for most transitions.

For a general solution, we need to find a method that does not assume a particular STG structure and is not heavily constrained in the number of state variables to use. We will use the probabilistic model developed in the previous section to obtain state assignments that minimize the average number of signal transitions on the state lines for a general STG.

6.3.1 Problem formulation

Our algorithm must be valid for an arbitrary STG, and must avoid constraints on the number of state variables used. The algorithm should be able to find the number of state variables n_{var} that gives the minimum number of transitions and is close to

the minimum $\lceil log_2 n_s \rceil$, to keep the size of the combinational part small.

We can describe a state encoding as a Boolean matrix (i.e. a matrix with 0-1 elements) $\mathbf{E}$ with rows $\{\mathbf{e}_i,\ i = 1, 2, ..., n_s\}$ corresponding to state codes and columns corresponding to state variables. Let $\{e_{i,j},\ i = 1, 2, ..., n_s;\ j = 1, 2, ..., n_{var}\}$ be the elements of $\mathbf{E}$. Our problem of finding a state encoding that results in minimum switching activity can then be formalized as an integer programming (IP) problem:

Given:

The reduced graph $G = (S, E, W)$, with weights $W = \{w_{i,j},\ i = 1, 2, ..., n_s;\ j = 1, 2, ..., n_s\}$,

Minimize:

$$\sum_{i=1}^{n_s} \sum_{j=1}^{n_s} w_{i,j} \sum_{l=1}^{n_{var}} e_{i,l} \oplus e_{j,l} \tag{6.38}$$

With constraints:

$$\sum_{l=1}^{n_{var}} e_{i,l} \oplus e_{j,l} \geq 1, \qquad \forall\, i, j,\ i \neq j \tag{6.39}$$

The cost function expresses the desire to assign adjacent codes to states with high-probability transitions. The constraint inequalities (6.39) express the fact that no two states can be allowed to have the same code.

Example 6.3.3. If we decide to use a minimum length encoding for our example STG, two state variables are needed ($log_2 4 = 2$). The encoding matrix $\mathbf{E}$ has therefore 4 rows and 2 columns. The constraint equations are:

$$e_{1,1} \oplus e_{2,1} + e_{1,2} \oplus e_{2,2} \quad \geq \quad 1$$

$$\begin{aligned} e_{1,1} \oplus e_{3,1} + e_{1,2} \oplus e_{3,2} &\geq 1 \\ &\ldots \\ e_{3,1} \oplus e_{4,1} + e_{3,2} \oplus e_{4,2} &\geq 1 \end{aligned}$$

while the cost function to minimize is:

$$\begin{aligned} Cost = \; & 6(e_{1,1} \oplus e_{2,1} + e_{1,2} \oplus e_{2,2}) + 9(e_{2,1} \oplus e_{3,1} + e_{2,2} \oplus e_{3,2}) + \\ & 9(e_{2,1} \oplus e_{4,1} + e_{2,2} \oplus e_{4,2}) + 27(e_{3,1} \oplus e_{4,1} + e_{3,2} \oplus e_{4,2}) \end{aligned}$$

The problem involves $2 * 4 = 8$ variables and $3 + 2 + 1 = 6$ equations. □

Note that the number of state variables used, n_{var}, is an additional degree of freedom. In theory, the IP should be solved more than once to find the n_{var} that gives the minimum cost. Because we know that the optimum lies between $\lceil log_2 n_s \rceil$ and n_s, we search on n_{var} to find the minimum. However, area considerations (to be discussed later) force n_{var} to be close to the minimum, keeping the number of iterations on n_{var} small in most practical cases.

The number of inequalities is $O({n_s}^2)$, and the solution space to be explored is $O(n_s 2^{n_s})$. For small FSMs, the exact solution of the IP problem can be found by using either a traditional approach [nehm88] or BDD based techniques [jeon92]. For larger STGs, the exact solution may be unattainable, being the integer programming problem NP-complete. However, the exact formulation is still interesting because it gives insights into more practical heuristic solutions.

Two more observations are of interest. First, for several problems a solution with distance one between all connected states is impossible; the presence of an odd cycle in the reduced graph is an example of constraint not satisfiable with any distance-one encoding [dmc86]. However, we do not need a distance-one encoding to reach the minimum cost. Second, although the exact solution of the problem always yields the exact minimum of the cost function, it does not guarantee that the power dissipation

of the synthesized circuit is minimum, because our cost function does not model the switching activity in the combinational part.

6.4 Algorithms for state encoding

The high computational complexity of the general state assignment problem has motivated the use of many heuristic approaches to its solution [dmc86, deva88, du91, esch92, dmc94]. We propose a column-based approach [dolo64, dmc86] that considers one state variable (one column of the encoding matrix) at a time and assigns its value for each state in the reduced graph, targeting the reduction of the average switching activity. The procedure is carried out iteratively for each state variable until the codes have been completely specified. The algorithm tries to give states that are linked by high-weight edges the same value for most state variables, while ensuring that each state has a unique code.

The column-based framework for the solution of the state encoding problem focuses on one column of $\mathbf{E}$ at a time. For each column l, the state bit are optimally assigned. The cost function is similar to the one introduced in the previous section: a weighted sum of bit differences multiplied by edge weights. After assigning one column, the weight are updated. The adjustment of the edge weights between iterations allows us to bias the assignment of the new state variables toward regions of better global optimality in the search space. This step is useful because we find an optimal solution for a single column at a time, and the column-based approach has no notion of global optimality across multiple columns.

Moreover, when minimizing the cost function, we need to enforce *class constraints*. The class constraints are based on the notion of *indistinguishability classes*. Two states having the same partial code are said to belong to the same *indistinguishability class*. Similarly, two rows of $\mathbf{E}$ belong to the same indistinguishability class when

the two corresponding states do. If the maximum number of state variables that we want to use is n_{var} and we are assigning bit codes for the l-th variable, the maximum number of indistinguishable partial state codes after the assignment must be less than $2^{(n_{var}-l)}$, otherwise we cannot create unique codes for this set of states with the remaining unassigned variables.

6.4.1 Column-based IP solution

We present a column-based algorithm that solves a set of simplified IP problems, with lower average complexity than the exact IP solution (although the final solution is not guaranteed to be optimum). Notice however that, since the simplified IP problems are still NP-complete, the worst-case complexity is still exponential. Hence, we will describe next a polynomial-time column-based heuristic that finds good solution in short time. The column-based IP can be formalized as follows.

Given:

Column l of encoding matrix $\mathbf{E}$

$G = (S, E, W)$, the reduced graph with vertex set S equal to the state set of the FSM, and edge set W with weights $w_{i,j}$,

$\{C_k,\ k = 1, 2, ..., n_{class}\}$, the indistinguishability classes after the assignment of $l-1$ columns.

Minimize:

$$\sum_{i=1}^{n_s} \sum_{j=1}^{n_s} w_{i,j} \left(e_{i,l} \oplus e_{j,l}\right) \tag{6.40}$$

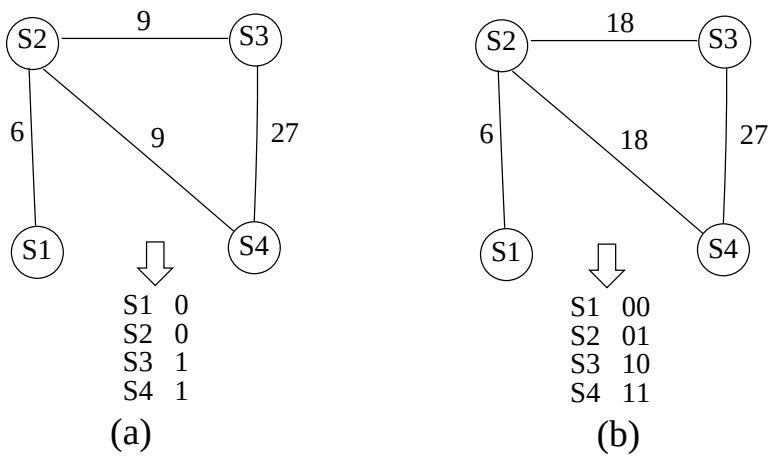

Figure 42: (a) Reduced graph and assignment of the first state variable (b) New reduced graph and assignment of the second state variable

With constraints:

$$\begin{cases} \sum_{e_i \in C_k} e_i & \leq & 2^{n_{var}-l} \\ \sum_{e_i \in C_k} e'_i & \leq & 2^{n_{var}-l} \end{cases} \qquad \forall C_k \tag{6.41}$$

We clarify the IP formalism through an example.

Example 6.4.4. Consider the reduced graph in Figure 41. We select $n_{var} = 2$. Initially, no state variable has been assigned, so all states belong to the same indistinguishability class $C_{1,1}$. We want to assign the codes for the first state variable (the first column in the encoding matrix). Since we have four states, the constraint Inequalities 6.41 require that we assign 0 to a pair of states and 1 to the other pair. One assignment that minimizes (6.40) is $e_{3,1} = e_{4,1} = 1$ and $e_{1,1} = e_{2,1} = 0$, as depicted in Figure 42 (a). □

This approach reduces the size of the problem that must be solved at each step. However, because the column-based IP solution does not consider the impact that the choice of one state variable has on the other state bits, the solution is not globally optimal. To improve the the final outcome, we can bias the decision at each step by the results of preceding assignments. This is done by updating the weights in the cost function after each variable (column assignment) using the following formula:

$$w_{i,j}^{l} = w_{i,j}(d_{i,j}^{(l-1)} + 1) \tag{6.42}$$

where $d_{i,j}$ is the Hamming (Boolean) distance between the partially assigned codes for states s_i and s_j: $d_{i,j}^{(l-1)} = \sum_{k=1}^{l-1} e_{i,k} \oplus e_{j,k}$

Example 6.4.5. In Figure 42 (b) the new weights after assignment of the first variable are shown. The final solution is found by assigning the second variable in a way that gives the minimum cost and distinguishes all states. This is shown in Figure 42 (b). □

The column based approach produces a simpler set of IP problems than the global IP. Therefore, it can be successfully applied to a larger class of FSMs. Nevertheless, the core computation is still an IP and the worst case complexity has not been reduced. For this reason, we propose an column-based algorithm whose worst-case complexity is polynomial in the number of states.

6.4.2 Heuristic algorithm

We want to eliminate the exponential complexity still remaining in the column assignment step of the column-based IP approach. Therefore, we use a much simpler heuristic that considers pairs of states and tries to assign the same state variable value to states with high transition probability. We first describe the structure of the proposed algorithm, then we discuss its rationale and performance. The pseudo-code of the algorithm is shown in Figure 43.

The algorithm is based on a greedy choice of the constraint to satisfy; if it is impossible to assign the same bit code to two states because an indistinguishability class becomes too big, a different code is assigned. The function `select_bit` makes a choice between two possible assignments based on the already assigned neighbor states. Given a pair of states (or a single state), `select_bit` calculates the *total edge violation* (defined next) caused by the possible assignments (0 or 1) of the current

```
assign(S) {
  sort edges by weight in decreasing order;
  foreach edge {s_i,s_j} {
                  /* consider pairs of states with high transition probability */
    if(s_i and s_j not assigned) {
      if(no Class violations) {
             /* if the number of states with the same bit code is not too high */
        x=select_bit(s_i,s_j);           /* chooses a code for the pair of states */
        e_i = x  e_j = x;          /* the same bit code is given to both the states */
      }
      else {
        x=select_bit(s_i, s_j);
        e_i = x; e_j = x';       /* different bit codes are given to the two states */
      }
    }
    else if(s_i or s_j not assigned) {
      s_h=unassigned(s_i,s_j);               /* state whose bit code is unassigned */
      s_g=assigned(s_i,s_j);
      if(no Class violations) {
        x=select_bit(s_h);         /* choose a bit code for the unassigned state */
        e_h = x;
      }
      else
        e_h = e'_g;  /* only one choice available because of the class constraints */
    }
  }
}
```

Figure 43: Heuristic algorithm for column-based state assignment

state variable for the codes of the two states. The total edge violation for a bit code is defined as the sum of weights on all edges connecting one of the considered states with other states that have already been assigned a different bit code. The selected bit code is the one resulting in a smaller edge violation. At the end of the outermost iteration, the value (bit code) of the l-th state variable (corresponding to a column of the encoding matrix) has been assigned for all states.

Example 6.4.6. For our simple STG, the greedy algorithm gives the same result as the semi-exact IP based approach. In this case both heuristics find an exact minimum for the cost function:

$$Cost = 6 * 1 + 9 * 2 + 27 * 1 = 51$$

The minimality of the solution can easily be verified by inspection; note that the solution is not unique. □

The structure of the algorithm is very simple and its execution time is always small, in fact no backtrack mechanisms are present and we do not iterate to improve a solution. The complexity of the algorithm is $O(n_s n_{edges})$. The dependence on the number of states (n_s) comes from the outermost iteration, while the dependence from the number of edges (n_{edges}) is due to the iteration needed in `select_bit` to compute the total edge violation. One can envision cases where the greedy choice of the constraints leads to suboptimal solutions, but, in general, this heuristic gives good results.

In particular, notice that if our heuristic is run on a reduced graph where all the edges have equal weight, and n_{var} is chosen to be equal to n_s, the final encoding will be 1-hot (all states will have a single one in their codes and only one state will have the all-zero code), the reason being that we force the largest indistinguishability class to be reduced of at least one element at each step. 1-hot encoding is therefore a particular case of the class of codes that we can generate with our algorithm.

The greedy heuristic can be improved. We could, for example employ local search techniques like genetic algorithms [olso94] or simulated annealing to improve the results. If we are not constrained to use the minimum number of state variables, as is often the case, we can try different solutions for multiple values of n_{var}. Although increasing the number of state variables will likely violate fewer constraints, the n_{var} should still be kept close to the minimum to avoid an explosion in complexity of the combinational part of the FSM.

Another approach is to use the greedy heuristic for fast iteration over n_{var} to find its optimal value. Once the best n_{var} has been found, more powerful and expensive algorithms can be applied in order to improve the optimality of the result.

We have assumed that the FSM are given in state-transition table format. For

FSM described by sequential networks, even the simple heuristic algorithms may not be applicable, because the state table is too large to be extracted in a reasonable time. In this case symbolic techniques similar to those presented in Chapter 4 should be used. Hachtel et al. [hahe94] proposed a symbolic algorithm for *re-encoding* large FSMs described by synchronous networks. When the initial specification is a synchronous network, re-encoding bypasses STG extraction step since it assumes that the states are initially encoded (with the encoding provided by the initial specification) and searches for a *trans-coding* function. The trans-coding function translates the codes of the original encoding to the new codes of the low-power encoding.

6.4.3 Area-related cost metrics

Up to this point, we have used the weighted sum of the Boolean distances between state codes as the cost function. This only minimizes the switching activity in the sequential portion of the FSM (the flip-flops). The overall power dissipation is also dependent on the structure of the combinational part of the final synthesized FSM. Neglecting area considerations in the cost function may lead to non-minimal area implementations with total power dissipation close to that obtained using traditional area-related state-assignment techniques. By adding an area-related secondary objective to our cost metric, we can keep the area of the combinational logic under control.

To tackle this problem, we incorporated metrics for minimal area into our cost function, similar to those proposed in MUSTANG [deva88] and later upon improved in JEDI [lin89]. Two different metrics are provided: a fanout-oriented metric, well suited for FSMs with a small number of inputs and a large number of outputs, and a fan-in-oriented metric that performs better in the opposite case.

Details of how the metrics are computed are presented in [deva88]. However two points are worth remarking on:

- The area constraints are expressed with edge weights exactly like the power constraints, and we can allow specification of different trade-offs in terms of their relative importance according to the overall design objectives. To do that, a new parameter $\alpha \leq 1$ has been introduced, specifying the relative importance of power with respect to area constraints. The edge weights on the reduced graph are then calculated using the following equation:

$$w_{i,j} = (1-\alpha) w_{i,j}^{area} + \alpha w_{i,j}^{power} \tag{6.43}$$

  where the weights $w_{i,j}^{power}$ are calculated with the algorithms presented earlier, while $w_{i,j}^{area}$ are calculated using the heuristics described in [deva88].

- Even if our edge weight calculation for area minimization is similar to the one proposed in MUSTANG, our state assignment algorithm is column based, and this allows to dynamically adjust the weights, resulting in a potentially more effective state assignment.

In conclusion, to obtain low power dissipation in the final circuit, area must be taken into account. However, our experiments have shown that using high values of α in equation (6.43) typically give the best results, implying that there is a strong correlation between the power-related cost metric and the actual power dissipation.

6.5 Implementation and results

We implemented the heuristic algorithm and applied it to some benchmark circuits. We computed the total transition probabilities using the methods outlined in Chapter 2. We then applied our state assignment algorithm, POW3, on the reduced graph to obtain a state encoding. We then used the SIS [sent92] standard script `script.rugged` to obtain a multi-level implementation of the state-assigned FSM.

Circuit	n_{var}	Area Jedi/POW3	Tot. trans. Jedi/POW2	% Red.	St. trans. Jedi/POW3	% Red.
bbara	4	67 / 69	3630 / 3448	5	327 / 294	11
bbsse	4	126 / 131	8871 / 7970	11	1033 / 851	18
bbtas	3	25 / 25	2971 / 2690	10	610 / 456	26
dk14	4	120 / 114	7296 / 7083	3	1403 / 1104	22
dk17	5	76 / 77	5548 / 5463	2	1337 / 1081	19
dk512	5	67 / 87	7650 / 4825	38	2355 / 1538	35
donfile	5	102 / 214	5231 / 4573	14	1743 / 1378	21
planet	6	697 / 665	27859 / 19771	30	3204 / 1240	62
planet1	6	708 / 697	25735 / 16306	38	3205 / 1278	61
s1488	6	742 / 727	14073 / 13123	7	628 / 341	55

Table 8: Comparison between POW3 and JEDI after multiple level optimization.

We ran an area-oriented state assignment program, JEDI [lin89], on the same benchmarks, following the same procedure to generate an implementation. The implementations were then simulated with random patterns using the MERCURY [dmc90], a delay-based gate-level simulator, to measure the circuit activity, which gives a good estimate of the power consumption of the real circuits. The results are shown in Table 8.

For all benchmarks, our state assignment algorithm produced circuits with less switching activity than those produced by JEDI. In most cases, the area penalty (linked to the number of literals in the network) was small.

Figure 44 compares area overhead with power reduction. If we call M_{minA} the minimal area implementation obtained with JEDI and M_{minP} the minimal power implementation obtained with POW3, the plot shows:

- The area ratio $A_{M_{minP}}/A_{M_{minA}}$ (Literal increase).
- The total transition count ratio $PT_{M_{minA}}/PT_{M_{minP}}$ (Decrease in total transitions).

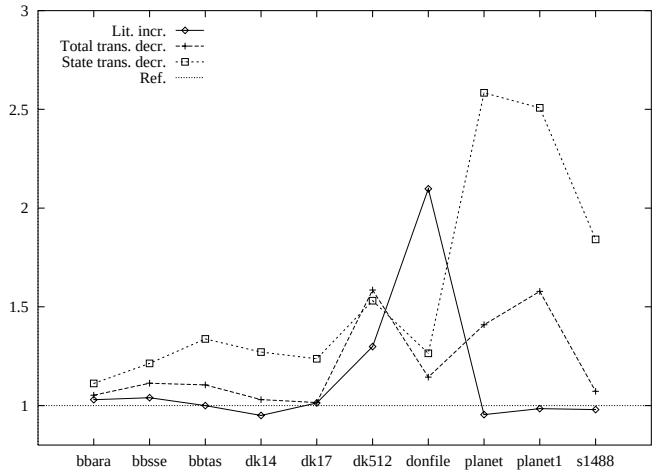

Figure 44: Increase in area and decrease in transition count of the low-power implementation (for both the complete circuit and the state variables only).

- The state transition count ratio $PS_{M_{minA}}/PS_{M_{minP}}$ (Decrease in state transitions).

It is clear that if the area overhead is large, the reduction in power dissipation is less significant, thus showing that the power dissipated in the combinational part plays an important role in the total power balance.

Figure 45 plots the average reduction in power dissipation as a function of the number of state bits. The reader can observe that our methods produce in the average better results for larger circuits, for which low power consumption is even more important.

All results use transition count as the estimate of power, because we have not mapped the circuits using a technology library. The algorithm described above is intended to be a preprocessing step in a complete synthesis tool that includes a low-power driven technology mapper, which we did not have. At this regard, notice that the power in the combinational part of the FSM can be divided in power dissipated in useful transition and glitch power. The reduced switching activity of the state lines

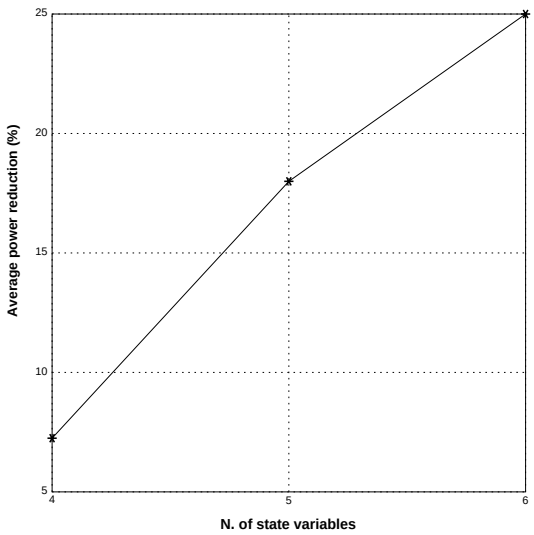

Figure 45: Average power reduction as a function of the number of state variables.

can be used to decrease both these quantities, in fact the intuition suggests that a network with low switching activity on part of the inputs and outputs could be synthesized with also reduced internal switching activity. This is still an open problem, but accurate power estimation techniques such as those presented in [tsui94b] could allow combinational synthesis and library binding tools to exploit the low-activity property of our state assignments.

The last column of Table 8 shows the reduction in switching activity on the state lines. Note that if power dissipation in the memory elements is significantly higher than the power dissipated in combinational gates, the power reduction of our implementation becomes more significant. Also, because the state lines have low activity, algorithms for optimization of the combinational logic can exploit this information for further power savings.

Two additional parameters help our algorithms in the search for optimal results. First, we can control the number of state variables used in the encoding. In all the examples we tried, the minimum number of state variables gave the best result, because increasing the number of state variables resulted in an area overhead that overcame

the (small) reduction in average number of transitions on the state lines. Second, our algorithms can accept different values of the parameter α, controlling the relative importance of power and area in the cost function. Our experiments with different values of α showed that setting $\alpha \geq .7$ produced the lowest power implementations. In fact, in some cases, setting $\alpha = 1$ resulted in a final implementation that was as small as the implementations obtained by using JEDI for state assignment. This confirms that the area-related cost metrics used are not very accurate, and more work has to be done in order to better estimate the area of multilevel implementations.

6.6 Relationships with clock gating and decomposition

There is no apparent connection between the state assignment problem and decomposition or clock gating. However, the relationships among these problems are deep. Let us consider FSM decomposition first.

The decomposition approach proposed in Chapter 5 is a based on partitioning the state set S of the FSM. Consider for simplicity a two-way partition $\Pi(S) = \{S_1, S_2\}$. A state belongs to either S_1 or S_2: this is a binary decision. The key observation is that a *state variable can be used to distinguish the states* [hart66]. If the state variable has value 1, a state belongs to to S_1, otherwise it belongs to S_2. The code for a state consists of two blocks: i) a set of state variables that identifies the partition block S_i to which the state belongs and ii) a set of state variables that uniquely identifies the state within the partition block.

Chow et al. [chow96] recently proposed a low power decomposition approach based on the relationship between state assignment and FSM decomposition. Compared to the method proposed in Chapter 5, the method by Chow et al. has a smaller area

overhead, a similar performance improvement but lower power savings. Our better power saving are attributed to the fact that Chow et al. do not use gated clocks in the decomposed implementation, while their smaller area overhead is due to the fact that block encoding requires a smaller number of flip-flops.

In Chapter 3 and 4 we proposed techniques for reducing the power dissipated when FSMs are idle. State assignment is related to such techniques as well. Remember that the key idea in Chapter 3 was to build a logic block that stops the clock when the FSM is in a some of its self-loops. We can chose the codes of the states whose self-loops are selected for clock gating in such a way that the implementation of the clock-control circuitry has reduced size, delay and power dissipation. A similar problem has been studied in the past and is known as symbolic input encoding [dmc86], a variation of the general state encoding problem.

The key idea in the symbolic encoding approach is that it is possible to minimize the number of cubes in the sum of products (SOP) representation of the activation function by minimizing a representation where implicants contain state values that are represented by symbolic names. The symbolic implicant list can then be minimized by building a minimum-cardinality prime cover. It can be shown [dmc86] that the cardinality of such cover is a lower bound for the cardinality of any cover of two-valued implicants that can be obtained after state encoding.

After building the minimum symbolic cover, we can perform state assignment. The implicants in the cover induce *constraints* for state assignment: they restrict the choice of state codes to those that do not impose the splitting of any symbolic implicant into two or more two-valued ones. In other words, we select a state assignment that guarantees the minimality of the SOP representation of the activation function. The main practical problem with this idea is that when we choose state codes to minimize the clock-control logic, we may produce sub-optimal logic in the combinational part of the FSM. Thus, a marginal improvement in the quality of the clock-control logic

may be swamped by the decreased quality of the much larger combinational part of the FSM.

6.7 Summary

In this chapter, we have presented a general framework for state assignment for low-power. Within that framework, we described a set of state assignment algorithms targeting low power consumption, varying in their exactness and computational complexity. We implemented one of the algorithms described, and ran it on standard benchmark circuits. We found that it compares favorably with existing state assignment tools targeting minimal area implementations, achieving a 16% average reduction of total switching activity, and a 34% average reduction of state variable related switching activity. We also explored the trade-offs between power-related and area-related cost metrics in the context of our algorithm. Our results confirm that state assignment has a large impact on power dissipation in the overall circuit.

The framework we have developed is general enough to open the way for exploration of new algorithms for the optimization of the FSMs combinational part that take into account the reduced switching activity on the present state inputs (flip-flip outputs). We believe that even larger power savings can be attained if new cost metrics are employed that relate more directly the power dissipated in the combinational part with the codes assigned to the states. Moreover, the state assignment step should be integrated with logic synthesis and library binding algorithms that can optimally exploit the reduced switching activity of the state variable inputs.

Compared to the clock-gating techniques presented in the previous chapters, state assignment produces in average lower power savings. This is a somewhat expected result, because state assignments targets only the power consumption on state lines while clock-gating techniques have been developed specifically for power minimization.

More specifically, clock-gating technique allow to decouple to a greater extent power optimization from area minimization, while state assignment has a strong influence on area.

Interestingly enough, the problem of minimizing power on the state lines has a mathematical model that allows us to formulate algorithms for its exact and heuristic solution. When the power dissipation of the combinational logic is taken into account, power minimization through state encoding becomes a much more complex problem, for which we do not have a clean mathematical formulation. Nevertheless, state assignment for low power is still an interesting optimization, especially for conservative design styles, where clock-gating techniques are not allowed.

Chapter 7

Conclusions

7.1 Thesis summary

Power dissipation is widely recognized as one of the hovering limiting factors to the exponential performance growth of digital CMOS circuits. In this thesis we presented a set of techniques for the automatic synthesis of digital circuits with reduced power dissipation. More specifically, we focused on the optimization of sequential synchronous logic, exploiting the basic technique of clock gating.

We proposed strategies for the minimization of the wasted power (i.e. the power dissipated in useless switching activity) as well as the reduction of the functional power. Sizable reductions have been obtained in both cases, although the minimization of wasted power is effective only for reactive system that remain idle for most of the operation time.

All power-reduction techniques analyzed in this thesis have some cost in area and/or timing. This is consistent with the characteristics of many engineering applications: optimization always involves trade-offs. However, the increasing density of modern VLSI circuits has lessened the importance of area as a cost metric, while timing is still the most important figure of merit. Fortunately, our techniques tend

to have a much smaller impact on timing than on area and we are optimistic on their practical relevance.

While Chapters 1 and 2 are dedicated respectively to a general introduction and to background information, Chapters 3 to 6 contain the original contribution of our work. We briefly summarize their content.

In Chapter 3 we introduced the first flavor of clock gating. We stop the clock of a finite state machine when the machine is idle and does not perform any useful computation. A limited amount of circuitry is added whose purpose is to detect the idle conditions (or a subset of them). Although the detection circuitry increases the area and may increase the delay, it reduces the power dissipation since its small size guarantees that the additional power it dissipates is smaller than that saved by stopping the clock for the original FSM. Moreover, some of the overhead can be eliminated by re-optimizing the original FSM using the knowledge that the clock will be stopped whenever the detection circuitry is active. The application of clock-gating on benchmark FSMs demonstrated that for reactive FMSs, power saving of more than 50% can be obtained, with small area (15%) and speed (8%) penalty.

In Chapter 4 we extended the techniques introduced in Chapter 3 to deal with larger sequential circuits. To this purpose we exploited algorithmic tools for the manipulation of large-size Boolean and discrete functions, namely BDDs and ADDs. Additionally, we investigated the relevance of the input probability distribution on the effectiveness of the clock gating procedures. The experimental results show that the results are competitive with those presented in Chapter 3 but the scope of applicability is

much increased. Moreover, we found that input statistics strongly influence the power reduction achieved by our technique. This confirms the usefulness of the accurate computation of the activation probability of the clock-stopping logic. The results obtained by the methods proposed in this chapter are comparable to, if not slightly better than, those obtained in Chapter 3. Power savings up to 40% have been obtained, with area overhead around 8% and speed penalty of 8%. When pattern with reduced transition activity are provided to the input of the gated-clock circuits the power savings rise to 60-70% compared to standard implementations.

In Chapter 5 we introduced a more aggressive flavor of clock gating that enables power optimization even for systems that are never idle. Clock gating is coupled with FSM decomposition to obtain an implementation where several sub-FSMs interact in a mutually exclusive fashion. In other words, whenever a given sub-machine is active, it is the only active one and it fully controls the input-output behavior of the circuit. Periodically, the active sub-machine disables itself and enables another sub-machine. The partitioning strategy targets the reduction of the interface overhead and the minimization of the frequency of control transfer among sub-FSMs. Experimentally we observed that the decomposition approach is very effective in minimizing power consumption and it has beneficial side effects on speed. Unfortunately, the area overhead is quite large. More in detail, power savings ranging between 16% and 43% have been obtained, with a speed improvement averaging around 12% and area overhead of 48% in average.

Finally, in Chapter 6 we investigated a more conservative technique for power minimization that does not involve clock gating. Starting from

a behavioral specification of a finite-state machine where the states are identified by symbolic names, we assign binary codes to the states so as to reduce the power dissipation on the state lines and the flip-flops. The basic intuition is that we reduce the number of state variables with different values for pairs of states that have a high transition probability. Our state assignment algorithm is very effective in reducing the average switching activity of the state lines. Unfortunately, state encoding has a strong effect on the area, delay and power dissipation of the combinational logic of the FSM. To take such effect into account, we employ a hybrid cost function that produces codes with reduced switching activity and keeps the combinational logic under control. On a set of benchmark FSMs, the power saving are in average around 16% with area and speed overhead around 10%.

It is important to notice that the techniques we introduced are *not* mutually exclusive: it is possible to apply them in cascade. For instance, we may first decompose FSMs, then apply state assignment and finally detect idle conditions. However, the power reduction of the combined techniques would not simply add up. The reason for this can be understood by observing that the techniques target slightly different classes of FSMs. While idle condition detection is very effective for reactive machines, decomposition gives best results for FSMs with high activity. Moreover, both techniques are based on clock gating which is not allowed in some conservative design styles. If clock gating is disallowed, state assignments is the only applicable technique.

In summary, we proposed a set of transformations that grants a good degree of flexibility. It is the designer's responsibility to choose the technique which is more suitable for the application at hand and merges seamlessly in the design flow.

7.2 Implementation and integration

The initial implementation of the techniques and algorithms presented in the previous chapters was in the form of *point tools*. Each tool was explicitly designed and optimized to perform a single functionality, and had its own dedicated user interface. While this implementation style is suitable for result collection and debugging, it is highly uncomfortable from the end user point of view.

We believe that user interfaces and usage paradigms are one of the main factors deciding the success of EDA tools (both for commercial and research applications). Indeed, a large amount of implementation effort has been dedicated to providing an uniform and effective user interface to the point tools described in this thesis and several other tools for power estimation and optimization that have been developed in our research group.

We have developed an integrated simulation and synthesis environment called *PPP* (to be read "p cube") with a modular and highly interactive Web-based interface [bbd96]. Geographically dispersed users can access our environment simply using a standard Web browser. No download of executables or compilation is required for testing the functionality of the tools and their performance. Many details of file format translation and parameter settings are abstracted away and results are presented through a simple and immediate graphical interface.

Integration of new features in the environment is simple and the selection of the computing resources to be used for running the tools is done automatically. The environment is intrinsically multi-user and distributed, but the end user does not perceive the complexity of managing several concurrent user sessions and computing resources.

The implementation of the distributed web-based environment and the optimization tools has been done in C and PERL. C was used for the computationally intensive

optimization tools, while PERL was used as "glue language" for file format translation and for managing the interaction with the Internet. Although lines of code are a poor measure of the amount of work, the implementation of the synthesis tools required approximatively 20,000 lines of code, while the user interface required approximatively 15,000 lines of code. *PPP* is freely available for access over the Internet and the source code of all its components is available as well.

7.3 Future work

Although a large body of research has been devoted to power optimization algorithms, this area has not yet reached complete maturity. The main limitation of the current power optimization techniques (including ours) is that they operate at a low level of abstraction. Even if we can reduce the power of a sequential unit by a factor of two, such reduction is obtained on a small portion of the entire system. Moreover, it is often claimed [raba96] that much larger power savings are possible if power optimization is performed at the system level or the algorithmic level.

The next generation of power optimization tools must rise the level of abstraction and the generality of the transformations. Modern system and appliances consist large part of commodity components that cannot be re-designed for cost and time-to-marked reasons. Even at the chip level, the use of optimized macros (such as memories, functional units, full microprocessor cores) is becoming widespread. Fine-grain optimization techniques like the ones we presented will always have a place in the design flow, but the most significant power savings will be obtained at the system level, where the granularity of the optimizations is much coarser.

An industry-promoted specifications for systems with advanced power management capabilities has been recently published [ACPI96]. An important assumption

in such specification is that hardware producers will provide components with a standardized power management interface. From the system perspective, it will be possible to dynamically set such components in several operation modes on the trade-off curve between performance and power dissipation. The diffusion of power-managed commodity hardware components opens a huge window of opportunity for system-level CAD tools, which can automatically generate an optimal power management strategy that minimizes the total power dissipation of a large system.

For systems with a predictable workload, system level power optimization can be done at design time. Extensive research and modeling effort is needed to develop algorithms that can automatically and effectively perform this task. An even more exciting challenge is the synthesis of dynamic schedulers that adaptively change the mode of operation of system components based on non-stationary workload, thermal control and battery conditions.

As system designers become more conscious of power dissipation issues and an increasing number of power-optimized commodity components is made available, the new generation of power optimization tools is expected to choose and manage such components, and guide the system designer towards power-efficient implementation. Numerous unsolved problems and open issues pave the road towards system-level tools for power optimization, but we believe that this is the main direction of research and evolution for the next few years.

Bibliography

[abra90] M. Abramovici, M. Breuer and A. Friedman, *Digital Systems Testing and Testable Design*. IEEE Press, 1990.

[alid94] M. Alidina, J. Monteiro et al., "Precomputation-based sequential logic optimization for low power," *IEEE Transactions on Very Large Scale Integration (VLSI) Systems*, vol. 2, no. 4, pp. 426–436, Jan. 19

[asha91] P. Ashar, S. Devadas and A. Newton, *Sequential logic synthesis*. Kluwer, 1991.

[atha94] W. C. Athas, L. J. Svensson et al., "Low-power digital systems based on adiabatic-switching principles," *IEEE Transactions on Very Large Scale Integration (VLSI) Systems*, vol. 2, no. 4, pp. 398–407, Dec. 1994.

[baha93] R. I. Bahar, E. A. Frohm et al., "Algebraic Decision Diagrams and their Applications," in *Proceedings of the International Conference on Computer Aided Design*, pp. 188-191, Nov. 1993.

[baha95] R. I. Bahar and F. Somenzi, "Boolean techniques for low-power driven re-synthesis," in *Proceedings of the International Conference on Computer-Aided Design*, pp. 428–432, Nov. 1995.

[bbd96] L. Benini, A. Bogliolo and G. De Micheli, "Distributed EDA tool integration: the PPP paradigm," in *International Conference on Computer Design*, pp. 448–453, Oct. 1996.

[beni94a] L. Benini, P. Siegel and G. De Micheli, "Automatic synthesis of gated clocks for power reduction in sequential circuits" *IEEE Design and Test of Computers*, pp. 32–40, Dic. 1994.

[benn88] C. H. Bennet, "Notes on the history of reversible computation," *IBM Journal of Research and Development*, vol. 32, no. 1, pp. 16, 1988.

[birt95] G. M. Birtwistle and A. Davis (editors), *Asynchronous digital circuit design* Springer-Verlag, 1995.

[bogl96] A. Bogliolo, L. Benini, and B. Riccò, "Power Estimation of Cell-Based CMOS Circuits," in *Proceedings of the Design Automation Conference*, pp. 433–438, June 1996.

[alpha96] G. Bouchard, "Design objectives of the $0.35\mu m$ Alpha 21164 microprocessor," in *Hot chips symposium*, Aug. 1996.

[brow90] F. M. Brown, *Boolean Reasoning.* Kluwer, 1990.

[brac90] K. S. Brace, R. Rudell, R. Bryant, "Efficient Implementation of a BDD Package," in *Proceedings of the Design Automation Conference*, pp. 40–45, June 1990.

[brya86] R. Bryant, "Graph-Based Algorithms for Boolean Function Manipulation," *IEEE Transactions on Computers*, Vol. C-35, No. 8, pp. 79–85, August 1986.

[bult96] K. Bult, A. Burstein et al., "Low power systems for wireless microsensors," in *International Symposium on Low Power Electronic and Design*, pp. 17–21, Aug. 1996.

[burd94] T. Burd, "Low-Power CMOS Library Design Methodology," *M.S. Report, University of California, Berkeley, UCB/ERL M94/89*, 1994.

[burd95] T. Burd and R. Brodersen, "Energy efficient CMOS microprocessor design," in *Proceedings of the Hawaii International Conference on System Sciences*, vol. 1, pp. 288-97, Jan. 1995.

[isca89] F. Brglez, D. Bryan, K. Koźmiński, "Combinational Profiles of Sequential Benchmark Circuits," in *International Symposium on Circuits and Systems*, pp. 1929–1934, May 1989.

[chan95] A. Chandrakasan and R. Brodersen, *Low power digital CMOS design.* Kluwer, 1995.

[chan95b] A. Chandrakasan, M. Potkonjak et al., "Optimizing power using transformations," *IEEE Transactions on Computer-Aided Design of Integrated Circuits and Systems*, vol. 14, no. 1, pp. 12–31, Jan. 1995.

[chan95] J. Chang and M. Pedram, "Register allocation and binding for low power," in *Proceedings of the Design Automation Conference*, pp. 29–35, June 1995.

[cho93] H. Cho, G. Hachtel and F. Somenzi, "Redundancy Identification/Removal and Test Generation for Sequential Circuits Using Implicit State Enumeration," *IEEE Transactions on Computer-Aided Design of Circuits and Systems*, vol. 12, no. 7, pp. 935–45, July 1993.

[cho94] H. Cho, G. Hachtel et al., "A State Space Decomposition Algorithm for Approximate FSM Traversal", in *Proceedings of the European Design and Test Conference*, pp. 137-141, Feb. 1994.

[chow96] S. H. Chow, Y. C. Ho et al., "Low power realization of finite state machines

- A decomposition approach," in *ACM Transactions on Design Automation of Electronic Systems*, vol. 1, no. 3, July 1996.

[clar93] E. M. Clarke, M. Fujita et al., "Multi-Terminal Binary Decision Diagrams: An Efficient Data Structure for Matrix Representation," in *International Workshop on Logic Synthesis*, pp. 6a:1-15, May 1993.

[coud89] O. Coudert, C. Berthet, J. C. Madre, "Verification of Sequential Machines Using Boolean Functional Vectors," in *IFIP Intl. Workshop on Applied Formal Methods for Correct VLSI Design*, pp. 111–128, Nov. 1989.

[coud92] O. Coudert and C. Madre, "Implicit and incremental computation of primes and essential primes of Boolean functions," in *Proceedings of the Design Automation Conference*, pp. 36–39, June 1992.

[dasg95] A. Dasgupta and R. Karri, "Simultaneous scheduling and binding for power minimization during microarchitecture synthesis," in *International Symposium on Low Power Design*, pp. 69–74, April 1995.

[davi78] M. Davio, J. P. Deschamps and A. Thayse, *Discrete and switching functions.* McGraw-Hill, 1978.

[debn95] G. Debnath, K. Debnath and R. Fernando, "The Pentium processor-90/100, microarchitecture and low power circuit design," in *International conference on VLSI design*, pp. 185–190, Jan. 1995.

[dmc86] G. De Micheli, "Symbolic Design of Combinational and Sequential Logic Circuits Implemented by Two-Level Logic Macros," *IEEE Transactions on Computer-Aided Design of Circuits and Systems*, vol. 5, no. 4, pp. 597–616, Oct. 1986.

[dmc94] G. De Micheli. *Synthesis and optimization of digital circuits.* McGraw-Hill, 1994.

[dmc90] G. De Micheli, D. Ku et al., "The Olympus synthesis system," *IEEE Design & Test of Computers*, pp. 37–53, October 1990

[denk94] J. S. Denker, "A review of adiabatic computing," in *Symposium on Low Power Electronics*, pp. 10–12, Oct. 1994.

[deva91] S. Devadas and K. Keutzer, "A unified approach to the synthesis of fully testable sequential machines," *IEEE Transactions on Computer-Aided Design of Circuits and Systems*, vol. 10, no. 4, pp. 39–51, Jan. 1991.

[deva95] S. Devadas and S. Malik, "A survey of optimization techniques targeting low power VLSI circuits," in *Proceedings of the Design Automation Conference*, pp. 242-247, June 1995.

[deva88] S. Devadas, Hi-keung Ma et al., "MUSTANG: State Assignment of Finite State Machines Targeting Multilevel Logic Implementations," *IEEE Transactions on Computer-Aided Design of Circuits and Systems*, vol. 7, no. 12, pp. 1290–1300, Dec. 1988.

[du91] X. Du, G. Hachtel et al. "MUSE: A MUltilevel Simbolic Encoding Algorithm for State Assignment," *IEEE Transactions on Computer-Aided Design of Integrated Circuits and Systems*, vol. 10, no. 1, pp. 28–38, Jan. 1991.

[dolo64] T. Dolotta and E. McCluskey. "The Coding of Internal States of Sequential Machines," *IEEE Teansaction on Electron. Comput.*, vol EC-13, pp. 549–562, October 1964.

[elli91] S. C. Ellis, "Power management in notebook computers," in *Proceedings of the Personal Computer Design Conference*, pp. 749–754, July 1991.

[esch92] B. Eschermann, "State assignment for hardwired control units," *ACM computing surveys*, vol. 25, no. 4, pp. 415–436, Dec. 1993.

[expo96] Exponential Corporation, "Exponential X^{704} microprocessor," *Press release*, Oct. 1996.

[fava96] M. Favalli, L. Benini, G. De Micheli, "Design for Testability of Gated-Clock FSMs," in *Proceedings of the European Design and Test Conference*, pp. 589-596, Mar. 1996.

[gajo93] M. R. Garey and D. S. Johnson, *Computers and intractability. A guide to the Theory of NP-completeness.* Freeman, 1983.

[gars96] J. Garside, "Amulet2e," in *Hot chips symposium*, Aug. 1996.

[geig91] M. Geiger and T. Muller-Wippefurth, "FSM decomposition revisited: algebraic structure theory applied do MCNC benchmark FSMs," in *Proceedings of the Design Automation Conference*, pp. 182–185, June 1992.

[ghos92] A. Ghosh, S. Devadas et al., "Estimation of average switching activity in combinational and sequential circuits," in *Proceedings of the Design Automation Conference*, pp. 253–259, June 1992.

[gold89] D. Goldberg, *Genetic Algorithms in search, optimization and machine learning*, Addison-Wesley, 1989.

[gref90] J. J. Grefenstette, *A user's guide to GENESIS*, 1990.

[hahe94] G. Hachtel, M. Hermida et al., "Re-Encoding sequential circuits to reduce power dissipation," in *Proceedings of the International Conference on Computer-Aided Design*, pp. 70–73, Nov. 1994.

[hama94] G. Hachtel, E. Macii et al., "Symbolic algorithms to calculate Steady-State probabilities of a finite state machine," in *Proceedings of IEEE European Design and Test Conference*, pp. 214–218, Feb. 1994.

[hach94] G. Hachtel, E. Macii et al., "Probabilistic Analysis of Large Finite State Machines," in *Proceedings of the Design Automation Conference*, pp. 270-275, June 1994.

[harr95] E. P. Harris, S. W. Depp et al., "Technology directions for portable computers," *Proceedings of the IEEE*, vol. 83, no. 4, pp. 636–658, April 1995.

[hart66] J. Hartmanis and H. Stearns, *Algebraic Structure Theory of Sequential Machines*. Prentice-Hall, 1966.

[hasa95] Z. Hasan and M. Ciesielski, "FSM decomposition and functional verification of FSM networks," *VLSI Design*, vol. 3, no. 3–4, pp. 249–65.

[henn68] F. C. Hennie, *Finite-State models for logical Machines*. Wiley, 1968.

[koha70] Z. Kohavi, *Switching and Finite automata theory*. McGraw-Hill, 1970.

[kuma95] N. Kumar, S. Katkoori et al., "Profile-driven behavioral sythesis for low-power VLSI systems," *IEEE Design & Test of Computers*, vol. 12, no. 3, pp. 70–84, Fall 1995.

[kuo95] M. Kuo, L. Liu and C Cheng, "Finite-State Machine decomposition for I/O minimization," in *IEEE International Symposium on Circuits and Systems*, pp. 1061–1064, April 1995.

[iman96] S. Iman and M. Pedram, "POSE: Power optimization and synthesis environment," in *Proceedings of the Design Automation Conference*, pp. 21–26, June 1996.

[inde94] T. Indermaur and M. Horowitz, "Evaluation of charge recovery circuits and adiabatic switching for low power CMOS design," in *Symposium on Low Power Electronics*, pp. 102-103, Oct. 1994.

[ACPI96] Intel, Microsoft and Toshiba,
"Advanced Configuration and Power Interface specification", available at *http://www.intel.com/IAL/powermgm/specs.html*, Dec. 1996.

[lai94] Y. T. Lai, M. Pedram, S. B. K. Vrudhula, "EVBDD-Based Algorithms for Integer Linear Programming, Spectral Transformation, and Function Decomposition," *IEEE Transactions on Computer-Aided Design of Circuits and Systems*, Vol. 13, No. 8, pp. 959-975, Aug. 1994.

[land95] P. E. Landman and J. M. Rabaey, "Activity-sensitive architectural power analysis for the control path," in *International Symposium on Low Power Design*, pp. 93–98, April 1995.

[land96] P. E. Landman, R. Mehra and J. Rabaey, "An integrated CAD environment for low-power design," *IEEE Design & Test of Computers* vol. 13, no. 2, pp. 72–82, Summer 1996.

[lin89] B. Lin and A. R. Newton, "Synthesis of multiple-level logic from symbolic high-level description languages," in *Proc. of IEEE Int. Conf. On Computer Design*, pp. 187–196, August 1989.

[madr88] J. C. Madre, J. P. Billon, "Proving Circuit Correctness using Formal Comparison Between Expected and Extracted Behavior," in *Proceedings of the Design Automation Conference*, pp. 205-210, June 1988.

[mail91] F. Mailhot and G. De Micheli, "Algorithms for technology mapping based on binary decision dBagrams and on Boolean operations," *IEEE Transactions*

on Computer-Aided Design of Circuits and Systems, pp. 599–620, May 1993.

[mang95] B. Mangione-Smith, "Low power communication protocols: Paging and beyond," in *Symposium on Low Power Electronics*, pp. 8–11, Oct. 1995.

[marc94] R. Marculescu, D. Marculescu and M. Pedram, "Switching activity analysis considering spatiotemporal correlations," in *Proceedings of the International Conference on Computer-Aided Design*, pp. 294–299, Nov. 1994

[mars94] A. Marshall, B. Coates and P. Siegel, "Designing an asynchronous communication chip," *IEEE Design & Test of Computers*, vol. 11, no. 2, pp. 8–21, Summer 1994.

[mart90] S. Martello and P. Toth, *Knapsack Problems. Algorithms and Computer Implementations.* Wiley, 1990.

[mart96] T. L. Martin and D. P. Sewiorek, "A power metric for mobile systems," in *International Symposium on Low Power Electronics and Design*, pp. 37–42, Aug. 1996.

[mccl86] E. McCluskey. *Logic design principles.* Prentice-Hall, 1986.

[mcg93] P.McGeer, J. Sanghavi et al., "ESPRESSO-SIGNATURE: a new exact minimizer for logic functions," *IEEE Transactions on Very Large Scale Integration (VLSI) Systems*, vol. 1, no. 4, pp. 432–440, Dec. 1993.

[mehr96] R. Mehra, L. Guerra et al., "Exploiting locality for low-power design," in *Proceedings of the Custom Integrated Circuits Conference*, pp. 401–406, May 1996.

[mein95] J. Meindl, "Low power microelectronics: retrospect and prospect," *Proceedings of the IEEE*, vol. 83, no. 4, pp. 619–634, April 1995.

[meng95] T. H. Meng, B. Gordon et al., "Portable Video-on-Demand in wireless communication," *Proceedings of the IEEE*, vol. 83, no. 4, pp. 659–680, April 1995.

[mina90] S. I. Minato, N. Ishiura, S. Yajima, "Shared Binary Decision Diagram with Attributed Edges for Efficient Boolean Function Manipulation," in *Proceedings of the Design Automation Conference*, pp. 52-57, June 1990.

[mont93] J. Monteiro, S. Devadas and A. Ghosh, "Retiming sequential circuits for low power," in *Proceedings of the International Conference on Computer-Aided Design*, pp. 398–402, Nov. 1993.

[mont94] J. Monteiro, S. Devadas and B. Lin, "A methodology for efficient estimation of switching activitiy in sequential logic circuits," in *Proceedings of the Design Automation Conference*, pp. 315–321, June 1994

[moor96] G. Moore, *Computerworld-Smithsonian Monticello Lecture*, Computerworld Leadership Series, May 1996.

[muss95] E. Mussol and J. Cortadella, "High-level synthesis techniques for reducing the activity of functional units," in *International Symposium on Low Power Design*, pp. 99–104, April 1995.

[najm95] F. Najm, "Power estimation techniques for integrated circuits," in *Proceedings of the International Conference on Computer-Aided Design*, pp. 492–499, Nov. 1995.

[nehm88] G. Nemhauser and L. Wolsey, *Integer and combinatorial optimization.* Wiley, 1988.

[niel94] L. S. Nielsen, C. Niessen et al., "Low-power operation using self-timed circuits

and adaptive scaling of the supply voltage," *IEEE Transactions on Very Large Scale Integration (VLSI) Systems*, vol. 2, no. 4, pp. 391–397, Dec. 1994.

[olso94] E. Olson and S. Kang, "State assignment for low-power synthesis using genetic local search," in *Proceedings of IEEE Custom Integrated Circuits Conference*, pp. 140–143, May 1994.

[raba96] J. M. Rabaey and M. Pedram (editors), *Low power design methodologies*. Kluwer, 1996.

[ragh94] A. Raghunathan and N. K. Jha, "Behavioral synthesis for low power," in *Proceedings of the International Conference on Computer Design*, pp. 318–322, Oct. 1994.

[ragh96a] A. Raghunathan, S. Dey et al., "Controller re-specification to minimize switching activity in controller/data path circuits," in *International Symposium on Low Power Electronics and Design*, pp. 301–304, Aug. 1996.

[ragh96b] A. Raghunathan, S. Dey and N. K. Jha, "Glitch analysis and reduction in register transfer level power optimization," in *Proceedings of the Design Automation Conference*, pp. 331–336, June 1996.

[ravi95] K. Ravi, F. Somenzi, "High-Density Reachability Analysis," in *Proceedings of the International Conference on Computer-Aided Design*, pp. 154-158, Nov. 1995.

[rofl96] R. Rofleich, A. Kobl and B. Wurth, "Reducing power dissipation after technology mapping by structural transformations," in *Proceedings of the Design Automation Conference*, pp. 789–794, June 1996.

[roy93] K. Roy and S. Prasad, "Circuit activity based logic synthesis for low power

reliable operations," *IEEE Transactions on Very Large Scale Integration (VLSI) Systems*, vol. 1, no. 4, pp. 503–513, Dec. 1993.

[royn93] S. Roy and H. Narayanan, "Application of the Principal Partition and Principal Lattice of Partitions of a graph to the problem of decomposition of a Finite-State Machine," in *IEEE International Symposium on Circuits and Systems*, pp. 2564–2567, May 1993.

[salz89] A. Salz, M. Horowitz, "IRSIM: an incremental MOS switch-level simulator," in *Proceedings of the Design Automation Conference*, pp. 173–178, June 1989.

[sanm96] R. San Martin and J. P. Knight, "Optimizing power in ASIC behavioral synthesis," *IEEE Design & Test of Computers*, vol. 13, no. 2, pp. 58–70, Summer 1996.

[schu94] J. Schutz, "A 3.3V 0.6μm BiCMOS superscalar microprocessor," in *IEEE International Solid-State Circuits Conference*, pp. 202–203, Feb. 1994.

[sent92] E. Sentovich et al., "Sequential circuit design using synthesis and optimization," in *Proceedings of the International Conference on Computer Design*, pp. 328–333, Oct. 1992.

[shen92] A. Shen, A. Ghosh, S. Devadas, and K. Keutzer, "On average power dissipation and random pattern testability of CMOS combinational logic networks," in *Proceedings of the International Conference on Computer-Aided Design*, pp. 402–407, Nov. 1992.

[slat95] J. Slaton, S. P. Licht et al., "The PowerPC 603e microprocessor: an enhanced, low-power, superscalar microprocessor," in *Proceedings of the International Conference on Computer Design*, pp. 192–203, Oct. 1995.

[some96] F. Somenzi and G. D. Hachtel, *Logic synthesis and verification algorithms.* Kluwer, 1996.

[stra94] A. J. Stratakos, S. R. Sanders and R. Brodersen, "A low-voltage CMOS DC-DC converter for a portable battery-operated system," in *Proceedings of the Power Electronics Specialists Conference*, vol. 1, pp. 619–26, June 1994.

[sues94] B. Suessmith and G. Paap III, "PowerPC 603 microprocessor power management," *Communications of the ACM*, no. 6, pp. 43–46, June 1994.

[tiwa95] V. Tiwari, S. Malik and P. Ashar, "Guarded evaluation: pushing power management to logic synthesis/design," in *International Symposium on Low Power Design*, pp. 221–226, April 1995.

[triv82] K. Trivedi, *Probability and Statistics with Reliability, Queueing, and Computer Science Applications*, Prentice-Hall, 1982.

[tsui93] C. Tsui, M. Pedram, and A. Despain, "Technology decomposition and mapping targeting low power dissipation," in *Proceedings of the Design Automation Conference*, pp. 68–73, 1993.

[tsui94] C. Tsui, M. Pedram and A. Despain, "Low-Power state assignment targeting Two-and Multi-level logic implementation," in *Proceedings of the International Conference on Computer-Aided Design*, pp. 82–27, Nov. 1994.

[tsui94b] C. Y. Tsui, M. Pedram and A. M. Despain, "Exact and Approximate Methods for calculating signal and transition probabilities in FSMs," in *Proceedings of the Design Automation Conference*, pp. 18–25, June 1994.

[veen84] H. J. Veendrick, "Short-circuit dissipation of static CMOS circuitry and its impact on the design of buffer circuits," *Journal of Solid-State Circuits*, vol. SC-19, no. 4, pp. 468–473, Aug. 1984.

[vitt94] E. Vittoz, "Low-Power design: Ways to approach the limits," in *Proceedings of the IEEE Solid-State Circuits Conference*, pp. 14–18.

[west92] N. Weste and K. Eshraghian, *Principles of CMOS VLSI Design (Second Edition)*. Addison-Wesley, 1992.

[mcnc91] S. Yang, "Logic Synthesis and Optimization Benchmarks User Guide Version 3.0," *Technical report, Microelectronics Center of North Carolina*, Jan. 1991.

[jeon92] S-W. Yeong and F. Somenzi. "A new algorithm for 0-1 programming based on binary decision diagrams," in *International Workshop on Logic Synthesis*, pp. 177–184, 1992.

[yeun94] N. Yeung et al., "The design of a 55SPECin92 RISC processor under 2W," in *Proceedings of the IEEE Solid-State Circuits Conference*, pp. 206–207, Feb. 1994.

Appendix A

Testability of gated-clock circuits

With the exception of state assignment (Chapter 6), all power minimization techniques presented in this thesis rely on clock gating to reduce switching activity. The main reason for using gated clocks is that they reduce power not only in the functional logic of the units whose clock is stopped, but also in the clocking circuitry itself.

On the other hand, gated clocks are regarded with suspect by many designers and explicitly disallowed in some conservative design styles. There are two reasons for this. First, clock gating requires the insertion of some logic on the clock distribution tree and increases clock skew. This issue was discussed in Chapter 3. Second, it is a common conception that gated clocks decrease testability. In this appendix we briefly discuss the testability issues raised by clock gating and we propose simple and effective solutions for designing highly-testable gated-clock circuits. Refer to [fava96] for a detailed treatment.

A.1 Testability issues

We adopt the *stuck-at* logical fault model to represent physical faults. Moreover, we focus on static single-fault testability, disregarding transient, intermittent and

multiple faults. In the following, a *fully testable* FSM is one in which there exist a test sequence that reveals any given single *stuck-at* fault.

The automatic synthesis of fully testable FSMs is considerably more difficult than the synthesis of testable combinational logic, nevertheless effective tools have been developed and are commonly used in industrial and academic [deva91, cho93] environments.

In many practical cases, full testability for single *stuck-at* faults is considered a minimum safety requirement. We will show that the addition of clock-gating circuitry makes the FSM not fully testable. Assume that we have modified our original FSM implementation by adding the clock-gating circuitry. Let us consider a *s-a-0* fault on the output wire of the activation function. In this case, the clock will always be enabled, and the FSMs will have the same behavior as in the original implementation. Observing the outputs, it is not possible to detect the fault. The same problem occurs for faults in the internal logic of the activation function that can be propagated only making the output of the activation function 0 for an input configuration that produces a 1 in the correct circuit.

In general, we cannot reveal a fault ϕ that transforms the activation function f_a into a faulty function f_a^ϕ with a smaller ON-set.

$$f_a^\phi \subseteq f_a \rightarrow \phi \; is \; untestable \tag{A.44}$$

This property implies the existence of at least one untestable fault in the gated-clock FSM (the *s-a-0* on the output of f_a). The gated-clock FSM is *never* fully testable.

While the existence of untestable faults in the activation function logic is quite intuitive, it may be possible to overlook that the insertion of clock-gating circuitry can decrease the testability of the combinational logic of the FSM as well. The activation function is active (one) in a sub-set of the self-loops. If a testable fault in the original

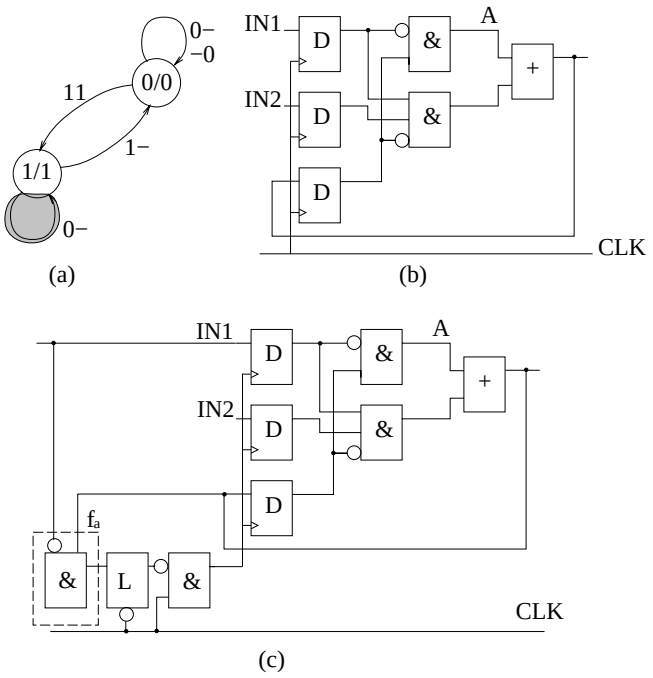

Figure 46: (a) STG of a simple two-state FSM. (b) Implementation of the FSM. (c) Gated-clock implementation.

FSM can be tested only with input sequences that imply traversing a self-loop in the ON-set of the activation function, the fault becomes untestable in the gated-clock FSM. This statement can be clarified through an example.

> **Example A.1.1**. In the FSM of Figure 46(b), consider a *s-a-0* fault on wire A. In the original FSM, the fault is testable. Assuming that the initial (reset) state is 0, an input sequence that reveals the fault is $(11, 01)$.
>
> The *s-a-0* fault on A is untestable in the gated-clock version of the FSM shown in Figure 46(c). The input value required at the AND gate to activate the fault is 01, but this value never appears on the output of the flip-flops. This is because the activation function is high when IN1 and the state are both one. When the activation function is high the clock is stopped and the value required for the activation of the fault is not propagated to the output of the flip-flops. □

We call I the set of possible input values for the combinational logic of the FSM. The presence of the activation function reduces the size of set I. In other words, the

controllability *don't care* set for the combinational logic of the FSM is increased, and we can exploit only a subset of the STG arcs to generate test vectors.

In application where testability is a primary requirement, the untestable faults generated by the clock-gating logic are not acceptable. We will show that it is possible to generate testable gated-clock FSMs with minimum overhead and no loss in performance. We will assume that the original FSM is fully testable, because in the following discussion we want to focus only on untestable faults that are created by the insertion of the activation function.

A.2 Increasing observability

We first address the problem of the *s-a-0* untestable fault on the output of f_a. Since we have shown that it is impossible to propagate the effect of such fault to the output, the only way to solve the problem is to increase the observability. If we make the output of the activation function observable, the *s-a-0* fault becomes trivially testable: any input-state configuration in the ON-set of the activation function is a valid test vector.

The penalty of increasing the observability is due to additional wiring needed to route the output of f_a to the closest observation point, or to an additional scan flip-flop in full-scan designs. These requirements are not excessive, especially for large FSM. We call *observability increase* the addition of one observable output in the FSM. Notice that the combinational logic of the FSM and the activation function are not modified.

The observability of f_a makes the generation of tests for faults in f_a not harder than the test generation for faults in the combinational logic of the original FSM. This can be intuitively understood observing that the inputs of the activation function are exactly the same as those of the combinational logic of the original FSM (anticipated

by one clock cycle). Notice that the inputs of the activation function do not come from the output of conditionally enabled flip-flops, therefore they can assume any value in the original set of allowed input values. If the activation function is synthesized without internal redundancies, the presence of the additional observation point is sufficient to guarantee its full testability.

While the use of an additional observation point solves the problem of testing the activation function, it still does not guarantee full testability of the gated-clock FSM, as we can see in the following example.

> **Example A.2.2**. Consider the gated-clock FSM of Figure 46(c). Requiring the observability of f_a guarantees the testability of the *s-a-0* fault on its output. Unfortunately, the *s-a-0* fault on line A is still untestable. The only input-state configuration that reveals it is never observed by the inputs of the combinational logic of the FSM, because the activation function freezes the clock when it occurs at flip-flop inputs. □

The gated-clock FSM with increased observability is not fully testable because even if the additional observation point makes the activation function irredundant, it does not improve the testability of the combinational logic in the FSM. The activation function reduces the set I of allowed input values to a set $I' \subset I$. We assumed full testability of the original FSM when the full I can be used for test generation, but nothing can be said on testability with respect to I'. Insertion of more observability points is not a viable solution, because the untestable faults are caused by the lack of fault activation conditions.

Fortunately, we can solve this problem employing the same tools used for the synthesis of the original fully testable FSM. Synthesis for testability of FSMs can be performed using standard *redundancy removal* techniques [cho93]. It is important to notice that redundancy removal can be applied to the gated-clock circuits only after the activation function has been made observable. If this is not the case, redundancy removal may eliminate the clock gating circuitry because it is functionally redundant.

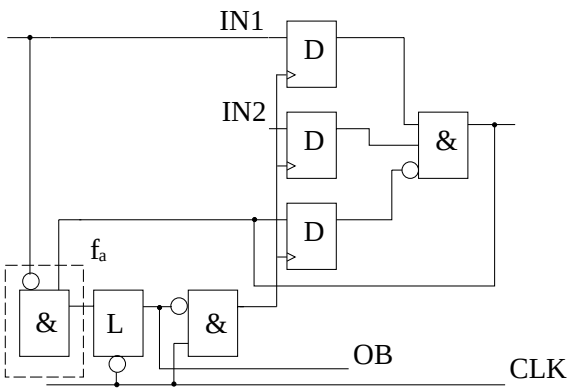

Figure 47: Optimized and fully-testable gated-clock FSM with increased observability

Example A.2.3. In the gated-clock FSM of Figure 46(c) the *s-a-0* fault on wire A is untestable. The redundancy removal algorithm detects it ad replaces wire A with a connection to the constant value 0. The constant can then be propagated to further simplify the circuit. The OR gate on the output can then be eliminated, and the and gate whose output has been blocked at 0 can be removed as well. The final optimized circuit is shown in Figure 47. It is not only fully testable, but has also better performance that the original gated-clock FSM, in terms of area, delay and power dissipation. □

A.3 Increasing controllability

Eliminating redundancy from a gated-clock FSM with increased observability is an effective way to obtain fully testable implementation with improved performance. Unfortunately, there are two important cases in which this procedure cannot be applied.

First, in many applications the combinational logic of the machine consists of blocks that cannot be modified. This is often the case when gated-clock synthesis is applied to data-path circuits: the combinational logic may consist of adders, multipliers, comparators or other standard components implemented by highly optimized cells that the designer is not allowed to modify. Faults inside the standard components may become untestable and they cannot be removed. Second, the redundancy removal

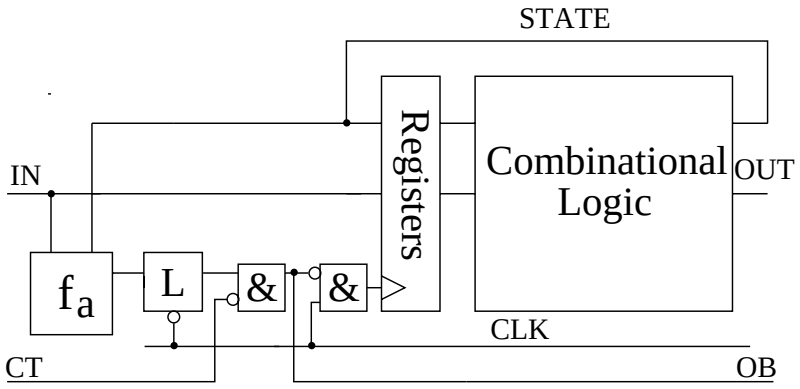

Figure 48: Gated-clock FSM with increased controllability and observability.

process may become very computationally expensive. If the redundancy removal algorithm fails, we do not have guarantees on the testability of our implementation. This is an unacceptable limitation for a general design methodology.

These problem can be avoided by adding an extra controllability input `CT` that inhibits the effects of the gating, as shown in Figure 48. When such input is set at logic 1, the combinational part of the FSM can be tested without worrying about the effects of the activation function. When the activation function becomes active, the clock is not stopped if `CT` = 1, and the flip-flops of the FSM sample the input and state value. Thus, the allowed input set I is exactly the same as the one of the original FSM. The availability of the complete I guarantees that no untestable faults exist in the combinational logic (under the assumption of full testability for the original FSM). If the activation function is observable (through the observability output `OB`), we can also guarantee the full testability of f_a, as discussed in the previous section.

The insertion of an additional controllability input has two advantages. First, since we do not need to modify the combinational logic of the FSM in the gated-clock version, the test set developed for the original FSM can be used to test the gated-clock FSM as well. More test vectors can just be appended to fully test the activation function. Second, while testing the gated-clock FSM without added controllability may

be substantially harder than testing the original FSM, the test generation process in the added controllability case is generally very efficient. The reason for this difference is that a large amount of time is spent in the first case to prove the untestability of redundant fault, and to subsequently remove the redundant wires, while the FSM with added controllability does not have redundant faults (if the original FSM is fully testable).

A.4 Summary

We proposed two transformations that solve the testability problems of gated-clock circuits. The first transformation, namely *increased observability*, allows the synthesis of fully testable gated-clock circuits with improved performance and it is applicable when the designer is allowed to modify the internal structure of the logic network whose clock has been gated. The test generation and redundancy removal steps for *increased observability* circuits are computationally expensive and should be applied in aggressive implementations.

The second transformation, namely *increased controllability and observability*, guarantees the full testability of the gated-clock circuit if the initial implementation was fully testable. This transformation is slightly more expensive than the previous one but does not require any modification of the logic in the gated-clock sub-system. Moreover, the test generation process is does not require substantially higher computational effort compared to the original implementation.

Both transformations can be seen as customized scan-based approaches [abra90]. Increasing controllability and observability is equivalent to assuming that the latch in the clock gating circuitry is transformed in a scan-latch and inserted in the scan chain. However, we presented the transformation in a more general setting, where scan-based design for testability may not be enforced in the entire design.